

pubs.acs.org/CR Review

Visible Light-Induced Transition Metal Catalysis

Kelvin Pak Shing Cheung, Sumon Sarkar, and Vladimir Gevorgyan*



Cite This: Chem. Rev. 2022, 122, 1543-1625

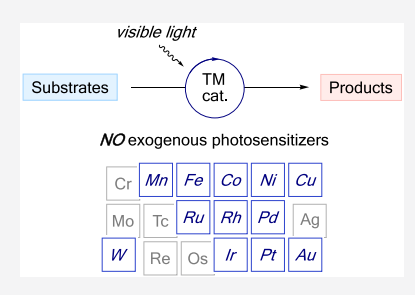


ACCESS |

III Metrics & More

Article Recommendations

ABSTRACT: In recent years, visible light-induced transition metal catalysis has emerged as a new paradigm in organic photocatalysis, which has led to the discovery of unprecedented transformations as well as the improvement of known reactions. In this subfield of photocatalysis, a transition metal complex serves a double duty by harvesting photon energy and then enabling bond forming/breaking events mostly via a single catalytic cycle, thus contrasting the established dual photocatalysis in which an exogenous photosensitizer is employed. In addition, this approach often synergistically combines catalyst—substrate interaction with photoinduced process, a feature that is uncommon in conventional photoredox chemistry. This Review describes the early development and recent advances of this emerging field.



CONTENTS

1. Introduction	1544
2. Cobalt	1545
2.1. General Overview	1545
2.2. Photolysis of Co(III)—Carbon Bond	1546
2.2.1. Giese-type Reactions	1546
2.2.2. Heck-type Reactions	1547
2.3. Transformations Involving LMCT of Co(II)	
Acetylides	1550
2.4. Fragmentation of P–H Bond of H-Phosphine	
Oxides	1551
3. Copper	1552
3.1. General Overview	1552
3.2. Photoinduced SET of Cu(I)—Nucleophile	
Complexes	1553
3.2.1. Heteroatom-Based Nucleophiles	1553
3.2.2. Alkynes as Nucleophiles under Redox-	
Neutral Conditions	1555
3.2.3. Alkynes as Nucleophiles under Oxida-	
tive Conditions	1558
3.2.4. Other Carbon-Based Nucleophiles	1562
3.3. Photoinduced SET of Standalone Cu(I)	
Complexes	1563
3.3.1. Difunctionalization of Alkenes and Al-	
kynes	1563
3.3.2. Decarboxylative Transformations	1565
3.3.3. Asymmetric Transformation	1567
3.4. Photoinduced Homolytic Ligand Dissocia-	
tion of Cu(II) Complexes	1567
3.5. Photoinduced EnT of Cu(I) Complexes	1569
4. Iron	1570
4.1. General Overview	1570
4.2. Transformations Involving LMCT of Fe(III)	

4.3. Difunctionalization of Alkenes	1572
4.4. Cross-Coupling Reaction	1572
5. Palladium	1572
5.1. General Overview	1572
5.2. Fragmentation of C(sp ²)—X Bond	1574
5.2.1. Desaturation	1574
5.2.2. Atom Transfer Radical Cyclization	1575
5.2.3. C–H Arylation	1575
5.3. Fragmentation of C(sp ³)—X Bond	1576
5.3.1. Desaturation	1576
5.3.2. Heck and Heck-type Reactions	1578
5.3.3. C–H Alkylation	1583
5.3.4. Multicomponent Reactions	1585
5.3.5. Atom Transfer Reactions	1588
5.3.6. Halogenation and Borylation	1589
5.4. Homolytic Cleavage of N–O Bond	1591
5.5. Miscellaneous	1591
6. Nickel	1593
6.1. General Overview	1593
6.2. Transformations Involving Photoexcitation	
of Ni(II) Aryl Halide Complexes	1593
6.3. Transformations Involving Photoexcitation	
of Ni(II)—Substrate Coordination Complexes	1594
6.3.1. Asymmetric β -Alkylation of Enones	1594
6.3.2. Cross-Coupling Reactions	1595
7. Iridium	1596
7.1. General Overview	1596

Special Issue: Photochemical Catalytic Processes

Received: May 7, 2021 Published: October 8, 2021





Carboxylates

1570

7.2. Iridium as Chiral Photoredox Catalyst 7.2.1. Asymmetric α -Alkylation of Ketones 7.2.2. Asymmetric Radical—Radical Cross-Cou-	1596 1596
pling	1598
7.3. Iridium as Chiral Triplet Sensitizer	1598
8. Rhodium	1600
8.1. General Overview	1600
8.2. Asymmetric α -Functionalization of Ketones	1600
8.2.1. Radical Addition to Enolates	1600
8.2.2. Radical—Radical Cross-Coupling	1602
8.3. Asymmetric Synthesis of β -Functionalized	
Ketones	1602
8.3.1. Radical—Radical Cross-Coupling	1602
8.3.2. β -Alkylation of Enones	1602
8.4. Asymmetric Photocycloaddition	1604
8.5. C(sp ²)—H Borylation	1605
9. Gold	1605
9.1. General Overview	1605
9.2. Carbofunctionalization of Alkynes and Al-	
kenes	1606
9.3. Cross-Coupling Reactions	1607
10. Tungsten	1608
10.1. General Overview	1608
10.2. C–H Alkylation	1609
10.3. C–H Alkynylation and Deuteration	1611
11. Other Transition Metals	1612
11.1. Manganese	1612
11.2. Ruthenium	1613
11.3. Platinum	1614
12. Conclusions	1614
Author Information	1615
Corresponding Author	1615
Authors	1615
Notes	1615
Biographies	1615
Acknowledgments	1615
References	1615

1. INTRODUCTION

Visible light photocatalysis has become a powerful tool in organic synthesis. This field can be classified into three subcategories, which are based on the catalytic system involved (Figure 1). The first class features a photocatalyst, which in its

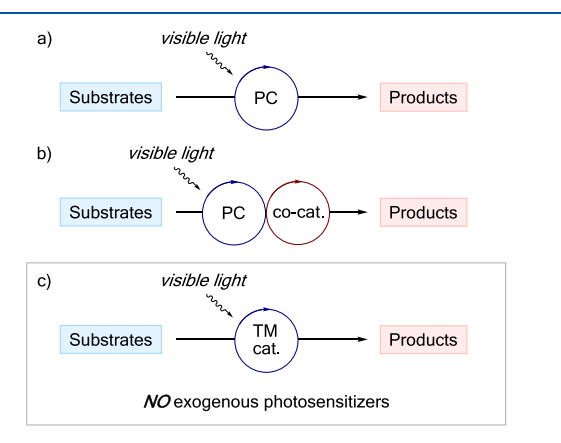


Figure 1. Visible light-induced transformations via (a) conventional photocatalysis, (b) dual photocatalysis, and (c) visible light-induced transition metal catalysis.

excited state is capable of activating an organic molecule via either single electron transfer (SET), energy transfer (EnT), or atom transfer (AT) processes (Figure 1a). Meanwhile, synergistic combination of organo-, transition metal, as well as the more recent enzymatic catalysis, in a dual catalytic manifold with photosensitizers, has been extensively developed, constituting the second mode of photocatalysis (Figure 1b). These two topics have been extensively reviewed, 1-12 and further discussion can be found in other Reviews of this issue.

Recently, another emerging area that distinguishes itself from the above paradigm, herein referred to as visible light-induced transition metal catalysis, is receiving a growing attention from the community (Figure 1c). In this case, a transition metal complex plays a double duty by harnessing photon energy as a photocatalyst and then by catalyzing bond breaking/forming events via traditional or new type of mechanism. As such, this duality of transition metal complex obviates the use of an exogeneous photosensitizer. Although this type of photocatalysis dates back to the 1980s, it has only made sporadic appearance in the literature in the following decades. Nevertheless, the recent resurgence of photochemistry has also promoted a rapid development in this area over the past few years, as evidenced by several review articles. ^{13–15}

Importantly, under this new paradigm, a catalyst-substrate interaction, an essential process in conventional ground state transition metal catalysis, is often synergistically combined with a photoinduced SET process. Notably, in this case, the SET process may proceed via an inner sphere mechanism, which is uncommon in conventional photoredox catalysis (Figure 1a). This catalyst-substrate interaction can be beneficial, as it essentially lowers the threshold for a redox process to occur, thereby enabling the activation of organic molecules with high redox potentials, which are sometimes beyond the reach for typical photoredox catalysts. In addition, transformations under this subcategory mostly operate via a single photochemical/ catalytic cycle, in contrast to a seemingly alike dual photocatalysis, where an exogenous photocatalyst, typically the sole light-absorbing species, 16 is required to harvest the energy of light (Figure 1b).

This Review aims at providing readers with an account of this emerging area from its early development to recent advances. The reaction scope is alluded for all methods, and mechanism is discussed for all new protocols. Since each transition metal exhibits its own excited-state reactivity character, we arranged this Review based on the identity of the metal. Given that newly developed synthetic methodology often focuses on the exploration of reaction scope, certain mechanistic aspects of newly developed protocols remain unclear. Accordingly, the reaction mechanisms presented herein only reflect the reasonable proposal by the authors, and thus may involve steps that are speculative.

We have limited our discussion to homogeneous catalysis under visible light irradiation (>390 nm). Thus, UV-induced transformations, which require the use of special glassware and methods employing transition metal complexes in stoichiometric quantities as well as heterogeneous transition metal or semiconductor photocatalysis, are not covered herein. In addition, there are reports where the role of light is limited to an off-cycle photoactivation of transition metal precatalyst via ligand dissociation, accelerated reduction of metal complex, or metal—metal bond homolysis. Since in these cases, the catalytic cycle does not require visible light irradiation, these types of

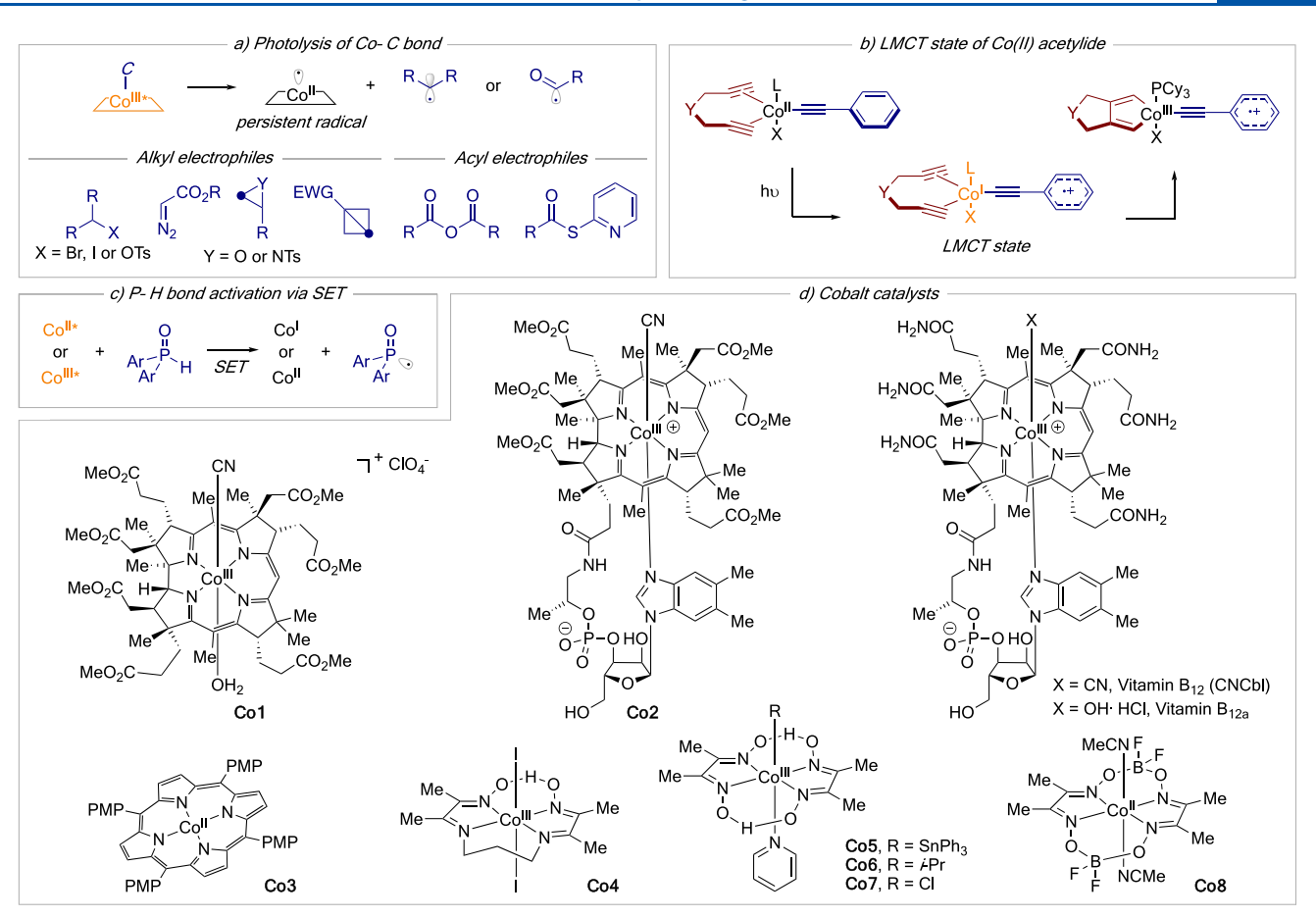


Figure 2. Outline of visible light-induced cobalt catalysis.

visible light-initiated chemistry are also beyond the scope of this Review, and, thus, are not discussed herein.

2. COBALT

2.1. General Overview

The ability of organocobalt(III) complexes to undergo facile homolytic Co-C (bond dissociation energy (BDE) $\approx 14-42$ kcal/mol) bond cleavage, via thermolysis, photolysis, or electrochemical reduction, to produce carbon-centered radicals and persistent Co(II) radicals is well-known. 17,18 These complexes are traditionally obtained from a Co(I) complex and an organic electrophile, and have been used as stoichiometric organic radical precursors. To achieve catalysis, the cobalt intermediate generated after photolysis needs to be reduced to its Co(I) form. This nucleophilic species can then react with the organic electrophile to regenerate organocobalt-(III) species. In 1983, Scheffold group disclosed a cobaltcatalyzed reductive acylation of Michael acceptors with acid anhydrides, thus representing the first example of cobalt photocatalysis.¹⁹ In this case, the catalyst turnover was enabled by electrochemical reduction. Several years later, Branchaud and co-worker revealed that elemental zinc could serve as a stoichiometric reductant for the Heck-type reaction of styrene with alkyl bromides.²⁰ However, the first practical, mild, and general catalytic method was developed by Carreira group in 2011. They utilized DIPEA as a base to formally reduce Co(III)H to an anionic Co(I) species via deprotonation, thereby obviating the use of electrolysis or metal reductants for similar reactions.²¹ In addition to acid anhydrides and alkyl

halides, other electrophiles have also been successfully employed to produce the corresponding organocobalt(III) intermediate (Figure 2a). Thus, in 2016, Gryko group introduced α -diazo esters, ²² followed by the report on epoxides and aziridines from the group of Morandi in the same year. ²³ Later, Gryko and co-workers employed 2-*S*-pyridyl thioesters as a source of acyl radical. ²⁴ The same group also showed that electron-deficient bicyclo[1.1.0]butanes (BCBs) could lead to the respective alkyl Co(III) intermediate upon strain-release ring opening. ²⁵ Very recently, Komeyama group reported the use of alkyl tosylates as an alternative to alkyl halides. ²⁶

The photochemistry of cobalt is not limited to the homolysis of Co–C bond. In 2018, Rovis group described an interesting example of photocycloaddition of diynes and terminal alkynes. This transformation involves the photoexcitation of a diyneligated Co(II) acetylide complex to its ligand-to-metal charge-transfer (LMCT) state, thereby formally generating a Co(I) center that is capable of oxidative cyclization with the diyne ligand (Figure 2b). Furthermore, the viability of photoinduced SET of cobalt complexes was also disclosed by Wu's group in 2019. In this case, excited Co(II) or Co(III) complex oxidizes *H*-phosphine oxide to its radical cation, which upon deprotonation produces phosphinoyl radical that subsequently adds to an alkene or alkyne (Figure 2c).

A vast majority of cobalt photocatalysis employs vitamin B_{12} derivatives and their close analogues such as Co(II) porphyrins and cobaloximes. The structures of these complexes are depicted in Figure 2d.

2.2. Photolysis of Co(III)-Carbon Bond

2.2.1. Giese-type Reactions. The first report on cobalt photocatalysis came from Scheffold group in 1983, in which they disclosed a vitamin B_{12a}-catalyzed reductive acylation of activated alkenes 1.1 with acid anhydrides 1.2 under photoelectrochemical conditions, with high-power incandescent bulbs as the light source. 29,19 Acrolein and its derivatives (1.4-1.7), as well as other electron-deficient alkenes (1.8-1.11), were all acylated in moderate to good yields. The proposed mechanism commences with the in situ formation of Co(I) species via electrochemical reduction of vitamin B_{12a}. This nucleophilic Co(I) complex then reacts with acid anhydride 1.2 to produce acyl Co(III) intermediate A, which upon photolysis releases acyl radical B along with the Co(II) species. The former then undergoes radical addition to alkene, followed by a direct hydrogen atom transfer (HAT) from solvent to afford product 1.3. In an alternative scenario, intermediate C undergoes a sequence of electron transfer/proton transfer (ET/PT). Meanwhile, the cobalt catalytic cycle is closed upon electrochemical reduction of Co(II) (Scheme 1).

Scheme 1. Reductive Radical Acylation of Michael Acceptors

Later in 1990, the same group achieved synthesis of prostaglandin $F_{2\alpha}$ precursor **2.3** under similar photoelectrocatalytic conditions (Scheme 2). ³⁰ In this case, Co(I) reacted with alkyl bromide **2.1** in an S_N2 fashion to form an alkyl Co(III) species, which underwent photolysis to generate alkyl radical. The latter then underwent 5-exo-trig cyclization followed by

Scheme 2. Photoelectrochemical Synthesis of Postaglandin $F_{2\alpha}$ Precursor

radical addition to ynone 2.2, eventually furnishing product 2.3 with two newly formed chiral centers.

Recently, Gryko and co-workers disclosed Co1-catalyzed generation of acyl radicals from 2-S-pyridyl thioesters 3.1, which efficiently added in a reductive manner to a wide range of Michael acceptors (3.4-3.10).²⁴ Notably, electron-deficient vinyl (hetero)arenes also reacted well (3.11-3.12). Various (hetero)aryl thioesters were also suitable substrates, with electron-rich ones being more efficient (3.13-3.18). Remarkably, product 3.13 containing a bromo functionality was obtained in high yield, despite the common dehalogenation side reaction in B₁₂ catalysis.³¹ In addition, alkyl thioesters proved to be viable substrates (3.19-3.21). Mechanistically, this reaction resembles that reported by Scheffold's group (Scheme 1), except that in this case, a stoichiometric amount of zinc was employed as the reductant. Accordingly, the catalytic cycle is initiated by the zinc-mediated reduction of cobalt catalyst to its active Co(I) form, followed by generation of an acyl Co(III) species A upon reaction with 3.1, as confirmed by MS. Photolysis of A, followed by trapping of the resultant acyl radical D with alkene 3.2, furnishes the reaction product. The deuterium-labeling studies revealed that the use of deuterated acetonitrile does not lead to a deuterated product. This disproves a possible direct HAT to intermediate E from the solvent. On the contrary, 70% deuterium incorporation was obtained when ND₄Cl was used, thus supporting the ET/PT pathway (Scheme 3).

In 2020, the same group reported synthesis of pyrrolidines 4.3 via dicarbofunctionalization of alkene-tethered alkyl bromides 4.1.³² As in the previous reports, different activated alkenes were appropriate radical acceptors (4.4–4.8). Significantly lower efficiency was, however, observed with enone (4.9) or alkene with α -substituent (4.10). Substrates bearing substituent at different positions delivered the respective products in moderate to good yields (4.11–4.15). Likewise, a fused bicyclic structure could be constructed using this approach (4.16). An alkynetethered substrate was also found to be reactive, leading to 4.17 as a mixture of stereoisomers (Scheme 4).

In the same year, Gryko's group also reported a bis-alkylation reaction of **5.1** featuring generation of radical from both pyridyl thioester and halide functionalities.³³ In general, alkyl bromides were more efficient than the chloro counterparts (**5.4**). Substrates of different chain lengths and substitutions were also reactive (**5.5–5.7**). Several examples of activated alkene were also demonstrated (**5.8–5.9**). The authors carried out kinetic studies to establish the reaction sequence. It was found that Co(III) complex **A** was formed at the outset of the reaction, indicating that generation of alkyl radical **B** preceded that of acyl radical. The concentration of **A** then decreased over time along with the formation of intermediate **C** and acyl Co(III) species **D**. The latter then produced acyl radical **E**, which eventually led to product **5.3** (Scheme **5**).

Several related reductive transformations using different electrophiles have been also reported. In 2020, Gryko and coworkers employed electron-deficient BCBs **6.1** as alkyl radical precursors. As in the aforementioned Giese-type reactions, alkylated products were obtained in moderate to good yields (**6.4–6.7**). Comparable amounts of *cis-* and *trans-*isomers were obtained in all cases. Besides alkylation, the authors also coupled cobalt and nickel catalysis to achieve arylation (**6.9**). Aryl iodides bearing a wide range of functionalities were effective coupling partners in this reaction (**6.10–6.14**) including a sterically demanding aryl iodide (**6.15**). This protocol was

Scheme 3. Generation of Acyl Radicals from 2-S-Pyridyl Thioesters

further applied to the synthesis of several drug derivatives such as 6.16 (Scheme 6).

Very recently, Komeyama's group utilized alkyl tosylates 7.1 in a Giese-type reaction. In addition to typical Michael acceptors (7.4-7.8), the authors also demonstrated an example of vinyl boronate (7.9). Various functionalized primary alkyl tosylates delivered the respective products in good yields (7.10-7.12). While reaction with secondary alkyl tosylate was less efficient using B_{12} , good yield of 7.13 was obtained by switching to Co_3 catalyst. This chemistry also works well in a more complex setting (7.14) (Scheme 7).

2.2.2. Heck-type Reactions. The examples described above demonstrate that the reductive Giese-type reaction typically occurs when electron-deficient olefins are used as radical acceptor under electrochemical conditions or in the presence of stoichiometric zinc or manganese reductant. In contrast, a Heck-type reaction dominates when aliphatic or styrene-type alkenes are employed, or when the reaction proceeds under less reducing conditions. As shown by Branchaud and co-worker in 1991, the reaction between alkyl bromides **8.1** and styrene under high-power incandescent bulb

Scheme 4. Dicarbofunctionalization of Alkene-Tethered Alkyl Bromides

Scheme 5. Sequential Alkyl- and Acyl Radical Generation

irradiation led to the Heck-type products 8.2. Primary and secondary α -bromoesters were reactive (8.3-8.4), while the tertiary counterpart was inactive (8.5). Several examples of unactivated primary alkyl bromides were also demonstrated (8.6-8.8) (Scheme 8). The proposed catalytic cycle commences with the *in situ* formation of Co(II) from CoCl₂, dimethylglyoxime (dmgH₂), and pyridine. It then abstracts bromine atom from substrate to produce radical **A** and a Co(III) complex. The former undergoes radical addition to styrene to

Scheme 6. BCBs as Alkyl Radical Precursor for (a) Giese-type Reaction and (b) Cross-Electrophile Coupling

Scheme 7. Alkyl Tosylates as Alkyl Radical Precursor

generate benzylic radical B, while the latter is reduced by zinc to close the left cycle. Intermediate B is not reduced by zinc but rather reacts with Co(II) to form Heck-type product 8.2 via the β -H loss along with formation of Co(III)H, which returns to its Co(II) form upon liberation of H_2 . Alternatively, the *in situ* formed Co(II) may first be reduced by zinc to produce nucleophilic Co(I) species, which then undergoes S_N2 -type oxidative addition with substrate to generate photoactive alkyl Co(III) complex (cf. Scheme 2).

Scheme 8. Heck-type Reaction of Alkyl Bromides and Styrene

Shortly after, Giese's group reported radical cyclization reactions of olefin-tethered alkyl bromides $9.1.^{34}$ With high catalyst loading and less reducing conditions, the authors were able to obtain Heck-type products 9.2, exclusively. Substrates with different degrees of substitution at the alkene moiety delivered the products in good to excellent yields (9.4-9.6). A high catalyst loading was required to facilitate the β -H loss. On the other hand, the same substrates provided Giese-type products 9.3 under more reducing conditions with low catalyst loading, as exemplified by 9.7. The authors also examined reactions using zinc as the reductant, but a less satisfactory product selectivity was observed in some cases (Scheme 9).

Scheme 9. Radical Cyclization of Alkyl Bromides

The catalyst turnover so far was achieved under reductive conditions, which, however, resulted in a limited substrate scope. In 2011, a fundamental advance was made by Carreira and co-workers, when they reported a cobaloxime-catalyzed intramolecular Heck reaction similar to that by Giese's group (Scheme 9), but under mild reaction conditions without resorting to electrochemistry or stoichiometric metal reductants. Diverse functionalized alkyl iodides were compatible with this transformation, delivering the cyclized products in good to excellent yields (10.3–10.5). Importantly, Heck-type product

was obtained in good yields, even with electron-deficient alkene (10.6). High functional group tolerance was further demonstrated by the successful synthesis of products 10.7–10.12. The synthetic utility of this method was highlighted by the expedient synthesis of **10.14**, an advanced intermediate toward (\pm) -samin. The mechanism of this reaction features a key catalyst turnover step, which involves the deprotonation of Co(III)H by DIPEA leading to regeneration of Co(I) species. Importantly, two cobalt catalysts enter the catalytic cycle by different means. Co5 is first photolyzed to a Co(II) intermediate and a triphenyltin radical.³⁵ The latter then abstracts iodine atom from substrate to produce alkyl radical, which then recombines with Co(II) to form intermediate A. For Co6, a photoinduced β -H loss leads to the formation of Co(III)H and propene. The former is then deprotonated by DIPEA before reacting with substrate (Scheme 10).

Scheme 10. Catalyst Turnover Enabled by Deprotonation of Co(III)H

The same group also applied this strategy to the total synthesis of (+)-daphmanidin E.³⁶ Under identical catalytic conditions, alkyl iodide 11.1 efficiently underwent Heck-type cyclization to afford key intermediate 11.2 in excellent yield (Scheme 11).

Later in 2013, the groups of Carreira and Martin further expanded this chemistry toward synthesis of allyl trifluoromethanes 12.3.³⁷ Various functionalized styrene derivatives (12.3–12.9), 1,1-disubstituted alkenes (12.10), and 2-vinylpyridine (12.11) were all viable substrates for this trans-

Scheme 11. Heck-type Cyclization en Route to (+)-Daphmanidin E

formation (Scheme 12). It is noteworthy that a flow photoreactor was also devised, which allowed for a substantial shortening of the reaction time (30 min vs 42 h for a 1 mmol reaction).

Scheme 12. Heck-type Reaction of Styrene Derivatives with 2,2,2-Trifluoroethyl Iodide

Carreira & Martin, 2013

12.5, R = OMe, 76%

12.7, R = SMe, 59% **12.8**, R = CH₂OH, 53%

12.6, R = NHCbz, 65%

R Ar 12.1 CF₃ Co5 (20 mol%) DIPEA MeCN, blue LED, rt 12.2 Br 12.3, R = CHO, 73% 12.9, 56%

12.10, 64%

12.11, 56%

In 2016, Gryko and co-workers generated alkyl radicals from α -diazo esters 13.2, which underwent intermolecular Heck-type reaction.^{22,38} Since a mixture of Heck- (oxidative) and Giese-(reductive) type products was obtained, the authors performed a subsequent hydrogenation to obtain reduced products 13.3. α -Diazo esters with different alkyl substituents underwent smooth transformation with 1,1-diphenylethylene in good to excellent yields (13.4-13.6). Notably, reactions with styrene derivatives proved to be challenging (13.7-13.9). Interestingly, aliphatic olefins, in contrast, were found to be efficient reaction partners (13.10). Other electron-rich systems, such as enamides (13.11), vinyl sulfides (13.12), and enol ethers (13.13), were also competent radical acceptors. Of note, 13.13 was formed selectively in this transformation. It is also worth mentioning that in all cases, the well-established in cobalt catalysis cyclopropanation process^{39–41} was not observed, thus highlighting the crucial role of visible light irradiation in this transformation. Deuterium-labeling experiment suggested that the additional proton at the α position of ester in the product comes from NH₄Cl. On the basis of this result, the authors proposed that the *in situ* formed Co(I) species reacts with α diazo ester 13.2 in the presence of NH₄Cl to produce the key alkyl Co(III) intermediate A, which then undergoes aforementioned homolytic cleavage to generate alkyl radical B (Scheme 13).

In the same year, Morandi's group utilized epoxides and aziridines 14.1 as radical precursors for regioselective coupling

Scheme 13. α -Diazo Esters as Alkyl Radical Precursors for Heck-type Reaction

with alkenes, leading to cyclic and acyclic homoallylic alcohols and amines $14.2.^{23}$ A range of methylene cyclopentanols were obtained in good yields (14.3-14.5). Notably, complete chirality transfer was observed when enantioenriched epoxide was used ((R)-14.3). A six-membered ring could also be constructed using this method (14.6). Likewise, reactions with aziridines led to methylene cyclopentylamines such as 14.7. Furthermore, the authors showed that intermolecular coupling with 1,1-diphenylethylene was also plausible, albeit with diminished efficiency (14.8-14.9) (Scheme 14).

Scheme 14. Regioselective Coupling of Epoxides and Aziridines with Alkenes

2.3. Transformations Involving LMCT of Co(II) Acetylides

In 2018, Rovis' group disclosed a cycloaddition reaction between diynes **15.1** and terminal alkynes **15.2** leading to fused arenes **15.3**.²⁷ Diynes with the tether possessing a quaternary carbon reacted smoothly with phenylacetylene to deliver the respective arenes in good to excellent yields (**15.4**–**15.6**). Similarly, diynes bearing heteroatoms were suitable substrates (**15.7**–**15.8**). This reaction was sensitive to electronic nature of the alkyne partner. Thus, electron-withdrawing groups

promoted the reaction rate as well as the yield, while electrondonating groups were detrimental (15.9–15.12). Aliphatic alkynes were less reactive under standard conditions (15.13) (Scheme 15). However, switching the light source to high-

Scheme 15. Diyne—Alkyne Cycloaddition via Photoinduced LMCT of Co(II) Acetylides

energy UV significantly improved the yield. The proposed catalytic cycle begins with the in situ formation of Co(II) acetylide A. The coordination of diyne is crucial, as it leads to a dramatic bathochromic shift of about 100 nm, rendering A photoactive at the employed wavelength. Photoexcited A* features LMCT character. The formally reduced cobalt center is therefore capable of oxidative cyclization with ligated diyne affording Co(III) intermediate **B**. The aryl radical cation in **B** is then reduced by DIPEA to produce metallacycle C, which upon migratory insertion with alkyne followed by reductive elimination, furnishes arene 15.3 and Co(I) acetylide D. The latter is then oxidized by DIPEA radical cation or A* to complete the catalytic cycle. The involvement of LMCT state was supported by fluorimetric analysis of reaction mixtures with different alkynes, which revealed a characteristic inverse correlation between emission energy and alkyne electronrichness.⁴² It is noteworthy that cobalt-catalyzed/-mediated [2 + 2 + 2] cycloaddition has long been recognized as a powerful method for construction of benzene or pyridine derivatives; and visible light irradiation has been incorporated occasionally, as

Scheme 16. Photoinduced P-H Bond Activation of H-Phosphine Oxides

exemplified by the early contributions from the groups of Vollhardt 43,44 and Oehme. 45,46 In those cases, however, the role of visible light irradiation is likely to induce ligand dissociation, thereby accessing the active Co(I) catalyst with free coordination sites.

2.4. Fragmentation of P-H Bond of H-Phosphine Oxides

In 2019, Wu's group employed cobaloxime catalysts for photoinduced P-H bond activation of H-phosphine oxides 16.1.28 With Co(II) catalyst Co8, H-phosphine oxides were coupled with alkenes 16.2 to produce alkenylphosphine oxides **16.3**, along with the reduction side products **16.4**. Electronically diverse 1,1-diarylalkenes delivered products in good to excellent yields (16.5-16.8). While reactions with styrene derivatives were less efficient, side product formation was substantially suppressed (16.9-16.12). Besides, the trans-isomer was exclusively obtained in all cases. Other diarylphosphine oxides were also competent substrates (16.13-16.14); however, diethylphosphite was not reactive (16.15). This transformation begins with the photoexcitation of Co8 catalyst, which in its excited state is highly oxidizing and thus capable of engaging Hphosphine oxide 16.1 in SET, thus producing phosphinoyl radical A and a Co(I) species. Potentially, the formation of A and Co(III)H species may occur via a direct HAT between 16.1 and Co(II)*. Intermediate A then reacts with alkene 16.2 to produce benzylic radical B, which is then captured by another Co(II) complex to form benzyl Co(III) intermediate C. Finally, β -H elimination of C affords the desired product 16.3. The Co(III)H

species, formed along with the product, selectively reduces excess alkene to **16.16** via HAT. The subsequently formed Co(III) complex may undergo radical-polar crossover (RPC) with radical intermediate **B** to return to its Co(II) form, meanwhile converting **B** to a carbocation, and eventually product **16.3** upon deprotonation. As Co(III)H does not reduce product, side product **16.4** may stem from protiodemetalation of Co(III) complex C. The intermediacy of phosphinoyl radical was confirmed by EPR studies as well as radical trapping experiment with 2-methyl-2-nitrosopropane (Scheme **16**).

In the same report, the authors also explored the reactivity of H-phosphine oxides toward alkynes 16.16. With a different catalytic system, terminal alkynes also provided alkenylphosphine oxides in moderate to good yields, albeit with diminished stereoselectivities in some cases (16.18-16.22). The photoexcited Co(III) cobaloxime (Co7) is an even more potent oxidant. Thus, the catalytic cycle commences with an SET event leading to phosphinoyl radical A, which undergoes addition to terminal alkyne substrate to form vinyl radical D. A subsequent recombination of Co(II) and D generates vinyl Co(III) species E, which upon protiodemetalation furnishes product and regenerates Co(III) catalyst. Reactions with internal alkynes at elevated temperature, on the other hand, led to benzophosphole scaffolds 16.23. Both aryl- and alkylsubstituted alkynes were reactive in this transformation (16.24-16.25). Notably, product 16.26 was obtained as a single regioisomer. Expectedly, H-phosphine oxides bearing para-

substituted aryl groups provided a 1:1 mixture of regioisomers (16.27). Similarly to the previous case, phosphinoyl radical A adds to internal alkyne to produce the respective vinyl radical, which in this case undergoes cyclization to afford cyclic intermediate F. Rearomatization of F upon HAT to Co(II) furnishes benzophosphole 16.23.

Later, the same group reported a similar phosphorylation of enamines and enamides $17.1.^{47}$ A wide range of functionalities at the *N*-aryl ring of β -cyano enamines are well tolerated (17.4–17.7). Unprotected enamine was also a competent substrate (17.8). Enamines, possessing an ester at the β -position reacted well, but provided the respective products with moderate degrees of diastereoselectivity (17.9–17.11). Enamides were also found to be reactive, providing the desired products in moderate to good yields (17.12–17.14). In addition, examining this phosphorylation method in a more complex setting proven efficient, as well (17.15) (Scheme 17).

Scheme 17. Phosphorylation of Enamines and Enamides

3. COPPER

3.1. General Overview

Despite enormous popularity of copper catalysis in organic chemistry, the reactivity of copper catalysts under visible light irradiation 48,49 remained underexplored until 2012, when Fu and Peters groups first disclosed a photoinduced Ullmann C-N

coupling reaction via an unprecedented radical pathway. 50 In the same year, Hwang's group showed that Sonogashira coupling, 51,52 which typically requires a copper/palladium dual catalytic system, under visible light irradiation could be achieved using a sole copper catalyst. 53 In both cases, a Cu(I)nucleophile complex (amide and acetylide, respectively) is involved, which upon photoexcitation serves as a single electron reductant and engages the aryl halide coupling partner in SET events. In 2015, the groups of Dolbier⁵⁴ and Reiser⁵⁵ independently reported excited-state reactivity of cationic Cu(I) complexes, such as Cu(dap)2Cl, toward fluoroalkyl sulfonyl chlorides. This type of Cu(I) catalyst is commonly referred as a standalone catalyst, as the formation of a Cu(I)nucleophile complex is not a prerequisite for the photoinduced transformation. These early works laid the foundation for Cu(I) photocatalysis, where a photoexcited Cu(I) species transfers a single electron to organic electrophiles in an inner sphere fashion, thereby engaging them in radical transformations (Figure 3a).

The photolysis of CuCl₂ salt to produce CuCl and chlorine radical upon irradiation has been recognized for almost 60 years, as described by Kochi in his pioneering work in 1962.56 However, the stage for catalysis by visible light-excited Cu(II) complexes⁵⁷ was set only in 2018 by Rehbein, Reiser, and coworkers.⁵⁸ It was shown that the mechanism of photocatalysis by Cu(II) complexes is different to that by Cu(I) counterparts. Thus, the *in situ* formed Cu(II) azide complex undergoes photoinduced homolytic ligand dissociation, commonly referred as visible light-induced homolysis (VLIH), to release an azide radical. Likewise, alkyl⁵⁹ and chlorine radicals^{60,61} can also be accessed from the respective Cu(II) complexes. This represents the general mechanistic scenario for Cu(II) photocatalysis (Figure 3b). Very recently, the detailed spectroscopic studies carried out by Reiser and Castellano groups have provided direct evidence for a homolytic Cu-Cl bond cleavage.62

There is also an example of EnT in copper catalysis. Thus, Liu's group demonstrated the ability of Cu(I) complexes to activate substrate via EnT, constituting another reactivity mode of excited-state Cu(I) complexes (Figure 3c).⁶³ In this case, a photoexcited $Cu(NCS)_2^-$ complex undergoes EnT to vinyl azide substrate, which upon liberation of N_2 forms a reactive 2H-azirine intermediate.

It is worth mentioning that the photochemistry of copper is an immense field of research. Thus, to keep the focus on catalytic properties of visible light-excited copper complexes, the reactions enabled by UV irradiation, $^{64-72}$ as well as visible

a) SET from Cu(l) complexes

$$L_{n}Cu^{l^{+}} + X - R \longrightarrow L_{n}Cu^{l^{+}} - X - R$$

$$Inner sphere electron transfer$$

$$Cu(l) complexes$$

$$Cu(l) complexes$$

$$Cu(l) - nucleophile complexes$$

$$Cu(l) - nucleophile complexes$$

$$Stand-alone copper(l) catalysts$$

$$D) Homolytic ligand dissociation of Cu(ll) complexes
$$L_{n}Cu^{l}L_{n} \longrightarrow X \longrightarrow L_{n}Cu^{l}L_{n}^{*} \longrightarrow X \longrightarrow L_{n}Cu^{l}Y$$

$$L_{n}Cu^{l}L_{n} \longrightarrow X \longrightarrow L_{n}Cu^{l}L_{n}^{*} \longrightarrow X \longrightarrow L_{n}Cu^{l}Y$$

$$L_{n}Cu^{l}L_{n} \longrightarrow X \longrightarrow L_{n}Cu^{l}L_{n}^{*} \longrightarrow X \longrightarrow L_{n}Cu^{l}Y$$

$$L_{n}Cu^{l}L_{n} \longrightarrow X \longrightarrow L_{n}Cu^{l}L_{n}^{*} \longrightarrow X \longrightarrow L_{n}Cu^{l}Y$$

$$L_{n}Cu^{l}L_{n} \longrightarrow X \longrightarrow L_{n}Cu^{l}L_{n}^{*} \longrightarrow X \longrightarrow L_{n}Cu^{l}Y$$

$$L_{n}Cu^{l}L_{n} \longrightarrow X \longrightarrow L_{n}Cu^{l}L_{n}^{*} \longrightarrow X \longrightarrow L_{n}Cu^{l}Y$$

$$L_{n}Cu^{l}L_{n} \longrightarrow X \longrightarrow L_{n}Cu^{l}L_{n}^{*} \longrightarrow X \longrightarrow L_{n}Cu^{l}Y$$

$$L_{n}Cu^{l}L_{n} \longrightarrow X \longrightarrow L_{n}Cu^{l}L_{n}^{*} \longrightarrow L_{n}Cu^{l}Y$$

$$L_{n}Cu^{l}L_{n} \longrightarrow X \longrightarrow L_{n}Cu^{l}L_{n}^{*} \longrightarrow L_{n}Cu^{l}Y$$

$$L_{n}Cu^{l}L_{n} \longrightarrow L_{n}Cu^{l}L_{n}^{*} \longrightarrow L_{n}Cu^{l}L_{n}^{*} \longrightarrow L_{n}Cu^{l}Y$$

$$L_{n}L_{n}Cu^{l}L_{n} \longrightarrow L_{n}Cu^{l}L_{n}^{*} \longrightarrow L_{n}Cu^{l}L_{n}^{$$$$

Figure 3. Outline of visible light-induced copper catalysis.

light-induced transformations utilizing copper either as a photoredox catalyst $^{73-80,48,81-84}$ or in stoichiometric fashion, are not discussed herein.

3.2. Photoinduced SET of Cu(I)-Nucleophile Complexes

3.2.1. Heteroatom-Based Nucleophiles. Copper photocatalysis involving heteroatom-based nucleophiles enables carbon—heteroatom bond formation under mild conditions. Although transformations vary, they share a general mechanism depicted in Scheme 18. The catalytic cycle begins with the *in situ*

Scheme 18. General Mechanism of Cu(I) Photocatalysis Involving Heteroatom-Based Nucleophiles

formation of Cu(I)-nucleophile complex A, which upon photoexcitation (A^*) engages electrophilic substrate 18.1 in SET process. The resultant intermediate may possess radical character as in B, or exist as a conventional Cu(III) oxidative addition complex C. A subsequent carbon-heteroatom bond formation furnishes product 18.2 and releases Cu(I) species D. The photoactive complex A is then regenerated upon ligand exchange with another molecule of nucleophile.

3.2.1.1. C-N Cross-Coupling. In 2012, Fu and Peters groups first explored the photochemistry of Cu(I) amide complexes.⁵ They found that visible light irradiation promoted the reaction between iodobenzene and Cu(I) carbazolide complex 19.2 at room temperature, or even −40 °C, to produce N-phenylcarbazole in good yield. The bromo- and chloro counterparts were less reactive, as would be expected on the basis of their reduction potentials. Nonetheless, good yields were obtained under mercury lamp irradiation. Notably, the authors achieved the catalytic version of this reaction with iodobenzene and lithium carbazolide 19.3. As alluded to in Scheme 18, one plausible mechanism involves SET from photoexcited complex 19.2 to halobenzene 19.1. Alternatively, 19.1 may undergo halogen atom transfer (XAT) to photoexcited 19.2, thereby directly leading to phenyl radical and the respective Cu(II) complex. The radical nature of this transformation was supported by mechanistic studies. First, low-temperature EPR data confirmed the formation of a copper-containing radical species with partial Cu(II) character. Additionally, deuterated substrate 19.4 furnished a 1:1 diastereomeric mixture of cyclized product 19.5, thus supporting the intermediacy of aryl radical A. To distinguish between SET and concerted oxidative addition pathways, the authors performed competition experiment using 4-chlorobenzonitrile and 1-bromonaphthalene. The former would be more reactive if SET is operative, while coupling with the latter would be favored if oxidative addition is at play. Indeed, consistent with the SET pathway, product 19.6 over 19.7 was preferentially formed (Scheme 19).

Later in 2016, the same groups accomplished an asymmetric C-N cross-coupling of α -chloroamides **20.1** with carbazoles or

Scheme 19. First Example of Photoinduced Radical Ullmann C-N Coupling

indoles 20.2 by incorporating chiral phosphine ligand (S)-20.4. Notably, for the first time, copper played both roles: participating in a photoinduced SET, and inducing chiral induction. A wide range of α -chloroamides reacted with carbazole derivatives to provide coupling products in high yields and enantioselectivities (20.5–20.9). Introduction of an electron-donating or electron-withdrawing group at the arene of substrate did not affect the efficiency of the coupling process. In addition, indoles were also found to be compatible nucleophiles (20.10–20.11) (Scheme 20).

Seemingly trivial selective monoalkylation of primary aliphatic amines with alkyl halides has been a longstanding challenge. The N-nucleophiles employed so far in visible light-induced copper catalysis were restricted to π -systems such as carbazoles and indoles. The π -conjugation in the resultant Cu(I) amide complex is necessary for its photoexcitation in the visible light region, or its suitable excited-state reactivity as a reductant. Nevertheless, in 2017, Peters, Fu, and co-workers accomplished photocatalytic, selective alkylation of aliphatic amines 21.2.87 To circumvent the limitation of N-nucleophiles, they strategically employed rac-BINOL as a ligand. The corresponding Cu(I) binaphtholate complex is likely the photoactive species responsible for alkyl radical generation. 68 Notably, primary neopentyl iodide, a notorious substrate in S_N2 reactions, underwent efficient amination to afford 21.4 in good yield. Secondary alkyl iodides were also reactive, however, the coupling efficiency was dependent on the steric environment (21.5-21.7). Besides, this protocol was also applicable in a more complex setting (21.8). Furthermore, a broad range of

Scheme 20. Asymmetric C-N Cross-Coupling of Alkyl Chlorides with Carbazoles and Indoles

primary aliphatic amines was suitable substrates for this reaction (21.9–21.13) (Scheme 21).

Scheme 21. Selective Monoalkylation of Aliphatic Primary Amines

3.2.1.2. Carbo- and Hydrofunctionalization of Alkenes. In addition to a direct coupling with nucleophile as mentioned above, the alkyl radical, prior to the coupling event, can be intercepted by alkene. Hence, in 2018, Fu and Peters disclosed a three component coupling of alkenes 22.1, alkyl halides 22.2, and nucleophiles 22.3. With NMe₄SCF₃ as nucleophile, a wide variety of alkenes, ranging from unactivated alkenes to styrenes and Michael acceptors, reacted well to deliver the respective carbofunctionalization products in good yields (22.5–22.7). Different electron-deficient alkyl bromides and iodides were found to be suitable substrates for this transformation (22.8-22.9). Notably, this protocol was applicable to other ammonium salts, furnishing carboazidation (22.10), -cyanation (22.11), and -bromination (22.12) products in moderate to good yields. As discussed previously, the catalytic cycle commences with photoinduced SET from Cu(I)—nucleophile complex A to alkyl

halide 22.2. In this case, the resultant alkyl radical B adds to alkene 22.1 to form another alkyl radical D, which subsequently reacts with Cu(II) complex C to afford product 22.3. As mentioned earlier, the identity of nucleophile plays an important role in the photocatalytic behavior of the respective copper complex. To validate the intermediacy of A as a photoactive species, the authors synthesized dimeric Cu(I) complex $[(BINAP)Cu(SCF_3)]_2$ (22.13), which exhibits a broad absorption band in the UV region tailing into the visible light region up to 520 nm. Complex 22.13 catalyzed the benchmark reaction with virtually the same efficiency, thus supporting the involvement of A in this transformation. Further support was obtained from stoichiometric reaction in the absence of NMe₄SCF₃, which provided moderate yield of product 22.14 (Scheme 22).

In 2019, Zhang group reported analogous carboamination protocol using a diverse array of amine nucleophiles (23.3). Various styrene derivatives underwent smooth transformation in good yields (23.5–23.7). An example of unactivated alkene was also demonstrated, albeit with diminished efficiency (23.8). Both α -functionalized and simple alkyl halides delivered the

Scheme 22. Three Component Coupling of Olefins, Alkyl Halides, and Nucleophiles

Conditions

MeCN, blue LED, rt

CF₃ 22.13

BrCF2CO2Et

22.10

NMe₄SCF₃

Bn²

Bn

Conditions

22.13 (5 mol%)

22.13 (0.75 equiv.)

no NMe₄SCF₃

CF₂CO₂Et

22.14

81%

48%

respective products in moderate to good yields (23.9–23.11). Besides, other carbazole derivatives, indoles, as well as indazoles, were competent nucleophiles (23.12–23.14). For other amines, additional BINOL ligand was required to induce the reaction (cf. Scheme 21). A wide range of amines, such as indolines (23.15), anilines (23.16), sulfonamides (23.17), and aliphatic amines (23.18), were found to be compatible with these reaction conditions. Furthermore, structurally complex amines were also applicable (23.19–23.20) (Scheme 23).

Scheme 23. Three Component Carboamination of Alkenes

The same group also reported intermolecular Markovnikov hydroamination of alkenes 24.1 under similar catalytic system. 90 Electronically diverse styrene derivatives reacted smoothly with carbazole (24.4–24.7). Di- and trisubstituted alkenes were also compatible, furnishing the respective products in good yields (24.8-24.10). As in the previous case, employment of rac-BINOL allowed for a broader scope of amine nucleophiles (24.11–24.15). Furthermore, 1,3-dienes were also competent alkene substrates, as exemplified by allylic amine 24.16 formed via 1,4-hydroamination. Interestingly, performing the reaction in CD₃CN led to product d-24.17 with almost complete deuterium incorporation at the β -carbon, suggesting a plausible intermolecular HAT from solvent. The observed Markovnikov selectivity invoked the potential intermediacy of carbocation.⁹¹ However, the reaction of the benchmark substrate in the presence of additional nucleophiles did not yield the corresponding hydrofunctionalization product 24.18, except for para-methylbenzenethiol.⁶⁵ These results disputed involvement of a carbocation intermediate, thus providing further support for the radical mechanism (Scheme 24).

Scheme 24. Intermolecular Markovnikov Hydroamination of Alkenes

3.2.1.3. Aminocarbonylation Reactions. In the same year, Chen's group employed redox-active oxime esters (RAOEs) 25.1 as an alkyl radical precursor for aminocarbonylation reaction under high CO pressure.⁹² Differently substituted oxime esters underwent cascade fragmentation/aminocarbonylation to deliver amides 25.5-25.10 in moderate to good yields. Remarkably, a wide range of aniline derivatives (25.11-25.15), primary alkyl amines (25.16-25.17), as well as α -amino acid derivatives (25.18), were found to be suitable nucleophiles under these reaction conditions (Scheme 25). Of note, this reaction could also be performed under thermal conditions (60 °C), as exemplified by products 25.14-25.16 (yields in parentheses). The efficiency was, however, lower than under the visible light-induced protocol. The proposed catalytic cycle begins with an SET event from photoexcited Cu(I) amide complex A to RAOE 25.1 (path a) generating Cu(II) complex B and an iminyl radical C. The latter undergoes β -scission to form cyanoalkyl radical **D**, which then recombines with complex **B** to afford alkyl Cu(III) species E. A subsequent coordination with CO followed by migratory insertion produces acyl Cu(III) intermediate F or G, which upon reductive elimination furnishes product 25.3. Alternatively, the reaction can also be initiated by thermally induced SET from A to substrate (path b).

3.2.2. Alkynes as Nucleophiles under Redox-Neutral Conditions. 3.2.2.1. Direct Sonogashira Coupling. Traditionally, Sonogashira reactions in the absence of palladium cocatalyst proceed under harsh reaction conditions and require large excess of ligands. 93,94 This can be attributed to the sluggish oxidative addition of aryl halides to the copper catalyst. In 2012, Hwang and co-workers showed that visible light

Scheme 25. Aminocarbonylation of Cycloketone RAOEs

irradiation could address this problem.⁵³ In this case, simple CuCl salt at room temperature effectively catalyzes the reaction without additional ligands. Control experiment revealed that catalytic amount of PdCl₂ suppressed the reaction, thus confirming copper being the sole catalyst in this visible lightinduced transformation. The scope of this protocol was found to be remarkably broad. Aryl iodides with diverse electronic and steric properties reacted efficiently with phenylacetylene (26.4– 26.8). Less reactive bromo functionality (26.9), as well as heterocycles (26.10), was a competent substrate. It is noteworthy that n-BuI was also amenable to this transformation (26.11). The substituent at alkyne could also be broadly varied. Thus, aliphatic alkynes bearing a pendant functional group (26.12-26.13) and propargyl alcohols (26.14) delivered the respective products in excellent yields. Trimethylsilyl acetylene, however, produced the coupling product in low yield (26.15). Similarly, high functional group tolerance was observed in the case of aryl bromides (26.16–26.20). The proposed mechanism involves the in situ formation of Cu(I) acetylide A in the

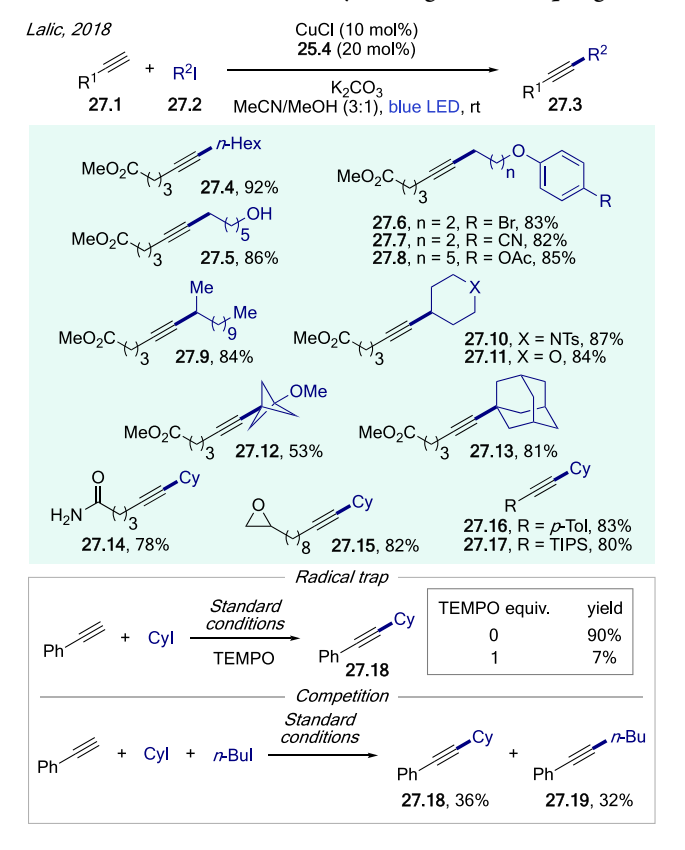
presence of base (B), which may exist in the bimetallic form B. Photoexcitation of complex B leads to enhanced polarization between Cu(I) and acetylide moiety, which then engages substrate 26.1 in concerted C–C bond formation (path a), thereby directly furnishing cross-coupling product 26.3 and regenerating Cu(I) catalyst. Alternatively, as suggested by von Wangelin and co-worker, the triplet excited state of B⁹⁷ can transfer a single electron to substrate, producing organic radical D and Cu(II) species E (path b). Recombination of the two, followed by reductive elimination, then affords product and completes the catalytic cycle (Scheme 26).

Scheme 26. Photoinduced Sonogashira Coupling

In 2018, Lalic's group developed a general photocatalytic alkyl Sonogashira coupling. It is worth mentioning that terpyridine ligand 25.4 was the key to success of this reaction, as it minimized undesirable di- and polymerization of alkynes. Unactivated primary and secondary alkyl iodides delivered the cross-coupling products in good to excellent yields (27.4–27.11). However, reactions with tertiary alkyl iodides proved to be more challenging due to rapid solvolysis, and only bridgehead iodides were efficient in this reaction (27.12–27.13). In addition, functionalized alkyl-, aryl-, and silyl-substituted alkynes were also smoothly alkylated in good yields (27.14–27.17). Addition of (2,2,6,6-tetramethylpiperidin-1-yl)oxyl (TEMPO) shut down the reaction between phenylacetylene and CyI, and

the Cy-TEMPO adduct was isolated and unambiguously confirmed. In line with the small difference in reduction potentials between primary and secondary alkyl iodides, ⁹⁹ the competition experiment using CyI and *n*-BuI provided comparable amounts of products **27.18** and **27.19** (Scheme 27).

Scheme 27. Photoinduced Alkyl Sonogashira Coupling



In continuation of their previous report on asymmetric alkyl Sonogashira coupling using secondary alkyl halides, 100 Liu and co-workers recently reported the use of redox-active esters (RAEs) 28.1 as secondary alkyl radical precursors for analogous transformation. 101 Thus, RAEs with different alkyl substituents afforded the coupling products in excellent enantioselectivities (28.5-28.7). The aryl fragment could accommodate a broad range of functionalities, some of which were not compatible with the previous method (28.8-28.11). RAEs derived from bioactive molecules, as well as heteroarenes, were also well tolerated (28.12-28.13). However, replacing the aryl group with other substituents, such as vinyl, led to decrease in enantioselectivity (28.14). Moreover, the use of simple aliphatic RAEs led to racemic products (28.15). On the other hand, various acetylene derivatives delivered the products in good yields with excellent enantiocontrol (28.16-28.22). Mechanistic studies, such as radical clock experiment using substrate 28.23, supported radical pathway. Besides, stoichiometric reactions of RAE 28.26 with Cu(I) complex 28.27 revealed that ligand 28.4 was essential not only for inducing chirality but also for promoting the reaction (Scheme 28).

3.2.2.2. Cascade Sonogashira Coupling. In addition to aminocarbonylation (Scheme 25), Chen's group also utilized RAOEs for carboalkynylation of vinyl (hetero)arenes 29.1. A diverse array of styrene derivatives were converted to the corresponding products, demonstrating a high functional group

Scheme 28. Asymmetric Alkyl Sonogashira Coupling

tolerance of this protocol (29.5–29.9). Heteroarenes (29.10), as well as natural product derivatives (29.11–29.12), all reacted well. Differently substituted RAOEs were also viable substrates, furnishing products in moderate to good yields (29.13–29.16). Besides, the aryl group on alkyne could be replaced by heteroaryl- (29.17) or alkyl- (29.18) substituents. Reaction in a more complex setting was also successful (29.19) (Scheme 29).

In 2020, Zhang, Zhang, and co-workers reported the asymmetric variant of analogous transformation using alkyl or aryl iodides 30.2. ¹⁰³ Of note, large excess of iodides (6 equiv) was necessary in this case. Excellent enantiocontrol was observed in most cases with respect to vinyl (hetero)arenes (30.5–30.9). Likewise, other silyl- and alkyl-substituted alkynes were competent coupling partners (30.10–30.12). However, (hetero)arylacetylenes delivered products with diminished enantioselectivities (30.13–30.14). Different fluoroalkyl-(30.15–30.17) and simple aliphatic (30.18) iodides underwent smooth transformation with excellent enantioselectivities. Notably, aryl iodides were also viable substrates, furnishing

Scheme 29. Carboalkynylation of Alkenes with RAOEs

highly enantioenriched products in moderate to good yields (30.19-30.21) (Scheme 30).

Very recently, the groups of Cao and Zhang employed silyl-tethered alcohols $^{104-106}$ for remote $C(sp^3)$ –H alkynylation. 107 Secondary and tertiary aliphatic alcohols underwent efficient γ -C-H alkynylation with various (hetero)arylacetylenes (31.4-**31.11**). However, alkyl-substituted alkynes did not provide any desired products. Reaction with primary alcohol was also feasible, albeit with lower efficiency (31.12). As established by Gevorgyan's group (Schemes 73 and 80), for silylmethyl tether, γ -functionalization via 1,6-HAT is preferable over β - and δ functionalization, which proceeds via 1,5- and 1,7-HAT, respectively. Thus, products 31.9 and 31.10 were obtained in excellent regioselectivity. Nonetheless, in the absence of weaker γ -C-H bonds, β - and δ -alkynylation products could be accessed (31.13-31.14). In the same report, the authors showed that carbazoles could be employed as nucleophiles delivering the respective remote γ -amination products in good yields (31.16– 31.18) (Scheme 31).

3.2.3. Alkynes as Nucleophiles under Oxidative Conditions. *3.2.3.1.* Oxidative Annulation. In 2013, Hwang's group reported an oxidative copper-catalyzed three component heteroannulation reaction. In this annulation reaction, orthophenylenediamines **32.1** reacted with arylacetylenes **32.2** under aerobic condition to produce quinoxalines **32.3**. Symmetrical substrates delivered the products in almost quantitative yields (**32.4–32.6**). Unsymmetrical substrates reacted equally well,

Scheme 30. Asymmetric Carboalkynylation of Alkenes with Alkyl or Aryl Iodides

Scheme 31. Remote C(sp³)-H (a) Alkynylation and (b) Amination of Aliphatic Alcohols

albeit producing regioisomeric products (32.7–32.8). Besides, various functionalities at alkyne, including iodo substituent, were perfectly tolerated (32.9–32.13) (Scheme 32). This transformation differs from the previous examples because molecular oxygen, rather than an organic electrophile, serves as

Scheme 32. Oxidative Coupling of *ortho*-Phenylenediamines and Arylacetylenes

$$\begin{array}{c} \text{Hwang, 2013} \\ \text{R} \stackrel{\text{II}}{\text{II}} \\ \text{NH}_2 \\ \text{32.1} \\ \end{array} + \underbrace{ \begin{array}{c} \text{Ar + O}_2 \\ \text{32.2} \\ \text{1 atm} \\ \end{array} }_{\text{1 atm}} \underbrace{ \begin{array}{c} \text{CuCl (3-5 mol\%)} \\ \text{K}_2\text{CO}_3 \\ \text{MeCN/MeOH (1:1)} \\ \text{blue LED, rt} \\ \end{array} }_{\text{32.3}} \\ \text{R} \stackrel{\text{II}}{\text{II}} \\ \text{NOH} \\ \text{32.4, R = H, 96\%} \\ \text{32.5, R = Me, 99\%} \\ \text{32.6, 93\%} \\ \text{32.7, R = Cl, 94\%} \\ \text{32.8, R = COPh, 74\%} \\ \text{32.11, R = 4-Ac, 96\%} \\ \text{32.11, R = 4-Ac, 96\%} \\ \text{32.12, R = 2-CN, 95\%} \\ \end{array}$$

the single electron acceptor from the photoexcited Cu(I) acetylide.

Since then, a number of oxidative Cu(I)-catalyzed transformations have been reported. A general mechanistic path is outlined in Scheme 33. First, the *in situ* formed Cu(I) acetylide A

Scheme 33. General Reactivity of Cu(I) Acetylide Complexes under Oxidizing Conditions

oxidant oxidant
$$\stackrel{-}{\longrightarrow}$$
 $R \xrightarrow{-} Cu^{II} \xrightarrow{+} \longrightarrow$ products

is oxidized via a photoinduced SET process with an oxidant, such as molecular oxygen or quinone derivative, to produce Cu(II) acetylide B and the reduced oxidant. The former is then engaged in various transformations. Importantly, the oxidative conditions allow for the coupling of another nucleophilic reaction partner to alkyne, thus complementing the redoxneutral transformations in which an electrophilic reactant is employed.

In 2015, the same group reported a regioselective synthesis of highly functionalized indoles 34.4 from anilines 34.1, terminal alkynes 34.2, and benzoquinones 34.3. ¹⁰⁹ Anilines functionalized at different positions all reacted well (34.5–34.9). The scope of arylacetylenes was also found to be broad (34.10–34.14). In addition, primary and secondary aliphatic alkynes delivered the indole products in good yields (34.15–34.16). Several successful examples employing substituted benzoquinone were also demonstrated (34.17–34.18) (Scheme 34).

In 2019, Hwang and co-workers employed *N*-tosylhydrazones **35.11** as nucleophiles for denitrogenative annulation toward 3-arylcoumarins **35.13**. The reaction efficiency was not influenced by the electronic properties of *N*-tosylhydrazones, providing good yields of the products in all cases (**35.4–35.6**). Coumarin derivatives with the C4 substituent were also accessible, albeit in lower yields (**35.7**). A range of (hetero)-arylacetylenes reacted efficiently to afford the products in good yields (**35.8–35.14**). However, enynes (**35.15**), as well as aliphatic terminal alkynes (**35.16–35.17**), delivered the respective products in low yields (Scheme **35**).

3.2.3.2. Oxidation of Alkynes to Carbonyl Compounds. In 2015, Hwang's group disclosed another oxidative C-N coupling of anilines 36.1 with terminal alkynes 36.2. In this case, the use of molecular oxygen instead of benzoquinones (Scheme 34) led to the formation of α -ketoamides 36.3. Various functionalized anilines reacted well in this transformation (36.4–36.9).

Scheme 34. Three Component Coupling of Anilines, Terminal Alkynes, and Quinones

Scheme 35. Oxidative Coupling of N-Tosylhyrdazones and Terminal Alkynes

However, diminished yields were obtained for less electron-rich anilines, as a consequence of their lower nucleophilicity. A broad range of (hetero)arylacetylenes delivered the products in good to excellent yields (36.10–36.15). Likewise, reactions with aliphatic terminal alkynes proceeded uneventfully (36.16–36.17) (Scheme 36).

A year later, the same group reported transformation that utilizes closely related 2-aminopyridine 37.1 as nucleophile. 112 Interestingly, pyridyl amides 37.3 were obtained, indicating cleavage of the triple bond. 2-Aminopyridines bearing functional groups at different positions delivered the respective amides in good to excellent yields (37.4–37.8). As in the case of anilines, both (hetero)aryl- (37.9–37.12) and alkyl-substituted (37.13–37.14) alkynes were efficient coupling partners (Scheme 37).

Scheme 36. Oxidative C-N Coupling of Anilines and Alkynes Leading to α -Ketoamides

Scheme 37. Oxidative C-N Coupling of 2-Aminopyridines and Alkynes Leading to Pyridyl Amides

The same group further expanded the chemistry of related oxidative transformations involving the intermediacy of dioxetene. In 2018, they reported analogous synthesis of α ketoesters 38.3 from aliphatic alcohols 38.1 and arylacetylenes 38.2. 113 Primary, secondary, as well as tertiary alcohols, were all appropriate substrates, furnishing the products in moderate to good yields (38.4-38.8). Diverse (hetero)arylacetylenes also reacted well (38.9-38.14). In this case, 2-picolinic acid serves as a ligand for Cu(II) acetylide, which captures molecular oxygen and forms dioxtene. Ring opening of the latter gives a glyoxal intermediate, which is then trapped by alcohol to produce α ketoester. Furthermore, Hwang group demonstrated the viability of a direct oxidation of internal alkynes 38.15. Thus, ynamides and ynamines yielded the corresponding α -ketoimides (38.17–38.25) and α -ketoamides (38.26–38.28), respectively. 114 Both aryl- and alkyl-substituted alkynes were competent substrates for this transformation. More recently, the direct oxidation of diarylacetylenes was also reported. 115 As in the previous cases, this protocol exhibits high functional group tolerance (38.29-38.33) (Scheme 38). Internal alkynes bearing alkyl substituents were, however, incompatible due to overoxidation.

Interestingly, employment of phenol nucleophiles **39.1** also leads to the cleavage of the triple bond of alkyne (cf. Scheme 37), as shown by Hwang group in synthesis of 4-hydroxyaryl ketones **39.3**. ¹¹⁶ Both phenol and hydroquinone formed product **39.4** with comparable efficiency. Besides, the same product was

Scheme 38. Synthesis of α -Dicarbonyls via Oxidative Transformations of (a) Arylacetylenes and (b) Internal Alkynes

obtained regardless of the substitution at the ortho- or metaposition (39.5). The scope of arylacetylenes was found to be broad and not sensitive to electronic and steric factors (39.6-39.8). Heteroaryl-, vinyl-, and alkyl-substituted terminal alkynes also reacted efficiently to form coupling products in good yields (39.9-39.11). The authors found that benzoquinone could deliver ketone 39.4 with the same efficiency, suggesting that the reaction begins with the oxidation of phenol to benzoquinone A under the reaction conditions. ¹¹⁷ Photocatalytically generated Cu(II) acetylide B then engages A in a Paterno-Büchi-type [2+ 2] cycloaddition ¹¹⁸ to form oxetene **C**, which upon ring opening affords quinone methide D. A subsequent homolysis of the Cu-C bond produces acyl radical E, which forms peracid F upon reaction with molecular oxygen, followed by an HAT from another phenol molecule. Finally, extrusion of CO2 and tautomerization of G deliver the reaction product 39.3 (Scheme 39). ¹⁸O-labeling experiment confirmed that molecular oxygen not only is involved in the oxidation of phenols to A, but also gets incorporated in the final product.

Recently, the same group showed that under basic conditions, the oxidative coupling of anilines **40.1** and arylacetylenes **40.2** delivered amides **40.3**, ¹¹⁹ complementing the previous method, which gives α -ketoamides (cf. Scheme 36). Electron-rich anilines reacted efficiently with electronically diverse (hetero)-arylacetylenes (**40.4–40.10**). Interestingly, derivatives of 2-aminobenzoic acid **40.11** were also good substrates for this reaction, smoothly reacting with arylacetylenes to give amides in good yields (**40.14–40.16**). In addition, alkyl acetylenes were

Scheme 39. Synthesis of 4-Hydroxyaryl Ketones via Oxidative Coupling of Phenols and Alkynes

also found to be viable coupling partners (40.17-40.19) (Scheme 40).

3.2.3.3. Oxidative Alkynylation. In 2016, Hwang group disclosed a dehydrogenative C-H/C-H Glaser-type crosscoupling of terminal alkynes to produce unsymmetrical conjugated diynes 41.3. Diverse electron-deficient arylacetylenes were well tolerated, furnishing cross-coupling products in excellent yields (41.4–41.7). As such, this protocol complements the known methods, which are less efficient with electron-poor alkynes. 121-129 Alkynes bearing electron-donating groups were also reactive, albeit in some cases delivered products with diminished yields (41.8-41.11). In addition, aliphatic alkynes also underwent smooth transformation to produce diynes in good yields (41.12–41.13). The formation of heterodimeric complex B by preferential formation of Cu(I) acetylide A from the relatively electron-rich alkyne 41.1⁵¹ and its favored coordination to the electron-deficient counterpart are the keys for achieving chemoselective cross-coupling. Indeed, isothermal titration calorimetry (ITC) revealed heat release upon titration of 41.1 into the solution of A, thus indicating a favorable complexation. This was further supported by the UVvis studies, which showed a bathochromic shift in a 1:1 mixture of A and 41.1 (Scheme 41). Interestingly, ITC indicated that homodimeric Cu(I) complex did not form, which is along the line of the high cross-selectivity observed. In the same year, the

Scheme 40. Oxidative C-N Coupling of Anilines and Alkynes Leading to Amides

Hwang, 2020
$$Ar^{1}NH_{2} + = Ar^{2} + O_{2}$$

$$40.1 40.2 1 atm \frac{K_{2}CO_{3}}{MeCN/MeOH (1:1)}$$

$$Ar^{1} + Ar^{2}$$

$$40.3 1 atm \frac{R^{1}}{MeCN/MeOH (1:1)}$$

$$Ar^{1} + Ar^{2}$$

$$40.3 1 atm \frac{R^{1}}{MeCN/MeOH (1:1)}$$

$$Ar^{1} + Ar^{2}$$

$$40.3 1 atm \frac{R^{1}}{MeCN/MeOH (1:1)}$$

$$Ar^{1} + Ar^{2}$$

$$40.4 1 3 atm \frac{R^{1}}{MeCN/MeOH (1:1)}$$

$$Ar^{1} + Ar^{2}$$

$$40.6, 59\%$$

$$40.8, R = 4-RBu, 82\%$$

$$40.9, R = 3-NO_{2}, 71\%$$

$$40.10, 78\%$$

$$40.11 1 atm \frac{K_{2}CO_{3}}{MeCN/MeOH (1:1)}$$

$$Ar^{1} + Ar^{2}$$

$$40.6, 59\%$$

$$40.10, 78\%$$

$$40.11 1 atm \frac{R^{1}}{MeCN/MeOH (1:1)}$$

$$Ar^{1} + Ar^{2}$$

$$40.3 1 atm \frac{R^{1}}{MeCN/MeOH (1:1)}$$

$$Ar^{1} + Ar^{2}$$

$$40.6, 59\%$$

$$40.10, 78\%$$

$$40.11 1 atm \frac{R^{1}}{MeCN/MeOH (1:1)}$$

$$40.13 1 atm \frac{R^{1}}{MeCN/MeOH (1:1)}$$

Scheme 41. Synthesis of Unsymmetrical Conjugated Diynes

authors also reported a homocoupling reaction of electronically diverse alkynes. 130

In 2018, the same group reported synthesis of 2-alkynyl-pyridines 42.3 from 2-hydrazinylpyridine derivatives 42.1 and terminal alkynes 42.2. Differently substituted 2-hydrazinyl-pyridines reacted smoothly with phenylacetylene to give alkynylpyridine products in good yields (42.4–42.7). As in most cases, a wide range of (hetero)arylacetylenes (42.8–42.13), regardless of steric and electronic factors, as well as vinyl- (42.14) and alkyl-substituted alkynes (42.15–42.17), were efficient in this reaction. Notably, hydrazines without the pyridine moiety, as well as 3- and 4-hydrazinylpyridines, did not provide any alkynylation product 42.19, thus suggesting that 2-hydrazinylpyridine may serve as a bidentate ligand for copper (Scheme 42).

Shortly after, Hwang and co-workers reported a three component coupling of anilines 43.1, alkynes 43.2, and alcohol 43.3, which was used as a solvent. ¹³² In this case, the use of

Scheme 42. Denitrogenative Cross-Coupling of 2-Hydrazinylpyridines and Alkynes

secondary anilines led to the formation of propargyl amines 43.4 instead of indoles 34.4. Various N-alkyl aniline derivatives were found to be viable substrates (43.5–43.10). (Hetero)aryl-(43.11–43.15), as well as alkyl-substituted (43.16) terminal alkynes, delivered the corresponding propargyl amines in moderate to good yields. The presence of electron-withdrawing groups either at anilines or alkynes decreased the reaction efficiency. Propargyl amines with α -substituents could be obtained by switching methanol to its higher homologues (43.17–43.20). Increased steric hindrance, however, compromised the reaction efficiency. The radical clock experiment using N-ethyl aniline, phenylacetylene, and cyclopropylmethanol revealed the formation of ring-opened product 43.21 along with 43.22, thus providing support for radical nature of this transformation (Scheme 43).

3.2.4. Other Carbon-Based Nucleophiles. 3.2.4.1. Cyanide as Nucleophile. In 2019, Wang and Xu's groups reported an asymmetric cyanofluoroalkylation of styrene derivatives 44.1 with fluoroalkyl iodides 44.2 and TMSCN. 133 Electron-neutral and -rich styrenes reacted smoothly to afford highly enantioenriched products in good yields (44.5-44.9). However, the electron-deficient counterparts were not effective substrates (44.10). More complex substrates were also amenable to this transformation (44.11). Unactivated alkenes delivered the respective products under UV irradiation, but at the expense of nearly complete loss of enantioselectivity (44.12). Other fluoroalkyl groups could also be efficiently introduced (44.13-44.15) (Scheme 44). It is noteworthy that a mixture of CuI and ligand 44.4 shows a similar absorption profile as the one with additional TMSCN in the visible light region but of lower absorbance. In addition, NMR studies revealed a rapid ligand exchange between the Cu(I)I complex and TMSCN. On the basis of these results, the authors proposed an in situ formed Cu(I)CN complex as the photocatalyst.

3.2.4.2. Azoles as Nucleophiles. In 2020, Zhang's group reported a C-H arylation of azoles 45.1 with aryl iodides 45.2

Scheme 43. Internal Alkynes Formation via Oxidative Three Component Coupling

Scheme 44. Asymmetric Cyanofluoroalkylation of Styrene Derivatives

under photocatalytic conditions. ¹³⁴ Various aryl iodides were moderately efficient (45.4–45.8). 3-Iodopyridine also furnished the respective product 45.9, albeit in low yield. Benzoxazole derivatives (45.10–45.11), other azoles (45.12), and electron-deficient thiophene derivative (45.13) were found to be competent substrates. The authors proposed a photoinduced double electron transfer from the *in situ* formed photoactive Cu(I) azolide complex to aryl iodide. However, based on literature precedents, an alternative SET pathway may be also operative. ^{50,53,96}

More recently, the same group achieved analogous C–H alkylation of azoles in an asymmetric fashion. ¹³⁵ Different benzyl

bromide derivatives provided the corresponding products in moderate to good yields with high level of enantiocontrol (45.16–45.21). However, functionalities such as methoxy- and cyano groups were not tolerated (45.22–45.23). Bromides bearing a heteroarene (45.24), as well as allylic bromides (45.25), were found to be reactive. A diminished enantioselectivity was, however, observed in the latter case. As in the case above, other azoles were also viable substrates, furnishing alkylated products in good yields and enantioselectivities (45.26–45.28). In this case, the proposed mechanism involves a photoinduced SET event, leading to the formation of Cu(II) azolide and an alkyl radical. A subsequent recombination in a stereocontrolled manner, followed by reductive elimination, affords the enantioenriched product (Scheme 45).

Scheme 45. Photoinduced C-H (a) Arylation and (b) Alkylation of Azoles

3.3. Photoinduced SET of Standalone Cu(I) Complexes

3.3.1. Difunctionalization of Alkenes and Alkynes. As in the case of Cu(I)—nucleophile complex, photocatalysis using a standalone Cu(I) complex enables a range of difunctionalization reactions of alkenes and alkynes. A general mechanism, typically involved in such transformations, as illustrated on difunctionalization of alkene, is depicted in Scheme 46. It begins with the visible light excitation of Cu(I) complex **A**, followed by the subsequent SET to an electrophile **46.1** to produce radical **B** and Cu(II) species **C**. The former is then captured by alkene

Scheme 46. Mechanisms of Difunctionalization of Alkenes

46.2 to afford alkyl radical **D**. Finally, formation of the C–X bond furnishes product **46.3**. Depending on the reaction, the C–X bond-forming step may follow different pathways. In the first scenario, Cu(II) complex C undergoes ligand transfer to **D** via **B1** to afford product directly. The overall transformation therefore represents a nonchain atom transfer radical addition (ATRA) reaction. Alternatively, recombination of **C** and **D** leads to Cu(III) intermediate **B2**, which upon reductive elimination constructs the C–X bond of the product. Other pathways, such as RPC (**B3**) and radical chain (**B4**), are also plausible. However, the RPC mechanism renders the copper catalyst a traditional photoredox catalyst, while a radical chain process does not involve copper in the propagating steps. Therefore, transformations operating via these mechanisms are not covered in the following sections.

3.3.1.1. ATRA Reactions. In 2015, Dolbier's group reported the first visible light-induced copper-catalyzed ATRA reaction of electron-deficient alkenes 47.1 with fluoroalkyl sulfonyl chlorides 47.2.54 Mono- and disubstituted acrylamides with different substitution patterns delivered the difunctionalized products in moderate to excellent yields (47.4-47.6). Other Michael acceptors were also viable substrates (47.7–47.9). Employment of other less reactive fluoroalkyl sulfonyl chlorides required elevated temperatures (47.10-47.12). Overall, this reaction works well with various electron-deficient alkenes (47.13–47.15) and shows high functional group tolerance (47.16–47.18). The alkyl radical formed upon radical addition is electrophilic in nature; thus, RPC and radical chain mechanisms are improbable. On the contrary, a ligand transfer mechanism, wherein the chlorine atom is transferred from a Cu(II) chloride species, is polarity-matched and therefore the favorable pathway (Scheme 47).

Shortly after, Reiser's group independently reported analogous transformation of unactivated alkenes 48.1 with triflic chloride under green LED irradiation. Interestingly, the SO₂ moiety was retained in some cases, furnishing a range of trifluoromethylchlorosulfonylation products in moderate to good yields (48.3–48.8). This turned out to be substrate dependent, as alkenes possessing a donor atom delivered chlorinated products, instead (48.9–48.12). Sterically hindered, 1,1-disubstituted alkene also favored trifluoromethylchlorination (48.13). The authors proposed that [Cu(II)-

Scheme 47. ATRA Reaction of Electron-Deficient Alkenes with Fluoroalkyl Sulfonyl Chlorides

 SO_2CI]⁺ intermediate, initially formed after photoinduced SET of Cu(I) to triflic chloride, may have a labile Cu-S bond and therefore is prone to extrusion of SO_2 in the presence of a donor atom. The transfer of bulky SO_2CI group is also impeded by steric factors, thus explaining formation of different products 48.4 and 48.13. An example of electron-deficient styrene was also demonstrated (48.14) (Scheme 48).

Scheme 48. ATRA Reactions of Unactivated Alkenes with Triflic Chloride

A year later, the same group reported a similar intramolecular transformation using olefin-tethered alcohols 48.15 toward sultones 48.16. The reaction efficiency was found to be dependent on the length of the tether in alkenol substrate (48.17–48.19). Substituted alcohols were also compatible, furnishing sultones in good yields (48.20–48.22).

In 2019, Reiser and co-workers disclosed a chlorosulfonylation reaction of alkenes 49.1 with sulfonyl chlorides **49.2**. ¹³⁷ In contrast to the previous reports, wherein a fluoroalkyl radical is involved (cf. Schemes 47 and 48), the less favorable formation of alkyl or aryl radical from 49.2 results in the generation of a sulfonyl radical. In addition to Cu(dap), Cl, the closely related Cu(II) catalyst, Cu(dap)Cl₂, was also effective (yields in parentheses). A wide range of aryl sulfonyl chlorides delivered the products in good to excellent yields regardless of the electronic and steric environments (49.4–49.7). Aliphatic counterparts were also highly effective (49.8). Excellent yields were also obtained with diverse styrene derivatives (49.9-49.15). Notably, benzylic- (49.11) and allylic chloride (49.14) groups remained intact, highlighting the functional group tolerance of this protocol. An array of unactivated alkenes were also viable substrates for this reaction (49.16-49.19). The authors also examined the scope of alkynes. Terminal arylacetylenes afforded the trisubstituted alkenes in excellent yields (49.20), while an internal alkyne gave moderate yield (49.21). Of note, unactivated aliphatic alkynes were unreactive in the transformation. It is worth mentioning that in the case of Cu(dap)Cl₂, the authors proposed VLIH of the Cu–Cl bond via LMCT to generate catalytically relevant Cu(I) (Section 3.4). In a separate report, the same group strategically utilized the VLIH process and demonstrated the versatility and robustness of Cu(II) catalyst in a range of ATRA reactions and other transformations such as decarboxylative alkynylation of RAEs (Scheme 49).138

In addition to sulfonyl chlorides, (perfluoro)alkyl iodides have also been utilized by Reiser group in related ATRA reactions. Thus, in 2018, they reported an iodoperfluoroalkylation reaction of alkenes and alkynes. 139 Various perfluor-

Scheme 49. Chlorosulfonylation of Olefins

oalkyl iodides were found to be viable reactants (50.4-50.6). Different styrene derivatives afforded the respective products in moderate to good yields (50.7–50.10). However, the presence of para-methoxy group led to polymerization of starting material (50.11). β -Methylstyrene was also a capable substrate, providing product 50.12 as a 1:1 mixture of diastereomers. Interestingly, the α -analogue furnished product 50.13 via a formal HI elimination. In addition, unactivated alkenes underwent efficient transformation in good yields (50.14-**50.16**). It is worth mentioning that the products derived from styrene derivatives are not readily accessible via Ru- or Ir-based photoredox catalysis. Notably, little electronic dependence was observed at the alkyne component. Thus, diverse arylacetylenes were smoothly converted to the corresponding iodo alkenes in good to excellent yields (50.17-50.19). In contrast to their previous report on chlorosulfonylation of alkynes (cf. Scheme 49), high E/Z selectivity was observed in this case. Importantly, this protocol enabled synthesis of tetrasubstituted alkene 50.20 with complete diastereocontrol. Likewise, aliphatic alkynes afforded the corresponding alkenes in good yields (50.21-50.25).

More recently, the same group demonstrated the use of iodoform as reaction partner in ATRA reactions of alkenes, 140 where diverse styrene derivatives furnished the difunctionalized products in good to excellent yields (50.27-50.30). Interestingly, highly electron-rich styrenes provided products 50.31 and 50.32, respectively, indicating the formation of a carbocation via RPC (cf. Scheme 46), which was then trapped by methanol solvent. As in the latter case, β -methylstyrene was a competent substrate for this transformation (50.33). Vinyl heteroarenes were also compatible, with reaction outcome dependent on the substrate (50.34-50.35). Furthermore, Michael acceptors (50.36-50.37), as well as conjugated diene (50.38), were found to be reactive alkene partners. Naturally, the products of this transformation are highly versatile synthons for further transformations. For instance, product 50.39 could be transformed to 2-pyrazoline derivative 50.40. Alternatively, it could undergo chemoselective thiocyanation at the benzylic position, followed by difluorination with AgBF4 to produce polyfunctional compound 50.41 (Scheme 50).

In 2018, Li, Yu, and co-workers reported a fluorotrifluoromethylation of unactivated alkenes 51.1 with Umemoto's reagent 51.2 and CsF. 141 Both visible light irradiation and elevated temperature were required. Under these conditions, various 1,1-disubstituted alkenes bearing a pendant functional group were smoothly converted to the products in moderate to good yields (51.6-51.10). More sterically demanding substrates were also reactive (51.11-51.13). However, monosubstituted alkene was found to be much less efficient, as hydrotrifluoromethylation became the dominant side pathway (51.14). An alcohol functionality in 51.15 was perfectly tolerated to produce 51.16, thus refuting the intermediacy of a carbocation via RPC, which would lead to the cyclized product 51.17 (Scheme 51). Of note, the authors also explored fluorotrichloromethylation in the same report. In that case, visible light irradiation was not necessary.

3.3.1.2. Dicarbofunctionalization. In 2018, Xiao, Chen, and co-workers disclosed a three component coupling of RAOEs 52.1, alkenes 52.2, and arylboronic acids 52.3. Diverse (hetero)aryl boronic acids were effective coupling partners, delivering products in moderate to excellent yields (52.5–52.10). The scope with respect to styrene derivatives was also found to be broad (52.11–52.14). Besides, heteroarenes, such

Scheme 50. ATRA Reactions with Iodoalkanes

as 2-vinylpyridine, were also reactive (52.15). However, reactions with β -substituted styrene derivatives were less efficient (52.16). In addition, conjugated dienes (52.17) and enynes (52.18) could also be engaged in this transformation. A mixture of 1,2- and 1,4-adducts was obtained in the former case. Finally, more complex RAOEs could also be used (52.19-**52.24**). In case of monosubstituted RAOEs, the products were obtained as a 1:1 mixture of diastereomers. Although closely related to their work on carboalkynylation (cf. Scheme 29), this reaction does not involve the in situ formation of the Cu(I)nucleophile complex. In this case, Cu(II) complex A, formed upon photoinduced SET of Cu(I) catalyst to RAOE 52.1, as supported by EPR experiments, undergoes transmetalation with boronic acid 52.3 to give aryl Cu(II) intermediate B. Meanwhile, the resultant radical from 52.1 undergoes a sequence of β -scission and addition to **52.2** to produce radical intermediate C. Recombination of B and C affords Cu(III) species D, which upon reductive elimination furnishes reaction product 52.4 (Scheme 52).

3.3.2. Decarboxylative Transformations. In 2017, the groups of Peters and Fu disclosed a decarboxylative C-N coupling of primary and secondary aliphatic RAEs **53.1**, ¹⁴³

Scheme 51. Fluorotrifluoromethylation of Unactivated Alkenes

Scheme 52. Three Component Coupling of RAOEs, Alkenes, and Arylboronic Acids

representing an azide-free, radical alternative to Curtius rearrangement. Primary alkyl RAEs bearing a wide range of functionalities underwent efficient coupling to deliver the respective products in moderate to good yields (53.3-53.9). In case of more hindered substrates, higher catalyst loading was required to achieve good yields (53.10-53.11). The secondary counterparts were also competent substrates, furnishing the C-N coupling products in moderate to good yields (53.12-53.15). Of note, both ligands were crucial to this transformation, as no product was obtained when either sole ligand was used. In addition, the UV-vis spectra indicated the only combination of CuCN, dmp, and Xantphos being the visible light-absorbing species. These results suggest the *in situ* formation of a Cu(I) complex featuring a mixed ligand environment. The radical nature of this transformation was supported by the radical clock and radical trapping experiments. Interestingly, crossover reaction of substrates 53.16 and 53.17 led to a statistical mixture of the four possible products (53.18-53.21), suggesting that the escape of radical from the solvent cage precedes the C–N bond formation process (Scheme 53).

Scheme 53. Decarboxylative C-N Coupling of RAEs

More recently, Loh, Tian, and co-workers employed hypervalent iodine(III) reagents **54.2** for site-selective alkylation of heteroarene *N*-oxides **54.1**. Iodine reagents bearing primary and secondary alkyl groups underwent smooth transformation with quinoline *N*-oxide to deliver the *ortho*-alkylation products in moderate to good yields (**54.4**–**54.8**). Tertiary alkylation was also feasible, albeit with diminished yield (**54.9**). Other quinoline *N*-oxides (**54.10**), as well as those derived from phenanthridine (**54.11**), pyridine (**54.12**), and quinoxaline (**54.13**), were all found to be viable substrates. The proposed

catalytic cycle commences with the SET from photoexcited Cu(I) catalyst A^* to hypervalent iodine reagent 54.2 to produce alkyl radical B and Cu(II) complex C. The latter undergoes selective metalation at the C2 position of substrate to form intermediate D. A subsequent recombination of B and D leads to Cu(III) species E, which upon reductive elimination furnishes C-H alkylation product 54.3 and regenerates the copper catalyst (Scheme 54).

Scheme 54. Decarboxylative C-H Alkylation of Heteroarene N-Oxides

3.3.3. Asymmetric Transformation. In 2019, Gong group achieved an enantioselective α -aminoalkylation of hydrazones 55.1 with aminomethyl silanes 55.2. 145 Secondary arylamino derivatives of 55.2 delivered the products in moderate yields with excellent enantiocontrol (55.5-55.7). Tertiary anilines, however, provided the respective products with diminished enantioselectivity (55.8-55.10). Substitution at aryl group of hydrazone posed no problems (55.12-55.14). In contrast, a significantly lower enantioselectivity was observed in the case of aliphatic substituent (55.15). The proposed mechanism involves a dual catalytic cycle beginning with the in situ formation of the Cu(II)-substrate coordination complex A. It engages electron-rich amine 55.2 in the SET event, leading to the formation of α -amino radical C via aminium radical cation B, as well as photoactive Cu(I) complex D. Radical C can then undergo enantiodetermining radical addition to another molecule of A to construct the C-N bond in E. A subsequent SET from photoexcited complex D* produces intermediate F

and closes the photoredox cycle. Finally, protonation followed by ligand exchange furnishes product 55.3 and regenerates Cu(II) complex A. The formation of α -amino radical C was supported by radical trapping experiments. In addition, stoichiometric reaction of amine 55.16 with copper catalyst indicated that the formation of dimer 55.17 did not require visible light irradiation, consistent with the observation that Cu(II) complex showed only weak absorption in the visible light region (Scheme 55).

Scheme 55. Enantioselective α -Aminoal kylation of Acyclic Imines

3.4. Photoinduced Homolytic Ligand Dissociation of Cu(II) Complexes

The LMCT character of photoexcited Cu(II) complexes and its subsequent homolytic ligand dissociation have long been recognized. However, synthetic transformations exploiting this excited-state reactivity had not been reported until 2018, when the groups of Rehbein and Reiser disclosed an

oxoazidation reaction of vinyl arenes 56.1 with trimethylsilyl azide and molecular oxygen.⁵⁸ In this transformation, electronically diverse styrene derivatives underwent smooth reaction to deliver the respective ketoazides in good yields (56.3-56.7). Markedly, benzyl chloride functionality did not undergo substitution under the reaction conditions, highlighting notable chemoselectivity of this transformation (56.8). In addition, vinyl heteroarenes (56.9), as well as β -methylstyrene (56.10), were found to be competent substrates. However, no desired product was obtained when unactivated alkenes were employed (56.11). This transformation begins with an off-cycle photoinduced oxidation of Cu(I) catalyst to Cu(II) complex A, which upon ligand exchange with TMSN₃ forms photoactive, dimeric species B. A subsequent photoexcitation leads to the formation of azide radical and Cu(I) complex C. The former then undergoes radical addition to alkene substrate to afford stabilized radical D, which further reacts with molecular oxygen to produce peroxy radical E. Recombination of C and E, followed by release of product 56.2 regenerates complex A and closes the catalytic cycle (Scheme 56).

Scheme 56. Oxoazidation of Vinyl (Hetero)arenes

In the same year, Gong's group reported an asymmetric alkylation of imine derivatives 57.1 using alkyl trifluoroborates 57.2. Ligand 57.4 was used in the case of N-sulfonylimines. A wide range of electron-neutral and -deficient benzyl trifluoroborates delivered the respective sulfonamides in excellent yields and enantioselectivity (57.6-57.9). The electron-rich counterparts were equally reactive, however provided products with inferior enantiocontrol (57.10). Similarly, product 57.11

was obtained in almost quantitative yield, but with lower enantioselectivity. Secondary (57.12) and tertiary trifluoroborate (57.13) were also efficient, albeit giving rise to products with diminished stereoselectivity. Substrates possessing other α carbalkoxy groups were viable reactants, as well (57.14-57.15). However, replacement of α -carbalkoxy groups with methyl group shut down the reaction (57.16). The benzene ring of substrate could also be modified without compromising the reaction efficiency (57.17-57.18). The authors also explored the scope of ketimines in the presence of ligand 57.5. Notably, excellent enantiocontrol was maintained upon varying the substituent at the benzene ring (57.19-57.22). N-Methyl substrate also furnished the corresponding oxindole 57.23 in good yield with excellent enantiocontrol. In contrast to the case using electron-rich amines (cf. Scheme 55), an SET event, either photoinduced or not, is unlikely in this transformation as alkyl trifluoroborates are not capable of reducing Cu(II). Thus, the authors proposed Cu(II) catalyst A and trifluoroborates first undergo transmetalation to produce alkyl Cu(II) complex B. A subsequent visible light excitation leads to the homolytic cleavage of Cu-C bond, thereby producing alkyl radical C and Cu(I) species **D**. As in the previous case, the former then enters the asymmetric catalytic cycle, while the latter is responsible for its completion (Scheme 57).

Scheme 57. Enantioselective Alkylation of Imines with Alkyl Trifluoroborates

In 2020, Wan's group reported catalytic dichlorination of unactivated alkenes 58.1 with HCl.⁶⁰ Monosubstituted aliphatic alkenes possessing certain functional groups were efficiently dichlorinated in good yields (58.3-58.5). Allylic systems were also applicable, furnishing the corresponding products in moderate yields (58.6-58.7). Furthermore, a wide range of functional groups at aryl substituent, including an iodide, were compatible under these reaction conditions (58.8-58.12). In addition, 1,1-disubstituted alkenes underwent efficient transformation to provide dichlorination products in excellent yields (58.13). The proposed catalytic cycle begins with the photoexcitation of CuCl₂ to its LMCT state, which subsequently undergoes Cu-Cl bond homolysis to produce chlorine radical and CuCl. The former adds to alkene substrate to generate alkyl radical A, which upon reaction with CuCl₂ forges the second C-Cl bond in product 58.2. Meanwhile, CuCl is oxidized back to CuCl₂ in the presence of air and HCl to complete the catalytic cycle. TEMPO trapping experiment indicated the formation of TEMPO-Cl adduct, thus supporting the involvement of chlorine radical. Another piece of evidence comes from an interesting example of HAT from alkene 58.14 to chlorine radical, thereby furnishing trichlorinated product 58.15 (Scheme 58). Of note, the authors also explored dichlorination of styrene derivatives. In those cases, however, a superstoichiometric amount of CuCl₂ was required.

Scheme 58. Dichlorination of Alkenes via LMCT of CuCl₂

More recently, Rovis' group also utilized $CuCl_2$ as chlorine radical source for HAT in aliphatic C-H alkylation of alkenes $59.1.^{61}$ For activated systems, both primary and secondary C-H alkylations were efficient (59.4-59.6). Cycloalkanes underwent efficient alkylation in excellent yields (59.7). Linear aliphatics

were also reactive in this transformation (59.7). However, a mixture of regioisomers was observed in all cases. Notably, an example of selective tertiary alkylation was demonstrated (59.8). In addition, various Michael acceptors with different degrees of substitution proved to be competent substrates for this transformation (59.9–59.15). Furthermore, azodicarboxylate was also found to be an appropriate radical acceptor (59.16) (Scheme 59).

Scheme 59. C(sp³)-H Alkylation via Intermolecular HAT

3.5. Photoinduced EnT of Cu(I) Complexes

In 2017, Liu's group reported a denitrogenative coupling of vinyl azides 60.1 with ammonium thiocyanide involving EnT from the in situ formed Cu(NCS)2-, representing another excitedstate reactivity of copper complexes. 63,150 A broad range of (hetero)aryl vinyl azides reacted smoothly under these reaction conditions, affording the respective 2-aminothiazoles in good to excellent yields (60.3-60.9). Likewise, the aliphatic counterparts, bearing diverse functionalities, were found to be competent reaction partners (60.10-60.14). The authors proposed an EnT mechanism for this transformation, which begins with the in situ formation of visible light-absorbing Cu(NCS)₂ complex. Which upon photoexcitation transfers energy to vinyl azide 60.1, leading to the formation of highly strained 2H-azirine A, presumably via the intermediacy of the respective vinyl nitrene. 151 Coordination of A to a copper center then forms intermediate B. A subsequent nucleophilic ring opening constructs the C-S bond in C. Finally, intramolecular nucleophilic attack, followed by protonation, produces the cyclized product 60.2. Ir(ppy)₃ photocatalyst, which can also produce 2H-azirines from vinyl azides via EnT, 152 was found to be less effective in this transformation, indicating that the conversion from 2H-azirine to final product may be mediated by copper. Indeed, the reaction of 2H-azirine 60.16 with ammonium thiocyanate was tremendously accelerated by catalytic amount of copper catalyst, thus supporting the second role of copper as a Lewis acid catalyst (Scheme 60).

Scheme 60. Photoinduced EnT from Cu(NCS)₂⁻ to Vinyl Azides

4. IRON

4.1. General Overview

Iron complexes are well-known for undergoing rapid excited state relaxation via the low-lying metal-centered states. ^{153–155} This innate nature of iron limits its photochemical reactivities and thus renders it a less popular photosensitizer. Nonetheless, it has been recently shown that certain Fe(III) complexes possess excited-state lifetime up to 2 ns and, thus, are capable of participating in intermolecular quenching events. ¹⁵⁶ Therefore, the utilization of Fe-based photoredox catalysts has been reported, and these catalysts were recently reviewed. ¹⁵⁷ In the context of visible light-induced iron catalysis, the first example came from Jin's group in 2019, when they described a decarboxylative alkylation of heteroarenes with alkyl carboxylic acids. ¹⁵⁸ This transformation involves the *in situ* formed Fe(III)

carboxylate that upon blue LED irradiation undergoes LMCT to produce carboxyl radical and an Fe(II) intermediate (Figure 4a).

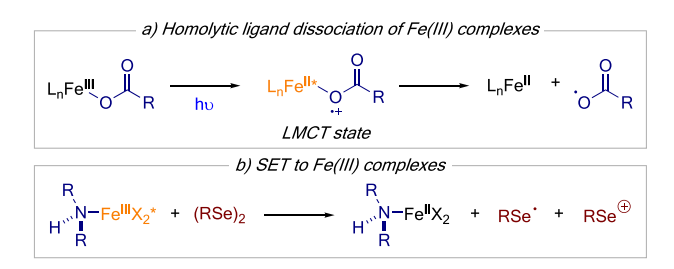


Figure 4. Outline of visible light-induced iron catalysis.

In 2020, Xia, Yang, and co-workers reported an aminoselenation of alkenes with amines and diselenides enabled by another excited-state reactivity of Fe(III) complexes. ¹⁵⁹ In this case, amine-coordinated Fe(III) complex undergoes photoinduced SET with diselenide to afford the respective Fe(II) intermediate, selenium radical, and selenium cation (Figure 4b).

Meanwhile, the groups of Alcázar and Noël observed an accelerating effect of visible light on iron-catalyzed Kumada coupling. Despite remaining elusive, the origin of acceleration is likely related to the enhanced oxidative addition of aryl chloride to Fe(I) catalyst.

4.2. Transformations Involving LMCT of Fe(III) Carboxylates

In 2019, Jin and co-workers disclosed a decarboxylative Miniscitype alkylation of heteroarenes 61.1 using carboxylic acids 61.2 as alkyl source. 158 Both simple aliphatic and functionalized primary carboxylic acids were viable substrates for this reaction, providing the respective products with moderate to good efficiency (61.4-61.9). Likewise, secondary and tertiary alkylation products were obtained in good to excellent yields (61.11–61.14). A remarkably broad scope of N-heterocycles, such as isoquinolines (61.15-61.16), pyridines (61.17), diazines (61.18-61.21), benzimidazoles (61.22), purines (61.23), and benzothiazoles (61.24), was shown, thus demonstrating the generality of this protocol. Of note, in cases where identical C-H sites are available, a mixture of mono- and bis-alkylated products was obtained (61.25). Besides, benzothiophenes were also found to be competent substrates (61.26). The postulated reaction mechanism begins with the in situ formation of Fe(III) carboxylate complex A. A subsequent photoinduced LMCT of A leads to the formation of carboxyl radical B and a Fe(II) intermediate. The former then extrudes CO₂ to produce nucleophilic alkyl radical C, which undergoes radical addition to protonated heteroarene **61.1** to form radical cation D. Finally, a sequence of deprotonation and oxidation by Fe(III) species affords the alkylation product **61.1**. Meanwhile, the Fe(II) intermediate generated in both cycles is oxidized by the terminal oxidant (NaClO₃ or NaBrO₃) to regenerate the Fe(III) catalyst. The radical nature of this transformation was supported by TEMPO trapping experiment (Scheme 61).

Later in the same year, Jin's group extended this chemistry by reporting a redox-neutral hydroalkylation of Michael acceptors 62.1. ¹⁶¹ In this case, addition of the initially formed nucleophilic alkyl radical to 62.1 leads to electrophilic alkyl radical, which is capable of oxidizing Fe(II) intermediate back to its Fe(III) state via RPC pathway, thereby completing the catalytic cycle without the use of an external oxidant. Various aryl- (62.5–62.8) and alkyl-substituted (62.9) malononitriles delivered the corresponding products in good to excellent yields. An example of

Scheme 61. Decarboxylative Alkylation of Heteroarenes

malonate derivative was also demonstrated (62.10). A broad range of carboxylic acids was found to be competent reaction partners, affording primary (62.11–62.14), secondary (62.15–62.16), and tertiary (62.17–62.18) alkylation products in moderate to excellent yields. Likewise, azodicarboxylates 62.19 proved to be competent radical acceptors, furnishing the respective products with good to excellent efficiencies under similar reaction conditions (62.21–62.25) (Scheme 62).

Me Me 61.27, 27%

More recently, Lei and Jin groups reported an intramolecular C–H acyloxylation of 2-arylbenzoic acids **63.1** to access lactones **63.2**. ¹⁶² It is speculated that in this case, formation of carboxyl radical from Fe(III) carboxylate is followed by a rapid intramolecular cyclization instead of decarboxylation. Substrates bearing diverse functional groups at the aryl substituent underwent smooth transformation to provide benzolactones in good to excellent yields (**63.6–63.10**). Likewise, variations

Scheme 62. Decarboxylative Alkylation of (a) Michael Acceptors and (b) Azodicarboxylates

could be made on the other phenyl ring without loss of efficiency (63.11–63.16). 2-Naphthoic acid derivative was also reactive, albeit with diminished efficiency (63.17) (Scheme 63).

Scheme 63. Intramolecular Lactonization of 2-Arylbenzoic Acids

4.3. Difunctionalization of Alkenes

Recently, Yang and Xia's groups reported aminoselenation of alkenes 64.1 with diselenides 64.2 and amines 64.3. 159 Electronically diverse styrenes reacted efficiently to provide the difunctionalized products in moderate to good yields (64.5– 64.9). However, 1,1-diphenylethylene did not provide any product, presumably due to increased steric hindrance (64.10). β -Methylstyrene was also a competent substrate, furnishing product 64.11 with excellent diastereoselectivity. Unactivated alkenes could also be employed, albeit with inferior efficiency (64.12-64.13). Remarkably, a broad range of aniline derivatives was found to be suitable reaction partners for this transformation (64.14-64.19). In general, electron-deficient anilines provided better yields than their electron-rich counterparts. In addition to anilines, azoles also furnished the respective products in good yields (64.20-64.21). In contrast, aliphatic amines were found to be unreactive (64.22). Several other diselenides also provided the desired products but were less effective than diphenyldiselenide (64.23-64.24). Finally, analogous reaction with disulfide was unsuccessful (64.25). The proposed mechanism commences with the *in situ* formation of Fe(III)—amine complex A. Photoexcited A* undergoes SET with diselenide 64.2 to generate selenium radical C and selenide cation D, which form alkyl radical E and carbocation F, upon addition to alkene 64.1, respectively. Under the oxidizing conditions, both radicals C and E can be oxidized to the corresponding cations. Subsequently, carbocation F either reacts with Fe(II)-amine complex B (path a) or with amine 64.3 (path b) to deliver product 64.3. However, given that electron-poor anilines are more efficient, path b is considered to be less likely. Finally, Fe(III) catalyst is regenerated upon oxidation by the external oxidant. A linear Stern-Volmer relationship confirmed the role of diselenide as a quencher. In addition, the formation of both E and F was supported by trapping experiments with TEMPO (64.27) and H₂O (64.28) (Scheme 64).

4.4. Cross-Coupling Reaction

Iron-catalyzed Kumada coupling is typically limited to electrondeficient aryl halides and primary aliphatic Grignard reagents. 163,164 To employ electron-neutral and -rich aryl chlorides, pressing conditions, such as elevated temperature, as well as prolonged reaction time, are required. ^{165,166} In 2019, the groups of Alcazar and Noël showed that visible light irradiation enables the use of diverse aryl chlorides 65.1 for Kumada coupling in flow under mild conditions. 160 Thus, differently substituted aryl chlorides underwent smooth transformation with CyMgCl to provide the cross-coupling products in good to excellent yield (65.4-65.7). Notably, substrate conversion was significantly lower in the absence of blue LED irradiation (shown in parentheses), thus confirming the essential role of light in this transformation. Similarly, heteroaryl chlorides provided the respective products in moderate to good yields (65.8-65.11). Of note, the effect of irradiation was marginal, or not noticeable at all, in the latter two cases. Moreover, other primary and secondary alkyl Grignard reagents were found to be suitable coupling partners (65.12-65.14). Kinetic studies, including light on/off experiments indicated crucial effect of visible light irradiation, especially in case of electron-rich aryl chlorides. The proposed mechanism begins with an off-cycle formation of photoactive Fe(I) complex A upon reduction of Fe(acac)₃ by Grignard reagent **65.2**. Then a light-accelerated oxidative addition occurs to afford aryl Fe(III) complex B. A

Scheme 64. Aminoselenation of Alkenes

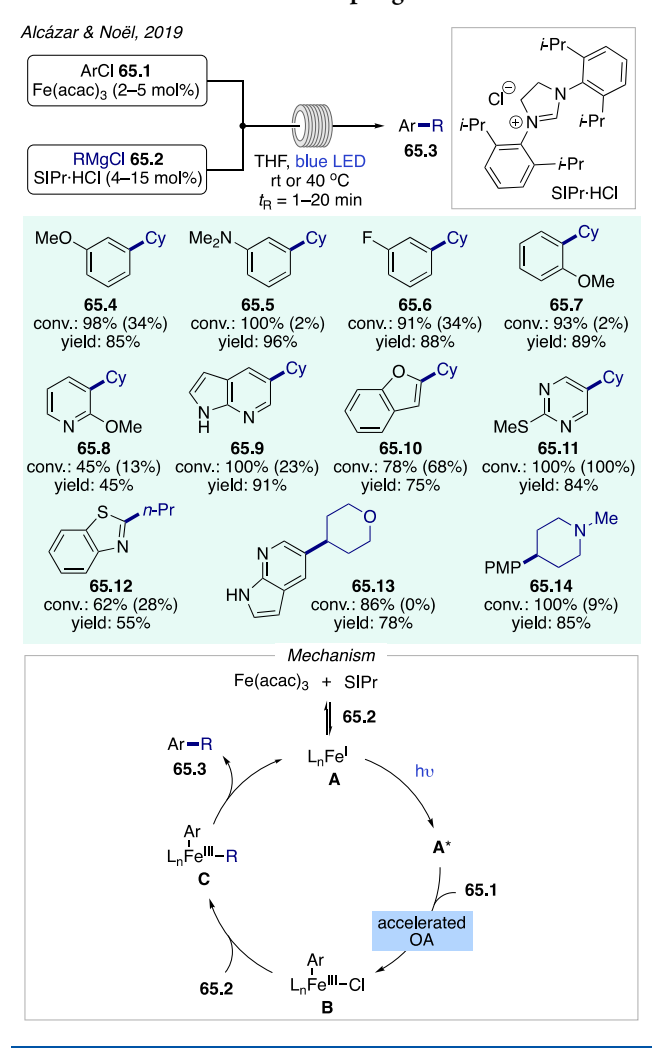
subsequent transmetalation with Grignard reagent, followed by the reductive elimination, furnishes the cross-coupling product 65.3 (Scheme 65).

5. PALLADIUM

5.1. General Overview

Photophysical properties of organometallic complexes of palladium have been a subject of research for decades. ^{167–172} For instance, in 1985, Caspar examined several zerovalent palladium—phosphine complexes, which exhibited rather long excited state lifetime up to 5.4 μ s. ¹⁶⁸ It was also found that the absorption maximum of Pd(PPh₃)₄, one of the common Pd(0) catalysts, lies in the UV region of about 330 nm and tails into the visible light region. Therefore, early examples of Pd(0) photocatalysis operate under UV irradiation. ¹⁷³

Scheme 65. Kumada Cross-Coupling in Flow



The first visible light-induced palladium-catalyzed transformation was reported by Gevorgyan's group in 2016 by disclosing the generation of an unprecedented hybrid aryl palladium-radical species from aryl iodides. ¹⁷⁴ In this case, visible light excitation led to the formation of a high-energy Pd(0) species, which was capable of transferring a single electron

to aryl iodide, thereby engaging it in hybrid palladium-radical chemistry. To date, the majority of palladium visible light photocatalysis operates via this oxidative quenching pathway, wherein an SET from photoexcited palladium to an organic halide or its equivalent occurs (Figure 5a). 13,175,14,176,15

Under this activation mode, visible light irradiation facilitates the "oxidation addition" step of otherwise unreactive substrates under milder conditions in comparison to thermally-177-180 and UV-induced methods, 173 thus encompassing a broader spectrum of substrates bearing more diverse functionalities. Furthermore, the formed hybrid aryl palladium-radical species opens up entry to a plethora of one-electron-based transformations, which are much less explored than the wellestablished two-electron chemistry of Pd. A striking difference between this SET event and that operating under typical photoredox methods³ is its loose relationship with the redox potentials. This can be attributed to a catalyst-substrate interaction, which would not be possible with typical coordinatively saturated photocatalysts. As a result of this inner-sphere SET mechanism, aryl and alkyl halides of reduction potentials beyond the reach for photocatalysts are reactive under the excited-state palladium catalysis.

Although examples remain scarce, visible light irradiation can also play a role in other catalytically relevant elementary steps. A recent example came from Arndtsen's group, in which they showed that reductive elimination of acyl palladium chloride complex could be promoted by photoinduced homolysis of C–Pd bond followed by an XAT to forge the C–Cl bond (Figure 5b). Besides, there were some reports on visible light-accelerated elementary steps of cross-coupling reactions, 182,183 however, in these cases, radical intermediates were not involved, and the origins of acceleration remain unclear.

Since the introduction of visible light-induced palladium catalysis in 2016, in just five years, tremendous progress has been made in this field. A historical outline on the development of electrophiles as substrates for the carbon-based hybrid palladium-radical species is presented in Figure 5c. After successfully engaging aryl iodides toward aryl radicals, in 2017, Gevorgyan's group realized the generation of analogous alkyl species from unactivated alkyl iodides and bromides, which was closely followed by the independent works on bromides from Yu's group 185 and Shang and Fu's groups, 186 respectively. Shortly after, Gevorgyan's group showed that tertiary alkyl

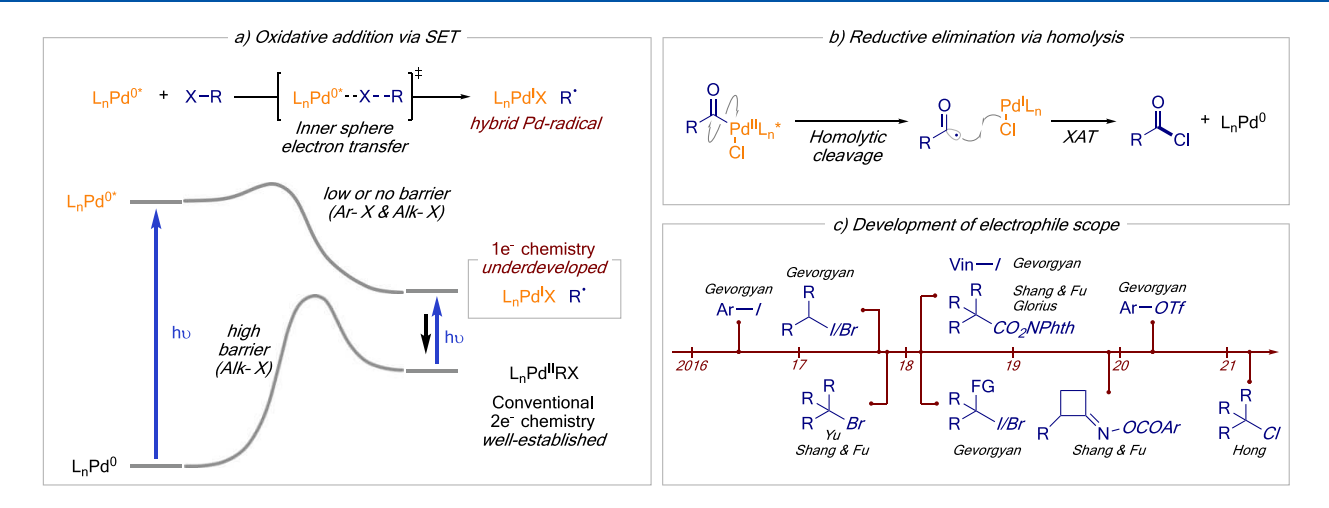


Figure 5. Outline of visible light-induced palladium catalysis.

iodides, as well as tertiary α -functionalized alkyl bromides, were also competent substrates. Weanwhile, they revealed the employment of vinyl iodides in a separate report. The same group also achieved the use of aryl triflates in 2020, providing a valuable alternative to aryl halides. Very recently, Hong's group utilized unactivated alkyl chlorides to access alkyl radicals, thus significantly expanding the scope of alkyl halides. RAEs and RAOEs also proved to be viable precursors of alkyl radicals, as shown by Glorius' group 191 and Shang and Fu's groups. 192,193

As mentioned above, the early reports have shown that aryl, vinyl, and alkyl radicals can be generated from the corresponding (pseudo)halides via visible light palladium photocatalysis. Different types of halides were therefore occasionally studied together in a single report. Accordingly, these references are arranged in Section 5.3 describing alkyl halides.

5.2. Fragmentation of C(sp²)-X Bond

5.2.1. Desaturation. In 2016, Gevorgyan's group disclosed a catalytic directed oxidation of silyl ethers 66.1 to silyl enol ethers 66.2, representing the first example of catalytic generation of aryl radical by Pd(0). 194,174 This protocol can be applied to structurally diverse substrates, ranging from cyclic (66.4–66.6) to acyclic (66.7–66.8) scaffolds, as well as complex molecules, such as androsterone derivative 66.9. Besides, the mild reaction conditions allowed for the introduction of various functional groups (66.10-66.13). Remarkably, selective oxidation of the silyl ether moiety was also achieved in the presence of unprotected alcohol functionality (66.14), highlighting the orthogonal chemoselectivity of this approach to that of the traditional oxidation methods. Mechanistically, the catalytic cycle begins with photoexcitation of the in situ formed Pd(0) species. SET from photoexcited Pd(0) catalyst to substrate 66.1 then occurs to produce a hybrid aryl palladium-radical intermediate A, which is capable of 1,5-hydrogen atom transfer (HAT) to form intermediate B. 195-197 The latter then undergoes β -H loss to afford product **66.2**. Finally, regeneration of Pd(0) from Pd(II) by base closes the catalytic cycle. Several pathways for β -H loss were proposed by the authors. In the first scenario, a sequential radical recombination/ β -hydride elimination via B1 is involved to yield the product. Alternatively, HAT to Pd(I) leads to the direct formation of the double bond (B2). Other potential mechanisms include RPC (B3) and XAT (B4), wherein the resultant intermediates can undergo a facile E2 elimination to furnish alkene product. Mechanistic studies strongly supported the radical nature of this transformation. Thus, addition of radical scavengers, such as galvinoxyl and TEMPO, completely suppressed the reaction. Furthermore, the radical clock experiment with 66.15 led to exclusive formation of the ring opening product 66.16, while formation of potential products of β -C elimination or direct β -H elimination, **66.17** and 66.18, respectively, was not detected. Moreover, deuteriumlabeled substrate 66.19 led to product 66.20 with ≥98% deuterium incorporation, thus providing additional evidence for 1,5-HAT to the hybrid radical species A (Scheme 66).

This unique reactivity of photoexcited Pd(0) to produce aryl radical was further exploited by the same group to achieve proximal and remote desaturation of aliphatic amines (Scheme 67). For this transformation, installation of tether, as well as the key desaturation step, can be carried out in a one-pot fashion. Primary and secondary amines are both compatible substrates for this transformation, leading to the respective enamines (67.3–67.8), allylic (67.9) and homoallylic amines (67.10–67.18) in good yields and high regioselectivity. Inportantly,

Scheme 66. Desaturation of Silyl Ethers Involving 1,5-HAT to Hybrid Pd Aryl Radical Species

it was shown that HAT can also occur at more challenging unactivated secondary C–H, affording the desaturation products in reasonable yield (67.17). In general, the carbonyltether (T^1) favors α -/ β -desaturation via 1,5-HAT, whereas the sulfonyl-tether (T^2) leads to desaturation at β -/ γ - and γ -/ δ -sites via 1,6- and 1,7-HAT, respectively. Thus, pinpoint desaturation can be accomplished by choosing the appropriate tether, as exemplified by products 67.5 and 67.9, which originated from the same substrate. To gain further insights into the SET step, the photophysical studies were performed to verify substrate's role as a quencher. Indeed, it was found that the emission intensity of the photoexcited Pd(PPh₃)₄ decreased as the

Chemical Reviews Review pubs.acs.org/CR

Scheme 67. Selective Proximal and Remote Desaturation of **Aliphatic Amines**

67.4, X = 0.90%

 β -/ γ - (1,6-HAT) & γ -/ δ - (1,7-HAT)

Parallel KIE

H H Conditions

$$C_6D_6$$
 C_6D_6
 C_6D_6

concentration of substrate 67.19 increased, resulting in a linear Stern-Volmer relationship. Deuterium-labeling studies were also performed, which confirmed HAT to the hybrid aryl radical intermediate. Besides, a primary kinetic isotope effect (KIE) value of 1.4 was obtained from the parallel reactions using 67.20 and d-67.20, suggesting that the HAT step could be the ratedetermining step in this transformation.

5.2.2. Atom Transfer Radical Cyclization. In 2018, Gevorgyan and co-workers advanced the chemistry of palladium photocatalysis to vinyl iodides. ¹⁸⁸ Electronically diverse iodovinylbenzene derivatives, as well as substrates possessing aliphatic tethers, underwent smooth transformation, leading to various iodomethyl hetero- (68.3-68.5) and carbocycles (68.6-68.12). It is noteworthy that an alkyl chloride moiety remained intact, thus delivering dihalide 68.10 bearing two convenient functional handles. Obviously, the overall transformation that features the preservation of the iodine atom follows a different mechanistic scenario from that of aryl radicals (Schemes 66 and 67). It was proposed that hybrid vinyl palladium-radical A, formed upon SET from photoexcited Pd(0) to substrate 68.1, undergoes 1,5-HAT to give a translocated radical species B. A subsequent 5-exo-trig cyclization of the latter at the double bond leads to the formation of cyclic intermediate C, which upon XAT from Pd(I) I species affords product 68.2 and regenerates the catalyst. A radical chain mechanism, where C would abstract iodine atom from another substrate molecule, is unlikely due to the large unfavorable BDE difference between vinyl- and alkyl-iodide bonds.²⁰⁰ It should be mentioned that alkene **68.13**, a product of potential β -H loss, was not observed (Scheme 68).

Scheme 68. HAT/ATRC Cascade Leading to Cyclic Motifs

5.2.3. C–H Arylation. In 2018, Ong, Jurca, Wang, and coworkers reported the use of palladium carbodicarbene catalyst 69.4 for light-induced directed C-H arylation with aryl diazonium salts 69.2.201 Good to excellent yields of arylation products were obtained with aryl diazonium salts bearing electron-withdrawing groups (69.5-69.7), whereas employment of their more electron-rich counterparts (69.8) was less efficient and required higher catalyst loading. Pyridines (69.9-69.12) and pyrimidine (69.13) were also suitable directing groups for this method (Scheme 69). The authors proposed a dual catalytic cycle composed of a photoredox cycle and a traditional cross-coupling cycle. 202 In the photoredox cycle, the photoexcited catalyst 69.4 undergoes oxidative quenching in the presence of diazonium salt, resulting in the formation of a Pd(III) species and an aryl radical. Of note, this represents a rare example of oxidative quenching cycle that starts from Pd(II). The formed aryl radical then adds to intermediate A, presumably generated via the concerted metalation-deprotonation (CMD) path, 203,204 leading to another Pd(III) species B bearing both coupling partners at the palladium. An oxidatively induced reductive elimination then occurs upon SET between these two Pd(III) entities, producing the coupling product 69.3. In the same report, the authors also utilized 69.4 as a photoredox catalyst for the oxidative amination of aldehydes 70.1. In this case, however, 69.4 only catalyzes the generation of hydrogen peroxide, which is known to promote the formation of 70.3 via hemiaminal A, 205,206 and is not directly involved in the bond forming/breaking event (Scheme 70).

Scheme 69. Directed C-H Arylation via Pd II/III/IV Cycle

Scheme 70. Oxidative Amination of Aldehydes

In 2019, Liang, Chen, and co-workers described an intermolecular, visible light-induced palladium-catalyzed C-(sp²)—H heteroarylation. ²⁰⁷ Employment of substantial excess of (hetero)arenes 71.2 or 71.3 (10 equiv) was necessary for this transformation. Pyrrole (71.6–71.7), indole (71.8), and electron-rich aromatics (71.9–71.10) were functionalized in moderate to good efficiency. In addition, triethyl phosphite was a suitable radical acceptor, furnishing phosphonate 71.11 in good yield (Scheme 71).

In 2020, Gevorgyan's group developed the method that allows for generation of aryl radicals from aryl triflates. ¹⁸⁹ Given wide availability of phenol precursors for aryl triflates, this method

Scheme 71. C-H Heteroarylation of (Hetero)arenes

substantially expands the pool of aryl radical precursors. In the reported protocol, the C-O bond of triflates 72.1 underwent fragmentation to produce aryl radical, which upon a sequence of 1,5-HAT, radical cyclization, and rearomatization afforded different heterocyclic cores 72.2. For oxindoles, various functional groups could be introduced at the aromatic ring (72.3-72.5). A tricyclic molecule was also obtained in good yield (72.6). Substitution at the α -carbon could also be varied (72.7). Substrate containing secondary α -C-H site also underwent cyclization, albeit with a diminished yield (72.8). Notably, substrates containing enolizable carbonyl groups reacted smoothly to give spirocyclic scaffolds 72.9 and 72.10 in good yields, showcasing the mildness of the reaction conditions. 208,209 Cyclization of meta-substituted substrate led to regioisomeric products (72.11). The observed unexpected preference for cyclization at α - over β -site may stem from the relative stability of the resultant radical upon cyclization. In case of a linear alkyl chain in which β -hydrogen atoms were present, enamide 72.12, the product of side desaturation reaction, was mainly obtained. By switching the linker connectivity, the same method allows for the access to isoindoline-1-one cores (72.13-72.16). The intermediacy of aryl radical in this transformation was confirmed by deuterium-labeling studies with substrates deuterated at the aryl ring (72.17) or the aliphatic C-H position (72.18). In both cases, formation of aryl radical would lead to the same intermediate A via either 1,5-DAT (72.17) or 1,5-HAT (72.18) (Scheme 72). The following cyclization step could occur at either C2- or C6-position, thus leading to a statistical loss of the deuterium label (47.5% or 37%). If the reaction proceeded via alternative CMD pathway, 210 no deuterium incorporation should be expected in the former case, whereas a complete preservation should be observed in the latter. 208,209 The latter mechanism was ruled out as the experimental values matched the theoretical values predicted for the radical mechanism.

5.3. Fragmentation of C(sp³)–X Bond

5.3.1. Desaturation. In 2017, Gevorgyan's group reported a remote desaturation of aliphatic alcohols 73.1. To achieve HAT beyond proximal C–H sites (Scheme 66), more flexible, easily installable/removable iodomethylsilyl tethers were employed. ^{211,212} This enabled desaturation of 73.1 to the

Scheme 72. Generation of Aryl Radicals from Aryl Triflates

corresponding allylic, homoallylic, and bis-homoallylic alcohols 73.2. In general, primary, secondary, and tertiary alcohols were all suitable substrates. For γ -/ δ -desaturation products, formed via 1,6-HAT, various functionalities, such as primary alcohol (73.3) and amide (73.4), were tolerated. Desaturation of (-)-menthol derivative occurred exclusively at one of the two tertiary γ -sites, which could be rationalized based on geometrical reasoning. ¹⁹⁹ A preference for γ - over β - or δ -C–H sites was also observed, thus allowing for the regioselective desaturation of substrates possessing C-H bonds of comparable BDEs (73.6). Excellent regiocontrol was maintained in more complex setting (73.7-73.8). Desaturation toward allylic alcohols proceeding via β-/γ-desaturation (73.9–73.11) also showed high regiocontrol. This method is also applicable to less common 1,7-HAT, furnishing δ -/ ε -desaturation products 73.12–73.14 in moderate to good yields. The high regioselectivity observed across the scope highlights the advantage of this protocol over those operating via RPC scenario. 199 A linear Stern-Volmer relationship confirmed the role of 73.1 as a quencher in the redox cycle. Besides, isotope-labeling experiments indicated the formation of silylmethyl radical and that the HAT being the rate-determining step (parallel KIE = 3.5). Furthermore, kinetic studies were

carried out using substrate 73.15, which revealed the following HAT aptitude: $1,6-(\gamma) > 1,5-(\beta) > 1,7-(\delta)$ (Scheme 73).

Scheme 73. Remote Desaturation of Aliphatic Alcohols

In 2018, the groups of Shang and Fu described the use of RAEs 74.1 as a source of alkyl radical 213,214 to produce desaturation products 74.2 upon β -H loss.²¹⁵ A dual ligand system was found to be crucial, as much lower yield was obtained without CyJohnPhos. A variety of primary (74.3-74.4), secondary (74.5-74.7), and tertiary (74.8-74.9) RAEs were successfully employed in this reaction. It is noteworthy that allyl arenes such as 74.4 did not isomerize to the more stable styrene derivatives under these mild reaction conditions. Complex molecules also underwent smooth transformation (74.10). α -Heteroatoms could also be tolerated; thus, an array of functionalized enol ethers (74.11) and enamides (74.12-74.13) were obtained in good yields. In addition, this method was applied to a three-step synthesis of chondriamides A and C in good overall yield. Involvement of alkyl radicals in this reaction was examined by EPR studies of 74.16 with 5,5dimethyl-1-pyrroline N-oxide (DMPO) as a spin trap. The EPR signals showed hyperfine coupling constant indicative of the adduct 74.17 upon blue LED irradiation, thus providing an additional evidence for alkyl radical formation under this visible light-induced palladium-catalyzed transformation (Scheme 74).

Scheme 74. Decarboxylative Desaturation of RAEs

5.3.2. Heck and Heck-type Reactions. *5.3.2.1.* Direct Heck and Heck-type Reactions. In comparison to their aryl counterparts, alkyl halides are notoriously less reactive toward oxidative addition with Pd(0) owing to the more electron-rich $C(sp^3)-X$ bond. Secondary and tertiary alkyl halides are in particular more challenging substrates, as they are also more prone to undesirable premature β -H elimination. Although palladium-catalyzed alkyl Heck reactions have been reported, $^{177-180}$ the harsh reaction conditions render these methods less stereoselective and less functional group-tolerant.

In 2017, Gevorgyan's group reported the first visible light-induced alkyl Heck reaction. ¹⁸⁴ This work was inspired by the successful generation of hybrid alkyl palladium-radical intermediates under thermal conditions, 178,179,212,180 as well as by the effective utilization of visible light for generation of hybrid aryl palladium-radical species (Scheme 66). This room-temperature alkyl Heck reaction allows for alkylation of vinyl (hetero)arenes **75.1** with excellent *E*:*Z* selectivity. Alkyl halides **75.2** containing a collection of α -heteroatoms, including pinacolboronyl- (75.4), phthalimidyl- (75.5), pivaloyl- (75.6), silyl- (75.7), phosphonyl- (75.8), sulfonyl- (75.9), germyl- (75.10), and stannyl-(75.11) methyl halides, were found to be competent reaction partners, furnishing valuable allylic synthons in good yields. In general, alkyl iodides were higher yielding than the corresponding bromides (yields in parentheses). Remarkably, these functionalized alkyl halides were not efficient under conditions of thermal alkyl Heck reaction. $^{177-180}$ It is worth mentioning that simple primary (75.12) and secondary (75.13) halides possessing β -hydrogen atoms gave comparable yields to those

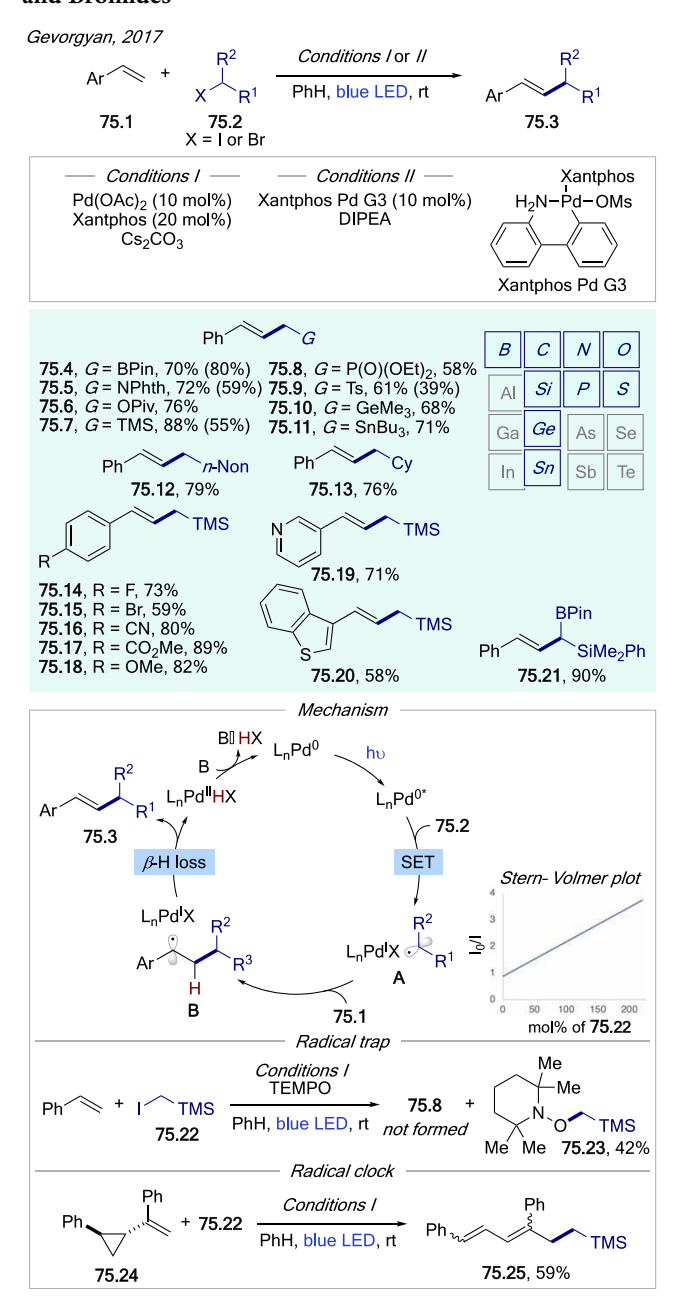
obtained under thermal conditions but with superior stereoselectivity. This transformation was found to be insensitive to the electronic nature of alkene 75.1, delivering the respective Heck products 75.14-75.18 with similar efficiency. Vinyl heteroarenes were also smoothly alkylated (75.19-75.20). Notably, this protocol allows for expedient access to a synthetically versatile mixed B/Si allylic synthon 75.21. Mechanistic studies provided support for Pd(0/I/II) catalytic cycle and involvement of alkyl radical intermediates in this novel light-induced transformation. Thus, analysis of UV-vis spectra confirmed palladium catalyst to be the single light-absorbing species in the reaction mixture, whereas fluorescence quenching studies indicated that alkyl halides were quenching the photoexcited Pd(0). The radical trapping experiment supported the formation of alkyl radicals, as the reaction of styrene and iodide 75.22 led to adduct 75.23 in 42% yield in the presence of TEMPO. Furthermore, the radical clock experiment using vinyl cyclopropane 75.24 gave only ring opening product 75.25, therefore supporting a radical addition step in the catalytic cycle (cf. Schemes 66, 75).

Shortly after Gevorgyan's group report, Shang and Fu's groups independently disclosed an alkyl Heck reaction with unactivated alkyl bromides 76.2. 186 Primary alkyl bromides with pendant functional groups efficiently participated in this reaction (76.4-76.6). Reactions with secondary and tertiary bromides also occurred with good to high yields (76.7–76.11). Diversely substituted styrene derivatives were viable substrates for this transformation (76.12–76.15). In particular, substrate bearing an aryl boronate ester fragment did not undergo side reactions such as Suzuki coupling or oxidative Heck reaction (76.12). 2-Vinylpyridine also proved compatible (76.16). Notably, 9-vinylcarbazole and acrylamide were also reactive substrates, affording the corresponding products in good yields (76.17–76.18). The radical clock experiments using bromides 76.20 and 76.21 were conducted to produce rearranged products 76.22 or 76.23, respectively. Importantly, competition experiment showed that tert-butyl bromide was more reactive than *n*-butyl bromide, contrasting the reactivity trend observed for S_N 2-type oxidative addition. Labeling experiment using *d*-76.24 revealed a small intramolecular KIE. This led the authors to propose β -H elimination, rather than bromine atom transfer/ elimination sequence, to be involved in the catalytic cycle (Scheme 76).²¹⁸ It should be noted that previous kinetic studies on Heck reaction of styrene with iodobenzene disclosed a substantially higher value of KIE (3.0); ²¹⁹ thus, β -H elimination may not be the only pathway in this radical Heck reaction. In addition, X-ray photoelectron spectroscopy (XPS) was employed, and the signals corresponding to Pd(II), Pd(I), and Pd(0) were detected, providing further support for the intermediacy of Pd(I) species in the catalytic cycle.

In the past few years, the visible light-induced palladium-catalyzed alkyl Heck reaction has enjoyed a substantial development. The contributions from different research groups toward the employment of various alkyl radical precursors are summarized in Scheme 77.

In 2018, Gevorgyan's group expanded the electrophile scope to activated and unactivated tertiary alkyl halides (77.4-77.10). Heck reaction with acrylonitrile was also found feasible (77.11). The authors also demonstrated that Heck reaction with tertiary alkyl halides bearing an activating group at the α -carbon, such as ester, boronate, phosphonate, and sulfonate, required no blue LED irradiation. Recently, Novák's group adopted a similar catalytic system for the fluoroalkylation

Scheme 75. Heck Reaction with Functionalized Alkyl Iodides and Bromides



of styrene derivatives, providing a complementary approach toward valuable fluorinated synthons (77.12–77.19). ²²⁰

In 2020, Shang, Fu, Chen, and co-workers reported the employment of α -amido- and α -siloxystyrenes in alkyl Heck reaction enroute to α -alkylated ketones and imines (77.20–77.32). For enamides, density functional theory (DFT) calculations suggested β -H elimination occurred at the nitrogenrather than at the carbon atom, thus affording imine products directly. The authors also provided computational evidence for the formation of a hybrid alkyl palladium-radical, which in its triplet state was kinetically stable against radical recombination. In addition, Pd(I) coordinated to one Xantphos and one PPh₃ ligand was found to be more stable than that with three PPh₃ ligands by 5.1 kcal/mol, which might explain why in many cases a dual ligand system is advantageous. More recently, Liang's group disclosed the use of α -bromosugars in Heck reaction for

Scheme 76. Heck Reaction with Unactivated Alkyl Bromides

synthesis of *C*-vinyl glycosides. Various styrene derivatives were compatible, delivering products in moderate to good yields (77.33–77.37). This protocol was also applicable to a range of carbohydrate derivatives (77.38–77.39). Importantly, the β -anomer was obtained as the major product in this transformation, contrasting the observed α -selectivity in related processes under free radical α -variable or photoredox conditions.

Very recently, Hong's group accomplished alkyl Heck reaction using unactivated alkyl chlorides, thus significantly broadening the scope of alkyl electrophiles. Similar to previous cases, high functional group tolerance was observed (77.40–77.44). Remarkably, secondary and even primary alkyl chlorides reacted smoothly under these reaction conditions (77.45–77.47). Besides, radical acceptors other than styrene derivatives (77.48–77.49), as well as natural product derivatives (77.50–77.51), were also compatible. It is noteworthy that this protocol could be applied to double Heck reaction with 1,5-dichlorides, thus delivering annulation products, such as piperidine derivative 77.52, in a single

Scheme 77. Heck Reactions of Different Alkyl Electrophiles

operation. On the basis of the kinetic studies and DFT calculations, the authors proposed that the catalytic cycle involves chlorine atom transfer to hybrid benzyl palladium-radical to form benzyl chloride, which then undergoes elimination in the presence of base to furnish the alkene product.

The use of RAEs in alkyl Heck reaction was independently reported by the groups of Shang and Fu, ¹⁹² and Glorius ¹⁹¹ in 2018. Differently substituted styrene derivatives were competent substrates (77.53–77.57, 77.62–77.65). Primary, secondary, and tertiary RAEs were all reactive under these reaction conditions. This method expands the scope of available electrophilic components for alkyl Heck reaction and is advantageous when the analogous halides are difficult, if not impossible, to obtain (77.59–77.61, 77.67–77.68).

In 2019, Rueping, Cavallo, and co-workers described an interesting decarboxylative alkylation of cinnamic acid derivatives 78.1 leading to olefins 78.3. Since cinnamic acid derivatives are broadly available, they can serve as a practical styrene surrogate for Heck-type reaction. Tertiary and secondary alkyl bromides were efficient coupling partners (78.4–78.9), whereas primary alkyl bromides led to diminished yields, as they were more susceptible to the side esterification reaction (78.10–78.12). It was found that electron-rich cinnamic acid derivatives were more effective in this Heck reaction (78.13–78.18). Notably, α -fluorocinnamic acid was successfully transformed to the fluorine-containing alkene 78.19. The DFT calculations supported selective radical addition at α -carbon over that at β -carbon (by 2.1 kcal/mol

for cinnamic acid). The computations also indicated that the decarboxylation step involves a concerted elimination of CO_2 and B·HBr from 78.20 via the transition state A, facilitated by a $[B \cdot H]^+$ -Br interaction. Importantly, the authors revealed a SOMO-LUMO interaction between photoexcited Pd(0) species 78.21 and alkyl bromide, which was calculated to be -10.6 kcal/mol (C) (Scheme 78). Since only 6.0 kcal/mol was

Scheme 78. Decarboxylative Alkylation of α,β -Unsaturated Carboxylic Acids

required for geometrical reorganization of the reactants, the generation of species \mathbf{D} could be considered barrierless (-4.6 kcal/mol). This interaction, as mentioned in the Introduction (Figure 5), provides an explanation for the ability of photoexcited Pd(0) to engage unactivated alkyl halides with high reduction potentials via an inner sphere pathway.

Radical addition to imines has long been recognized as a versatile approach toward synthesis of amines. ^{228,229} Current methods are largely reductive in nature; thus, the imine moiety is usually lost after the transformation. Very recently, Gevorgyan and co-workers reported a C–H alkylation of oximes **79.1**, which represents an "oxidative" process, wherein the imine double bond functionality is preserved. ²³⁰ A broad range of functionalized alkyl halides were compatible reaction partners (**79.4**–**79.9**). Complex molecules, such as β -D-ribofuranoside derivative **79.10**, were also accessible via this method. Secondary (**79.11**–**7914**) and tertiary (**79.15**–**79.17**) alkyl bromides and iodides served as efficient electrophilic component in this Hecktype reaction. Interestingly, a halide dependence of E/Z selectivity was observed (**79.13**–**79.14**). In addition to benzylic oximes, styryl- (**79.18**) and alkyl-substituted (**79.19**–**79.20**)

oximes were found to be viable substrates. Notably, substrates bearing easily removable trimethylsilylethoxymethyl (79.21) and benzyloxymethyl (79.22) groups were also amenable to this transformation. The authors proposed a catalytic cycle resembling that of alkyl Heck reaction. First, the photocatalytically generated radical species A undergoes radical addition to indium-activated substrate B to form hybrid aminyl palladiumradical species C. A direct HAT can then afford product 79.3 (not shown for clarity; cf Schemes 66 and 75). Alternatively, a recombination may occur to form Pd(II) complex D, which may in turn be in equilibrium with alkoxyamine E. Intermediate D then undergoes either classical (path a) or base-assisted (path b) β -H elimination to furnish product 79.3. The recombination pathway was supported by the observation of E in the reaction mixture. Besides, benzyloxyamine 79.24 was converted to oxime 79.14 in the reaction between substrate 79.23 and bromocyclopentane, validating the involvement of E, and therefore D, in the catalytic cycle (Scheme 79). A profound base effect on the stereochemical outcome was found when alkyl bromide was used, while the influence of base was marginal in the case of iodide. Thus, both paths a and b are plausible depending on the

5.3.2.2. Cascade Heck Reactions. Although Heck reaction represents one of the most efficient ways for alkenylation, a prefunctionalized reaction partner, such as an organic halide, is typically required. However, accessing such a molecule with the halide functionality at the desirable site may not be trivial, especially in aliphatic systems. To address this synthetic challenge, in 2019, Gevorgyan's group developed an aliphatic radical Heck reaction (Scheme 80), 105 which combined a remote C(sp3)-H activation and an alkyl Heck reaction (cf. Schemes 73 and 75). Substrates 80.1, which are readily synthesized via a routine silylation of the respective secondary or tertiary alcohols, underwent selective alkenylation at remote, unactivated β -, γ -, or δ -C(sp³)—H site to form alkenols **80.3**. It is noteworthy that switching the ligand from 66.3 to Xantphos proved to be crucial, as it substantially reduced the amount of the desaturation side product. Michael acceptors, such as acrylonitrile (80.4-80.6), and electronically diverse styrene derivatives (80.7–80.11) were competent alkene substrates. As established earlier, 1,6-HAT was found to be favorable over 1,5-HAT (80.6) and 1,7-HAT (80.12), resulting in excellent regioselectivity. Remarkably, alkenylation could also occur at more challenging secondary C-H sites (80.13). Likewise, alkenylation at tertiary β -sites afforded homoallylic alcohols in moderate yields (80.14-80.16). Diminished regiocontrol was observed in the presence of a secondary γ -C-H site (80.15). This protocol was also applicable to more challenging δ -Heck reaction (80.17– **80.19**). Analysis of the reaction profile revealed the formation of XAT intermediate at the early stages of the reaction, which was then gradually converted to the product. This was substantiated by a stoichiometric reaction of substrate 80.20, wherein translocated alkyl iodide 80.21 was formed in the absence of the alkene partner and the base. Furthermore, independently synthesized 80.21 was readily converted to the Heck products 80.22 or 80.23 when subjected to the standard conditions, thus providing additional evidence of the involvement of translocated alkyl iodide in this reaction (Scheme 80).

In 2020, Glorius' group described a cascade cyclization/Heck reaction of olefin-tethered aryl or alkyl bromides **81.1** in the presence of radical acceptors **81.2**, leading to diverse allylated heterocycles **81.3**. The reaction begins with photoinduced generation of aryl or alkyl radical, which upon 5- or 6-exo-trig

Scheme 79. Heck-type Reaction of Oximes

cyclization forms a translocated alkyl radical. The latter then undergoes an alkyl Heck reaction to furnish the product. It should be noted that this method represents one of the few approaches toward quaternary carbon synthesis via dicarbofunctionalization of olefins. ^{232–234} This protocol demonstrated high functional group tolerance. Thus, styrene derivatives (81.4–81.6) and vinyl heteroarenes (81.7) underwent smooth reaction to produce dihydrobenzofurans. Acrylamide was also fairly reactive (81.8). Fused ring structure 81.9 could also be

Scheme 80. Radical Relay Heck Reaction of Aliphatic Alcohols

obtained in good diastereoselectivity. Moreover, other types of heterocyclic cores were also accessible including fused pyridine (81.10), benzimidazole (81.11), indoline (81.12–81.14), oxindole (81.15–81.16), tetrahydrofuran (81.17), piperidine (81.18), and pyrolidine (81.19) (Scheme 81).

Recently, Duan's group demonstrated that, in addition to HAT and radical addition shown above, a Dowd-Beckwith reaction ^{235,236} could be coupled with alkyl Heck reaction leading to ring expansion products 82.3. ²³⁷ Various vinyl (hetero) arenes were examined in this reaction exhibiting a significant electronic effect (82.4–82.11). Low yields were obtained in case of electron-deficient styrene derivatives, presumably due to the polarity mismatch. 1,1-Disubstituted alkenes (82.12), as well as natural product derivatives (82.13), showed to be viable substrates. Silyl enol ethers and enamides were also compatible alkene partners. The authors also achieved ring expansion to larger than six-membered ring systems under slightly modified reaction conditions, albeit in moderate yields (82.14–82.16). Of note, rearrangement also occurred with the acyclic substrate

Scheme 81. Quaternary Carbon Synthesis via Cascade Cyclization/Heck Reaction

(82.17). On the other hand, chain extension proved to be challenging and dependent on the chain length. Thus, substrate 82.18 bearing two methylene units produced the premature Heck reaction product 82.20 instead of the targeted product 82.19, whereas substrate 82.21 bearing three methylene groups led to comparable amounts of products 82.22 and 82.23 (Scheme 82).

5.3.3. C–**H Alkylation.** In addition to Heck reaction, hybrid alkyl palladium-radical species could also engage in various types of C-H alkylation. Thus, in 2017, Yu group disclosed a $C(sp^3)$ -H alkylation of N-aryl tetrahydroisoquinoline (THIQ) derivatives 83.1. 185 A variety of primary (83.4-83.7), secondary (83.8-83.14), and tertiary (83.15-83.17) alkyl bromides were efficiently coupled with N-phenyl THIQ, showcasing the generality and good functional group tolerance of this protocol. The aryl group at nitrogen, as well as the substituent at the benzene ring of THIQ, could also be varied (83.18-83.21) to produce the respective alkylation products in moderate to good yields. As discussed above, the reaction begins with the formation of hybrid alkyl palladium-radical A upon SET from photoexcited Pd(0) to alkyl bromide. The next step involves another SET event from THIQ derivative 83.1 to A leading to the aminium radical cation \mathbf{B} and regenerated Pd(0) catalyst. It is worth mentioning that THIQ derivatives have been extensively used in related processes due to their ability toward facile single electron oxidation. 238,239 On the contrary, formation of analogous radical cation from other benzyl amines, such as N-methylbenzylamine, is much more difficult, thus explaining the lack of reactivity. Intermediate B then undergoes a facile deprotonation to form α -amino radical C, as evidenced by the formation of adduct 83.23 in radical trapping experiment.

Scheme 82. Dowd-Beckwith Ring Expansion/Heck Reaction Cascade

Intermediate C upon cross-recombination with alkyl radical-affords α -alkylation product 83.3 (Scheme 83).

In the same report, the authors also explored alkylation of heteroarenes (Schemes 84a and 88). Intramolecular alkylation of indole derivatives 84.1 was found to be feasible under similar reaction conditions to deliver cyclization products in good to excellent yields (84.3–84.6). Similarly, Liang, Chen, and coworkers employed α -haloamides 84.7 for synthesis of oxindoles 84.8. ²⁰⁷ Differently substituted oxindoles (84.9–84.18) could be obtained in moderate to excellent yields using this method. A tricyclic core was also accessible (84.19). Good regiocontrol was maintained in reaction of 3,3′-unsymmetrically disubstituted starting material (84.20).

Furthermore, Yu and co-workers showed that alkylation using 1-adamantyl bromide could also occur in an intermolecular fashion with electron-deficient heterocycles such as benzoxazole (85.4), thiophene (85.5), and pyridine *N*-oxide (85.6). Shang and Fu's groups carried out more detailed studies on the scope of heterocycles and alkyl bromides. In line with Yu's work, they found that electron-withdrawing groups on the heterocycles were crucial in this transformation (85.7–85.10). In addition, they showed that secondary alkyl bromides were also competent reaction partners (85.11–85.12) (Scheme 85).

In 2018, Zhou's group disclosed an intermolecular alkylation of electron-deficient arenes as a complementary approach to Fridel-Crafts alkylation of electron-rich systems. ²⁴¹ In this report, both thermal- $(100-130 \, ^{\circ}\text{C})$ and visible light-induced

Scheme 83. Alkylation of N-Aryl THIQ Derivatives

conditions were examined. Tertiary 1-adamantyl bromide gave product **86.4** with complete regiocontrol. Generally, under both conditions for secondary bromides a comparable regioselectivity at C2- over C4-position was observed (**86.5**, **86.7**–**86.9**). Notably, primary alkyl bromide was only reactive in the presence of light irradiation, highlighting its pivotal role in the formation of primary alkyl radicals (**86.6**) (Scheme **86**).

83.22

not formed

O 83.23, 16%

Ft

Εt

More recently, Hong group expanded the substrate scope to unactivated arenes. 242 In this case, the arene substrate was used as a solvent to guarantee efficient capture of alkyl radical. Although, primary alkyl bromides bearing a variety of functionalities reacted smoothly (87.4–87.11), higher yields were obtained in the case of secondary (87.12–87.15) and tertiary (87.16) bromides. Derivatives of aceclofenac (87.17) and febuxostat (87.18) were readily arylated in moderate yields. In case of substituted arenes, a mixture of regioisomers was obtained (87.19–87.21), with selectivity governed by both inductive and mesomeric effects. 243 Notably, the reaction yields diminished with the increasing number of fluorine substituents

Scheme 84. Intramolecular Alkylation en Route to (a) N-Fused Indoles and (b) Oxindoles

Scheme 85. Intermolecular Alkylation of Electron-Deficient Heterocycles

at the arene (87.22–87.24), culminating in completely unreactive pentafluorobenzene. The proposed catalytic cycle features a bromine atom transfer step of radical species B, which regenerates Pd(0) for the next cycle, while the concomitantly formed cyclohexadienyl bromide C undergoes rearomatization upon elimination of HBr to afford reaction product 87.3. The XAT step was supported by a series of mechanistic studies. First, significant electronic effect was observed (87.22–87.24), thus invoking a mechanism different than recombination/ β -H elimination. Accordingly, an inverse secondary KIE value of 0.88 was obtained from the parallel experiments of benzene and benzene- d_{6} , suggesting a rate-determining step involving change

Scheme 86. para-Selective Alkylation of Electron-Deficient Arenes

in hybridization of carbon from sp² to sp³.²⁴⁴ Besides, an absence of intramolecular KIE of substrate **87.26** was in good agreement with the computed value (Scheme 87).

5.3.4. Multicomponent Reactions. As detailed in Sections 5.3.2 and 5.3.3, it has been established by different groups that hybrid alkyl palladium-radical undergoes radical addition to unsaturated entities such as alkenes and (hetero)arenes. The resultant radical species then either recovers the alkene moiety or rearomatizes upon loss of hydrogen atom. On the other hand, engaging this radical intermediate in further reactions can lead to more complex transformations. In this regard, several multicomponent reactions (MCRs) have been developed. Thus, in 2018, Yu and co-workers reported an oxyalkylation of allylic amines 88.1 with alkyl bromides and CO₂, leading to diverse five-membered cyclic carbamates 88.3.²⁴⁵ In general, substrates bearing electron-rich aryl group gave better yields than those with electron-deficient ones (88.4-88.7). The substituent at nitrogen could also be varied (88.8-88.9). Notably, internal alkene moiety was also reactive, delivering product 88.10 in moderate yield. Other tertiary (88.11), as well as secondary (88.12-88.13) alkyl bromides, reacted smoothly to give products in good yields. Primary alkyl bromides were also compatible, featuring 88.14 containing a ketal functionality. Mechanistically, this transformation involves an off-cycle in situ formation of carbamate A via a nucleophilic attack of CO2 by substrate 88.1 in the presence of base. 246 Intermediate A then enters the catalytic cycle upon reaction with hybrid alkyl palladium-radical B. The resultant intermediate C undergoes RPC to generate carbocation D, which upon intramolecular nucleophilic trapping delivers cyclic carbamate 88.3. Control experiment without CO2 ruled out possible intermediacy of aziridine intermediate 88.16 (Scheme 88). This was further emphasized by its lack of reactivity under standard reaction conditions.

Later in 2019, a closely related transformation was disclosed by Cheng's group. In this case, six-membered cyclic carbamates 89.3 were synthesized from 2-(1-arylvinyl)anilines 89.1 under similar reaction conditions. As in the previous report, this protocol was applicable to a variety of alkyl bromides (89.4–89.8) and differently substituted anilines (89.9–89.12). Similar detrimental effect of electron-withdrawing substituents was also observed (89.13). It was also shown that the phenyl group could be replaced with heteroarenes (89.14–89.15) (Scheme 89).

Scheme 87. Intermolecular Alkylation of Unactivated Arenes

Although RAEs have been used as both carbon and nitrogen sources, 213,214 their use in palladium photocatalysis remained limited to an alkyl radical precursor (cf. Scheme 77). In 2020, Glorius group utilized RAEs as a bifunctional reactant to achieve 1,4-aminoalkylation of conjugated dienes 90.1. This work highlights a complementary radical approach toward synthetically useful π -allylpalladium intermediates. In general, RAEs derived from tertiary (90.4), secondary (90.5), and primary (90.6) carboxylic acids were all effective, with diminished regioselectivities observed in the latter cases. In addition to butadiene, various substituted dienes were also reactive, delivering the products in moderate to good yields (90.7–90.11). As in the previous cases, amino acid derivatives were competent reaction partners (90.12–90.14). The general-

Scheme 88. Oxyalkylation of Allylic Amines Leading to Five-Membered Cyclic Carbamates

Scheme 89. Synthesis of Six-Membered Cyclic Carbamates

ity of this protocol was further demonstrated by the successful modification of complex molecules (90.15-90.16). This

sequential transformation operates via alkyl radical addition to diene substrate leading to hybrid allyl palladium-radical **B** and its subsequent RPC to classical π -allyl complex **C**, whose intermediacy was verified by the observation of **D** by HRMS analysis. A nucleophilic substitution with phthalimide anion, concomitantly formed upon generation of hybrid species **A**, furnishes allylic amine **90.3** and recovers Pd(0) catalyst (Scheme 90).

Scheme 90. 1,4-Aminoalkylation via Radical Generation of π -Allylpalladium

Shortly after, the same group reported a related multicomponent reaction. In this case, alkyl bromides reacted with 1,3-dienes and a variety of nucleophiles, enabling the synthesis of diverse 1,4-carbofunctionalization products 91.4 with high functional group tolerability. Similarly, differently substituted alkyl bromides smoothly reacted to deliver products in good to excellent yields (91.5–91.7). The authors also demonstrated a remarkably broad scope of nucleophiles, ranging from aliphatic amines (91.10–91.11), carbon-based pronucleophiles (91.12–91.13), phenols (91.14–91.17), to sulfinates (91.18–91.22) (Scheme 91), highlighting the generality of this protocol. A related three-bond forming cascade radical cyclization/addition/allylic substitution was also achieved recently. 252

confirmed by HRMS

Scheme 91. Three Component 1,4-Carbofunctionalization of Conjugated Dienes

Simultaneously with Glorious group's report on 1,4-carbofunctionalization of dienes, a report from Gevorgyan group described a three component 1,2-carbofunctionalization of substituted dienes 92.1.²⁵³ This reaction tolerates a broad range of electronically diverse dienes and exhibits high levels of regioand stereoselectivities (92.5-92.11). Aliphatic dienes were also reactive, delivering allylic amines 92.12-92.13 in good yields. A mixture of 1,2- and 1,4-adducts was observed in the latter case, which could be rationalized by the formation of π -allylpalladium intermediate with almost indistinguishable steric and electronic environments at both termini. Trisubstituted alkenyl amine 92.14 could also be obtained via this approach. Various primary (92.15) and secondary (92.16-92.17) alkyl iodides were efficient reaction partners, leading to the corresponding allylic amines in good yields and high selectivity. Sterically demanding tertiary alkyl iodide, however, gave almost equimolar amount of regioisomers (92.18). Furthermore, various nitrogen- (92.19), oxygen- (92.20), and carbon-based (92.21) nucleophiles were capable reactants in this transformation. In line with the previous reports, 1,4-addition product was obtained exclusively when 2,3butadiene was used (92.22). Interestingly, the authors observed a substantial counterion effect in this reaction. Control experiments indicated that the reaction of the benchmark diene 92.23 gave desired product 92.25 in 44% yield only in the absence of AgNTf₂, in sharp contrast to 89% yield obtained with catalytic amount of AgNTf2. The diminished yield was attributed to the significant formation of radical dimerization side product 92.26. To gain further insights into the role of triflimide anion, π -allylpalladium complexes bearing iodide (92.27) or triflimide (92.28) counterion were subjected to the reaction with TEMPO under both thermal and visible light conditions. It was found that the iodide complex gave appreciable amount of TEMPO adduct 92.29 under both conditions, whereas the triflimide complex was less reactive, and

did not form the adduct under thermal conditions at all (Scheme 92). These results suggest that triflimide anion was capable of stabilizing π -allylpalladium against undesirable in this case photoinduced homolysis of Pd complex.

Scheme 92. Three Component 1,2-Carbofunctionalization of Conjugated Dienes

Transition metal-catalyzed carbonylation using CO has found numerous applications in synthesis of carbonyl compounds. ^{254–256} In 1974, Heck and co-worker disclosed the first palladium-catalyzed carbonylative transformation of aryl, vinyl, and benzyl halides under thermal conditions. ^{257,258} In their 1982 report on amidation of organic halides, Tanaka group showed that ethyl iodide could be efficiently transformed into the corresponding amide under high temperature and pressure. ²⁵⁹ Several years later, Watanabe group employed UV irradiation to achieve analogous reactions at room temperature and ambient pressure, ²⁶⁰ followed by Suzuki and Miyaura's work

in 1991.²⁶¹ A series of photoinduced carbonylative reactions of alkyl iodides using xenon lamp was then accomplished by Ryu and co-workers.^{262–269,173} In 2016, Alexanian's group reported a notable example of engaging unactivated secondary alkyl bromides in alkoxycarbonylation at low CO pressure and slightly elevated temperature.²⁷⁰

Although a broad range of organic halides and nucleophiles have been successfully employed in palladium-catalyzed carbonylation reactions, they are not without limitations. Broadly speaking, there is a trade-off between the generality of organic halides and nucleophiles. For instance, catalytic systems facilitating the oxidative addition step are less efficient at reductive elimination, thus limiting the choice of nucleophiles. This is further accentuated when coordination of nucleophile to palladium is needed. On the contrary, the systems with better reductive elimination enable reaction with a wide array of nucleophiles, but at the expense of the necessity to employ more reactive organic halides. Very recently, Arndtsen's group described a visible light-induced carbonylation reaction that bridged this gap. 181 Various electronically diverse aryl iodides and bromides reacted smoothly with nitrogen-, oxygen-, and carbon-based nucleophiles in good to excellent yields (93.6-93.10). Notably, sterically hindered anilines (93.11) and alcohols (93.12) were competent nucleophiles even when unactivated alkyl halides were used. (Hetero)arenes (93.13) and thiols (93.14) were also compatible nucleophiles. Furthermore, in the absence of nucleophiles, aliphatic acid chlorides, synthesis of which typically requires pressing reaction conditions, ²⁷¹ could be obtained using this mild protocol (93.15–93.19). The authors proposed a dual role of visible light irradiation in this transformation. Upon photoinduced generation of radical species A, an addition to CO occurs forming acyl Pd(II) complex B. A ligand exchange with n-Bu₄NCl then follows to generate C. Next, a second photoinduced event, a homolytic cleavage of Pd-C bond, leads to hybrid acyl palladium-radical species D. A subsequent XAT to the acyl radical moiety furnishes acid chloride 93.5, which can then be trapped in situ or ex situ by nucleophile to afford product 93.4. The pivotal role of light in the reductive elimination step was confirmed by control studies using complex 93.20, from which efficient formation of acid chloride 93.21 was observed only upon irradiation. Of note, a concomitant formation of palladium complex 93.3, used in some cases as the catalyst, was also confirmed (Scheme 93). Furthermore, radical trapping experiments using TEMPO and n-OctSH indicated the formation of acyl radical, thus corroborating a photoinduced homolytic cleavage of Pd-C bond at play.

Very recently, Koenigs reported a dicarbofunctionalization reaction of terminal alkynes 94.1 with alkyl iodides leading to enynes 94.3 with good to excellent stereoselectivity.²⁷² In general, electron-deficient alkynes were found to be more efficient (94.4–94.9). An interesting switch in E/Z selectivity was observed with substrate containing a para-cyano group (94.7). Heterocycle-substituted enynes were also accessible via this method (94.10). Variation of secondary or tertiary alkyl iodides posed no problem, as well (94.11-94.16). According to the authors, this reaction involves a less studied radical addition of hybrid radical species A to alkyne to give B, followed by recombination of Pd(I) and a vinyl radical. The observed stereoselectivity can be rationalized by the favorable interaction at the less hindered side of vinyl radical, which adopts a linear geometry. The formed vinyl Pd(II) complex C then reacts with another molecule of alkyne to produce intermediate D, which

Scheme 93. Carbonylative Transformation of Organic Halides Featuring a Dual Role of Visible Light

upon reductive elimination furnishes product **94.3** and closes the catalytic cycle (Scheme 94).

5.3.5. Atom Transfer Reactions. In the examples described so far, hydrodehalogenation of aryl or alkyl halides is typically considered an undesirable side reaction. However, one can strategically harness this process, or, in a broader sense, an atom transfer process, in synthetically valuable transformations. In 2019, Liang, Cheng, and co-workers reported a hydrodehalogenation of organic bromides and its extension to deuteration. Thus, a simple reduction using *i*-PrOH, as the hydrogen source, led to a selective reduction of primary alkyl bromides (95.3–95.4). Isolated examples of reduction of secondary (95.5) and tertiary (95.6) alkyl bromides were also

Scheme 94. Dicarbofunctionalization of Terminal Alkynes

demonstrated. This protocol was also applicable to various (hetero) aryl and vinyl bromides (95.7–95.9). By switching the solvent to i-PrOH- d_8 , the authors were able to perform deuteration on (hetero) aryl bromides (95.10–95.13) (Scheme 95). Deuteration of alkyl bromides proved to be more challenging, as desaturation became the major process.

Very recently, Ngai's group reported an interesting transformation featuring selective C2 reduction, deuteration, and

Scheme 95. Reduction and Deuteration of Organic Halides

iodination of carbohydrates 96.1 proceeding via a 1,2-spincenter shift (SCS).²⁷³ This protocol offered a straightforward access to 2-deoxy sugar derivatives, which find numerous applications in different fields, ranging from medicine and molecular imaging to cell engineering. This mild method allows for reduction by DIPEA as a hydrogen atom source. A wide range of protecting groups at α -bromosugars (96.3–96.10) are tolerated, further showcasing the mildness of this method. Natural product or drug derivatives were also viable substrates, delivering products in good to excellent yields and high C2 selectivity (96.11–96.12). Similarly, α -bromosugars were deuterated at the C2 position by switching the base and solvent to Cs₂CO₃ and THF-d₈ respectively, demonstrating high levels of regioselectivity and deuterium incorporation (d-96.9-d-96.10). This atom transfer reaction was further extended to access 2-iodo-2-deoxy sugars using α -iodosugars. In this case, Cs_2CO_3 and t-BuOH, in which no hydrogen atoms are available for HAT, were chosen. The presence of an axial substituent seemed to be beneficial, as excellent equatorial/axial selectivity was observed in 96.13, whereas the selectivity was compromised in the cases of 96.14 and 96.15. This protocol was also efficient in a more complex setting (96.16). The success of these transformations is built on a 1,2-SCS step in the mechanism, which is unprecedented in palladium photocatalysis. Accordingly, intermediate A readily undergoes conformational change to the $B_{2.5}$ boat form A' due to the favorable hyperconjugation between SOMO and σ^* orbital of C-O, which sets the right geometry for an extended anomeric interaction that arises from lone pair interaction of the endocyclic oxygen $(n_O \leftrightarrow SOMO \leftrightarrow$ σ^*_{C-O}). This interaction weakens the C-O bond and thereby drives forward the 1,2-SCS. Mechanistic studies support a concerted [2,3]-acyloxy rearrangement pathway (B). The rearranged radical species C then undergoes atom transfer to deliver reaction product 96.2 (Scheme 96).

5.3.6. Halogenation and Borylation. In 2020, Polyzos, O'Hair, and co-workers reported an example of $C(sp^3)$ -H halogenation of Pd(II) auxiliaries 97.1 using the respective halogen sources (97.2–97.4). ²⁷⁴ This reaction tolerates a range of palladacycles with different α -substituents (97.6–97.17). In general, iodination was more efficient than bromination and chlorination. β -iodination of more challenging α -halogenated substrate was also feasible (97.18). An example of functionalization of a more complex substrate was also demonstrated (97.19). Notably, this transformation could be accomplished in a catalytic fashion starting from substrate 97.20, albeit with a relatively low turnover number. UV-vis absorption studies performed on a benchmark substrate revealed a maximum at 418 nm. The proposed mechanism therefore begins with photoexcitation of substrate 97.1 that leads to excited state 97.1* with mixed MLCT/LLCT characters. Interestingly, upon SET to the halide reagent, Pd(III)X intermediate A is formed instead of the analogous complex bearing the alkyl fragment. Complex A then undergoes either disproportionation to form Pd(IV) complex B (path a) or one-electron oxidation by oxone leading to intermediate C (path b), followed by reductive elimination to furnish C-H halogenation product 97.5 (Scheme 97). Alternatively, a direct reductive elimination of A (path c) may be operative, although a higher energy barrier renders it less likely to be the major pathway. It should be mentioned that this work represents another example that involves less common oxidative quenching of photoexcited Pd(II) complex (cf. Scheme 69).

Scheme 96. Selective C2 Reduction, Deuteration, and Iodination of Carbohydrates via 1,2-SCS

More recently, Liang's group described a borylation reaction of various aryl, vinyl, and alkyl bromides 98.1. 275 Electronically diverse aryl bromides could be transformed into the corresponding aryl boronate esters in moderate to excellent yields (98.3–98.7). 2-Bromopropene also proved to be a viable substrate (98.8). Of note, aryl chloride was also reactive, albeit with lower efficiency (98.9). Besides, primary, secondary, and tertiary alkyl bromides were all reactive (98.10–98.14). Finally,

Scheme 97. C(sp³)-H Halogenation of Pd(II) Auxiliaries

allylic (98.15) and benzylic (98.16) boronates could also be obtained via this protocol. The proposed mechanism involves radical addition of A to B_2Pin_2 to form intermediate B, which upon coordination with phosphate base produces radical species D. An SET from D to Pd(I) then leads to homolytic cleavage of the B-B bond and releases reaction product 98.2 (Scheme 98).

Shortly after, the same group reported the use of olefintethered alkyl halides 99.1 for cyclizative iodination or borylation toward cyclic structures 99.2.²⁷⁶ A wide variety of hetero- and carbocycles with different substitution patterns were accessible via this method (99.3–99.11). It should be mentioned that iodination product 99.3 could be obtained without KI in comparable yield, suggesting that XAT might be operative in this method (Scheme 68). When tertiary alkyl radical forms upon cyclization, a desaturation side reaction instead of iodination occurred (99.12). Similarly, borylation could be performed to access different hetero- and carbocycles in moderate yields (99.13–99.16) (Scheme 99).

Scheme 98. Borylation of Aryl, Vinyl, and Alkyl Bromides

Scheme 99. Cyclization/Functionalization Cascade of Alkene-Tethered Alkyl Halides

В

Α

Liang, 2020

R1

$$X R^4$$
 R^5
 R^6
 R^7
 R^6
 R^7
 $R^$

5.4. Homolytic Cleavage of N-O Bond

The ability of photoexcited Pd(0) to transfer an electron has also been exploited in the cleavage of N–O bond of RAOEs. ^{238,239} In 2019, Shang and Fu's groups employed oxime esters **100.1** and silyl enol ethers **100.2** for synthesis of δ -cyano ketones **100.3**. ¹⁹³ Various (hetero)cyclobutanone oxime esters underwent smooth cascade transformation in good to excellent yields (**100.4**–

100.10). The scope of silyl enol ethers was also found to be broad without noticeable electronic effects (**100.11–100.16**). Notably, aryl iodide functionality was well tolerated under these reaction conditions (**100.12**). Heterocycle-containing substrates were also compatible (**100.17–100.18**). Of note, in the absence of alkene partner, the corresponding allylic cyanide was obtained. According to the proposed mechanism, the photoexcited Pd(0) undergoes SET with substrate **100.1**, leading to hybrid iminyl radical species **A**, which upon strain-release-driven β -scission produces hybrid alkyl palladium-radical **B**. As in alkyl Heck reactions, a subsequent radical addition to alkene followed by β -H loss delivers Heck product **D**, which is readily converted to a ketone product **100.3** under the reaction conditions (Scheme **100**).

Scheme 100. Cascade Ring Opening/Heck Reaction of Oxime Esters

A more recent example involving oxime esters was disclosed by Xia, Zhou, and co-workers.²⁷⁷ In this work, substrate **101.1** undergoes radical addition to tethered olefin upon generation of iminyl radical. The formed hybrid radical species is then trapped by an external alkene to furnish 1-pyrrolines **101.3**. The overall transformation represents an intermolecular Narasaka—Heck reaction.²⁷⁸ Good functional group tolerance was observed across different vinyl (hetero)arenes (**101.4–101.9**). Besides, the oxime ester substrate could be readily varied to access pyrrolines of diverse structures (**101.10–101.15**). Interestingly, when electron-deficient alkenes **101.17** were used, the three component coupling products **101.18** were produced instead. Several Michael acceptors were demonstrated as appropriate reaction partners (**101.19–101.21**) (Scheme **101**).

5.5. Miscellaneous

The examples presented so far feature the use of visible light irradiation to induce radical reactivities under mild conditions,

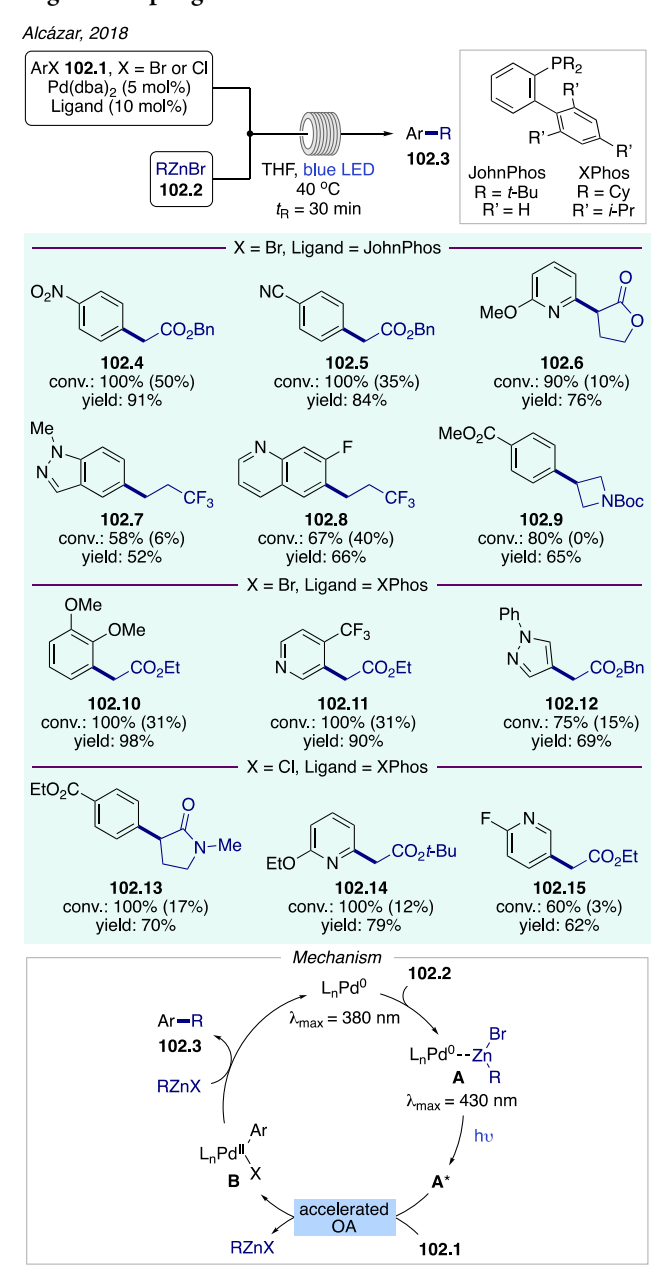
Scheme 101. Intermolecular Narasaka-Heck Reaction

which are uncommon for ground state palladium catalysis. The involvement of radical species is supported by mechanistic studies ranging from radical trapping, radical clock, isotopelabeling studies, to EPR experiments. This section briefly covers the reactions in which visible light irradiation was found to be beneficial but did not lead to a switch from classic two-electron mechanism to a radical pathway.

In 2018, Alcázar's group reported a visible light-accelerated Negishi coupling in flow. 182 Electronically diverse aryl bromides were efficiently coupled with organozinc reagents 102.2 to furnish the cross-coupling products in good to excellent yields (102.4-102.12). Notably, conversion of aryl bromides was significantly lower in the absence of blue LED irradiation (shown in parentheses), thus confirming its crucial role in the transformation. Likewise, aryl chlorides were successfully converted to products in good yields (102.13-102.15). To identify the light-absorbing species, the authors recorded absorption spectra of different combinations of reaction components and observed a bathochromic shift upon addition of organozinc reagent to a mixture of the palladium catalyst and the ligand. Therefore, the mechanism may involve the in situ complexation between Pd(0) and 102.2 leading to a photoactive species A. According to the authors, the photoexcitation of A accelerates the oxidative addition of substrate 102.1 to form Pd(II) complex B and release of the organizinc reagent. The latter then undergoes transmetalation with intermediate B to

furnish cross-coupling product 102.3. It should be mentioned that radical scavengers, diphenylethylene and di-tert-butylhydroxytoluene (BHT), did not affect product formation at all, suggesting that SET or other radical processes were not involved in this reaction (Scheme 102).

Scheme 102. Visible Light-Accelerated Oxidative Addition in Negishi Coupling



In 2019, Chu, Sun, and co-workers reported an oxidative reaction cascade between phenol derivatives 103.1 and α -bromoacetophenones 103.2 to access cyclic cores 103.3. ²⁷⁹ Both visible light irradiation and elevated temperature were required to achieve good yields of the products (103.4–103.10) (Scheme 103). Separately synthesized ether substrate using the corresponding phenol and bromide was converted to product without loss of efficiency, thus suggesting the *in situ* etherification followed by the palladium-catalyzed C–C bond

Scheme 103. Cascade Etherification/Oxidative Cyclization

formation. However, at this point, the reaction mechanism and the role of light remain elusive.

A more recent example came from Patel's group, who reported a cascade addition/cyclization of ketodinitriles 104.1 and 104.2 with arylboronic acids 104.3 to construct 3-cyanopyridines 104.4 and 3-cyanopyrroles 104.5, respectively. This protocol was applicable to a wide range of substrates of different electronic and steric properties (104.6–104.16). A broad scope of boronic acids was also demonstrated (104.17–104.20). Alkylboronic acid, however, was not reactive (104.21). A diverse array of 3-cyanopyrroles, such as 104.22 were successfully synthesized using this method (Scheme 104).

Scheme 104. Visible Light-Accelerated Transmetalation with Arylboronic Acids

The test experiments indicated that the addition of TEMPO led to a drastic decrease in the reaction yield. Nonetheless, based on the fact that no TEMPO adducts were detected, the authors refute a radical reaction pathway. Instead, it was proposed that visible light irradiation accelerates the transmetalation step between palladium species and arylboronic acids. Apparently,

more in-depth mechanistic studies are required to establish the exact role of visible light in this transformation.

6. NICKEL

6.1. General Overview

While nickel catalysts have been frequently used in combination with photocatalysts (cf. Figure 1b), ^{7,9} the catalytic reactivities of photoexcited nickel complexes are much less studied. In 2018, Doyle group demonstrated that visible light irradiation of Ni(II) aryl halide complexes led to the homolysis of Ni—C bond upon geometrical change, representing the first example of visible light-induced reactivity of nickel complexes. ²⁸⁰ Importantly, this offers a new way of generating catalytically active Ni(I) species (Figure 6a).

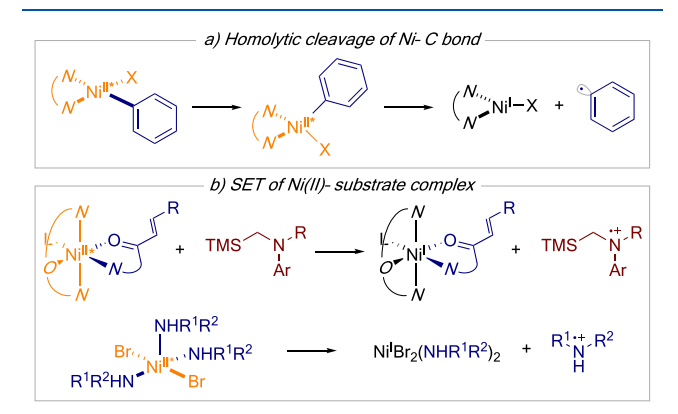


Figure 6. Outline of visible light-induced nickel catalysis.

Later in the same year, Gong and co-workers utilized chiral Ni(II) complex as dual Lewis acid and photoredox catalyst for asymmetric radical conjugate addition. In this case, a photoinduced SET from an electron-rich amine to the Ni(II)—substrate complex was involved. Almost at the same time, another example of reductive quenching of excited-state Ni(II) complex came from the group of Miyake, who coupled aryl halides with amines via a photoinduced generation of reactive aminium radical cation and Ni(I) complex (Figure 6b).

Furthermore, Alcázar's group observed an accelerating effect of visible light on nickel-catalyzed Negishi coupling reaction. ²⁸³ Despite a relatively unexplored area, these initial efforts clearly showcased the versatile reactivities of nickel complexes upon photoexcitation.

6.2. Transformations Involving Photoexcitation of Ni(II) Aryl Halide Complexes

In 2018, Doyle and co-workers studied the photophysics and photochemistry of Ni(II) aryl halide complexes, such as 105.1, using DFT calculations and ultrafast spectroscopy.²⁸⁰ It was found that these complexes displayed long-lived excited states, which were then computationally assigned to be ³MLCT in nature. Later in 2020, they studied a series of these complexes and came to the conclusion that the long-lived species was instead a ³d-d state 105.1b*, which originated from an initially formed short-lived MLCT state 105.1a*.²⁸⁴ This tetrahedral excited state featured an elongated Ni–Ar bond, which is predisposed to homolysis into Ni(I) complex 105.2 and aryl radical 105.3. The former readily dimerized, as observed by ¹H NMR studies, while the formation of the latter, rather than a chlorine radical, ²⁸⁵ was unambiguously confirmed by spin trapping experiment with 105.4 (Scheme 105). An important

Scheme 105. ³d-d Excited State of Aryl Ni(II) Complexes and Photoinduced Homolysis of Ni-Ar Bond

Doyle, 2018, 2020

$$t \to Bu$$
 $t \to Bu$
 $t \to B$

implication of these studies is that visible light irradiation enables a facile generation of catalytically relevant Ni(I) halide from Ni(0) and an aryl halide. As a proof of principle, the authors showed in their 2018 report that C-O coupling reaction between 4'-bromoacetophenone and n-butanol was significantly facilitated by blue light irradiation.

Following Doyle group's discoveries, Xue's group evaluated the scope of the C-O coupling of various aryl electrophiles 106.1 with primary or secondary aliphatic alcohols 106.2.²⁸⁶ Interestingly, purple LED was found to be superior, and elevated temperatures were necessary for this transformation. A wide range of (hetero)aryl chlorides were smoothly converted to the respective ethers in moderate to excellent yields (106.5–106.9). However, electron-rich aryl chlorides were unreactive. Various primary and secondary alcohols were competent coupling partners, delivering products in good yields (106.10-106.15). Sterically less hindered primary alcohols reacted selectively in the presence of their secondary counterparts (106.12). Study of the scope of aryl bromides showed good functional group tolerance, featuring an example of intact para-bromo substitution (106.16-106.19). Besides, aryl bromides with a tethered alcohol underwent intramolecular C-O bond formation leading to heterocycles 106.20-106.22 (Scheme 106). Notably, aryl triflates, tosylates, as well as mesylates, were also reactive under these reaction conditions. It is worth mentioning that continuous irradiation was required, presumably to convert catalytically inactive Ni(II) species back to Ni(I). The authors proposed several plausible pathways, including disproportionation, 280 homolysis, 284 and reduction by base. 28

Using the same nickel precatalyst, Xue and co-workers achieved C-N coupling of nitroarenes 107.1 with aryl halides 107.2.²⁸⁷ Electronically diverse nitroarenes provided the corresponding diarylamines in moderate to good yields (107.4–107.9). As in the previous report, electron-deficient aryl bromides were more reactive coupling partners (107.10–

Scheme 106. Cross-Coupling between Aryl Electrophiles and Aliphatic Alcohols

107.14). Aryl chlorides were also successfully coupled with nitroarenes, albeit with diminished yields (107.15–107.16). Notably, drugs such as fenofibrate, could be employed directly to yield aminated analog 107.17 in good yield. In addition, the authors applied this protocol to efficient synthesis of koenoline derivative 107.20 via a sequential C-N/C-C couplings. Preliminary mechanistic studies showed that aniline 107.21 was obtained in good yield upon reacting nitroso compound 107.22 with stoichiometric amount of Ni(II) aryl halide under the standard reaction conditions, thus supporting the intermediacy of 107.22. On the other hand, the involvement of other intermediates, such as aniline (107.23), hydroxylamine (107.24), diazene (107.25), and diazene oxide (107.26), was unlikely (Scheme 107).

6.3. Transformations Involving Photoexcitation of Ni(II)—Substrate Coordination Complexes

6.3.1. Asymmetric β -Alkylation of Enones. In 2018, Gong and co-workers developed a bifunctional Ni(II) catalyst for photoinduced asymmetric aminomethylation of enones 108.1.²⁸¹ Substrates bearing a wide range of substituents at the β -carbon afforded the corresponding products in moderate to good yields and excellent enantioselectivities (108.5-108.9). Tertiary anilines with various aryl groups were effective reaction partners (108.10–108.12). However, more sterically congested substrates, including ortho-tolyl- (108.13) or sterically demanding alkyl groups (108.14-108.15), compromised the reaction yield. Interestingly, secondary α -silylamines further reacted after the alkylation step to provide γ -lactams 108.16-108.18 (Scheme 108). Mechanistically, this transformation resembles reactions developed by Meggers and Kang groups (Scheme 122). Thus, in the photoredox cycle, an in situ assembled chiral Ni(II)-enone coordination complex undergoes photoinduced electron transfer with amine 108.2 to produce α -aminomethyl radical, which then undergoes enantiodetermining radical addition to another Ni(II)-enone complex to construct the

Scheme 107. Cross-Coupling of Nitroarenes with Aryl Halides

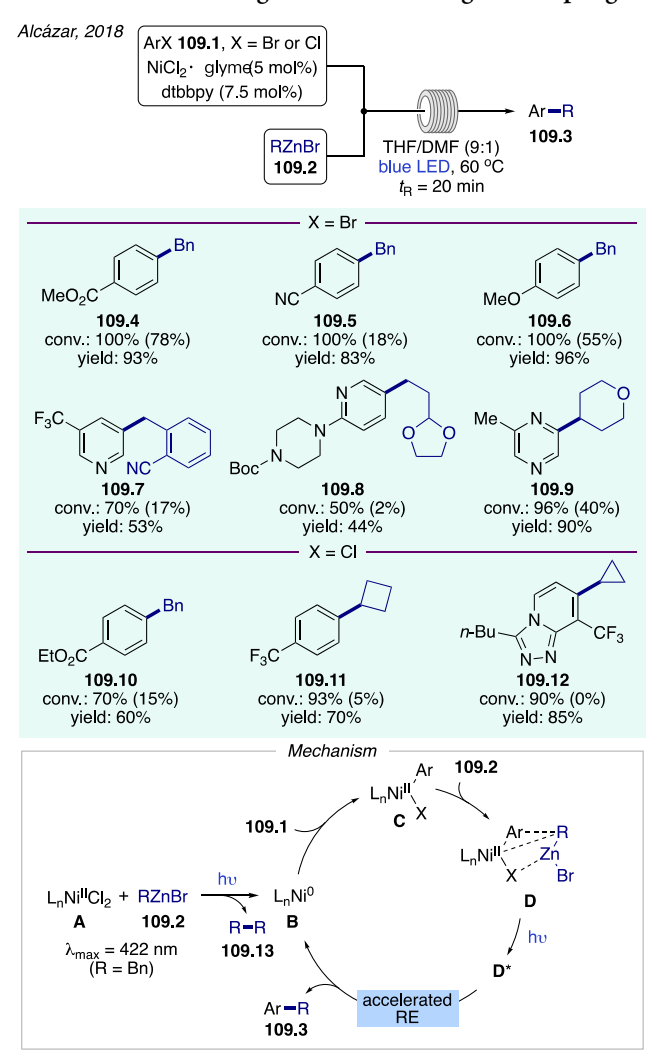
Scheme 108. Asymmetric Aminomethylation of Enones

C-C bond in the asymmetric catalysis cycle. Finally, the resultant radical undergoes a sequence of ET/PT (from water) to furnish product **108.3**.

6.3.2. Cross-Coupling Reactions. Prior to their report on the accelerating effect of visible light irradiation in palladiumcatalyzed Negishi coupling reaction (Scheme 102), Alcázar's group disclosed similar phenomenon in the nickel-catalyzed version. 283,288 Similarly, visible light irradiation enabled for higher conversion of aryl halides 109.1 and better yield of coupling products. Notably, aryl bromides, regardless of their electronic properties, provided the coupling products in excellent yields (109.4-109.6). Various organozinc reagents, which were otherwise much less reactive, underwent smooth transformation (109.7–109.9). Likewise, more challenging aryl chlorides were successfully employed, where a more profound impact of light was observed (109.10-109.12). The UV-vis studies revealed a mixture of Ni(II) precatalyst A and organozinc reagent 109.2 as the only combination that would give rise of an absorption band in the blue light region. Thus, the proposed catalytic cycle begins with the visible light-accelerated reduction of A by 109.2 to generate active Ni(0) species B. Indeed, dimer 109.13 was observed only when light was turned on. Next, complex B undergoes an oxidative addition with aryl halide 109.1 to form intermediate C, which upon complexation with zinc reagent affords another light-absorbing species D. A visible light-accelerated reductive elimination then occurs to furnish coupling product 109.3 and regenerated Ni(0) catalyst **B** (Scheme 109).

In 2018, Miyake's group disclosed a C(sp²)-N cross-coupling reaction involving photoexcitation of Ni(II) amine complexes.²⁸² Although the authors surveyed the scope of this reaction using 365 nm LED, they showed that violet LED was equally effective for the benchmark reaction. In general, aryl bromides were used, as they provided the best results among other halides rested (110.4). Various secondary alkyl amines were smoothly coupled demonstrating high functional group tolerance (110.5-110.10). Less reactive primary alkyl amines also worked, albeit sometimes in lower yields (110.11–110.12). Besides, aromatic amines were also competent coupling partners (110.13-110.14). Diverse electron-deficient aryl bromides provided the respective products in good yields (110.15-110.19). On the contrary, electron-neutral or -rich aryl iodides gave better yields than the bromide counterparts (110.20-110.22). The proposed catalytic cycle commences with the formation of Ni(II) amine complex A upon ligand substitution, with n = 3 being the dominant species. A photoinduced LMCT then occurs between amine and nickel center (B), leading to the formation of radical ion pair C. The aminium radical cation in C is then readily deprotonated, furnishing aminyl radical in D, which subsequently adds to substrate 110.1 to afford the coupling product 110.3 (path a). Meanwhile, Ni(I) amine complex E recombines with the displaced bromine radical to produce closed-shell intermediate G, which upon association with amine regenerates **A**. Since the Ni(I) complex in **D** is also a reactive species, an alternative pathway in which oxidative addition of substrate is plausible (path b). According to this route, a recombination of the formed Ni(III) intermediate and aminyl radical in F, followed by reductive elimination, leads to product formation and generation of complex G. In addition, parallel KIE experiments using piperidine and piperidine- d_{11} revealed a large primary KIE of 4.9, consistent with a ratedetermining step associated with the N-H bond breaking event $(C \rightarrow D)$ prior to the C-N bond formation step (Scheme 110).

Scheme 109. Visible Light-Accelerated Negishi Coupling



7. IRIDIUM

7.1. General Overview

Iridium photocatalysts are frequently employed in mainstream photocatalysis (cf. Figure 1a,b), 3,6,7,9,285 which is discussed in other review articles in this issue. In this chapter, we describe transformations, in which iridium photocatalysts are engaged not only in the process of harvesting light and subsequently transferring electron or energy, but also in asymmetric transformations. Previously, to achieve asymmetric photochemical transformations, dual-catalytic systems including an additional asymmetric cocatalyst, such as amine, 28 heterocyclic carbene (NHCs),²⁹² Brønsted or Lewis acid,^{293,294} and thiourea, ²⁹⁵ were required. The major breakthrough was achieved in 2014, when Meggers group reported an asymmetric photocatalyst capable of harnessing light energy, as well as inducing chirality. Thus, it was shown that chiral-at-metal Ir(III) complexes could catalyze enantioselective α -alkylation of ketones, hence representing the first example of asymmetric iridium photocatalysis. 296 The employed bis-cyclometalated complex features two labile acetonitrile ligands, which in situ are readily replaced by substrate to form an iridium-substrate complex, thereby enabling precise control over the stereodetermining step (Figure 7a). As with typical photoredox catalysts, either oxidative or reductive quenching cycles can be

Scheme 110. C(sp²)—N Cross-Coupling via Photoexcitation of Ni(II) Amine Complexes

operative depending on the reactants and conditions. In 2017, Yoon group utilized chiral hydrogen-bonding Ir(III) triplet sensitizers for asymmetric [2+2] photocycloaddition via EnT (Figure 7b). ²⁹⁷ In this case, the hydrogen-bonding to a substrate was enabled by a bidentate pyridylpyrazole ligand. Later, the same group reported an interesting intermolecular [2+2] reaction, which also occurred via EnT. ²⁹⁸ The chiral catalysts developed for the transformations detailed in the following sections are shown in Figure 7c.

7.2. Iridium as Chiral Photoredox Catalyst

7.2.1. Asymmetric α **-Alkylation of Ketones.** Previously, Meggers' group developed a family of chiral Ir(III) complexes

Figure 7. Outline of visible light-induced iridium catalysis featuring a single iridium as chiral photocatalyst.

for asymmetric Lewis acid catalysis. 299-302 These complexes share structural similarities with octahedral bis-cyclometalated cationic Ir(III) photocatalysts. In 2014, Meggers and co-workers achieved asymmetric α -alkylation of ketones 111.1 employing Λ-Ir1 photocatalyst. ²⁹⁶ A variety of electron-deficient benzyl bromides were found to be competent reaction partners (111.4–111.6). Substituent at the α -carbon of substrate could also be varied, including sterically and electronically diverse aryl-(111.7-111.9), thiophenyl- (111.10), and simple alkyl groups (111.11). Furthermore, phenacyl bromides were also reactive under these reaction conditions (111.12–111.14). Remarkably, in all cases, the reaction products were obtained in excellent yields and enantioselectivities. A dual-catalytic cycle of the proposed mechanism begins with the coordination of substrate with catalyst to form A, which upon facile deprotonation forms nucleophilic iridium enolate complex B. Next, electrophilic radical C, generated in the photoredox cycle, undergoes enantiodetermining radical addition to B to afford ketyl radical intermediate D. A subsequent single electron oxidation of D by iridium complex B+ leads to complex E and closes the photoredox cycle. Finally, intermediate E releases reaction product 111.3 upon exchange with another molecule of substrate, thus completing the catalysis cycle. Both intermediates A and B were isolated and unambiguously confirmed by Xray crystallography. High enantiocontrol of this transformation can be rationalized based on the X-ray structure of B, in which one face of the prochiral enolate moiety is sufficiently blocked by the tert-butyl group of one of the ligands. In addition, Stern-Volmer quenching studies indicated that B was quenched more efficiently than Λ -Ir1 by bromide, which is consistent with the redox potentials of these two species. Therefore, complex B serves not only as the key intermediate in controlling enantioselectivity, but also as an in situ formed photoredox catalyst. This radical mechanism was further supported by radical trapping experiments using 1,1-diphenylethylene and TEMPO (Scheme 111).

Subsequent to their initial report, Meggers and co-workers successfully extended the scope of electrophile to BrCCl₃³⁰³ and a range of perfluoroalkyl iodides.³⁰⁴ Substrates possessing

imidazole auxiliary underwent efficient α -trichloromethylation with good to excellent yields and remarkable enantiomeric excess (112.4–112.7). Besides, the authors demonstrated the use of quinoline and pyridine as competent directing groups (112.8–112.11). Importantly, α -bromination product was exclusively obtained when reaction was run in the dark, highlighting the pivotal role of light as a switch between single and two electron chemistry. Of note, the authors proposed that chain process was operative based on the measured quantum yield of 5. Thus, ketyl radical intermediate can directly reduce BrCCl₃ to yield another trichloromethyl radical, which then propagates the chain upon addition to iridium enolate.

In the reactions with perfluoroalkyl iodides, they employed the same strategy to obtain valuable chiral perfluoroalkylated products. As in the previous cases, the substituent at the α -carbon could broadly be varied without compromising the enantioselectivity (112.12–112.14). In addition to aliphatic iodides, this protocol is also applicable to perfluorobenzyl iodide (112.15) (Scheme 112).

In 2015, Meggers' group demonstrated that the same type of chiral catalyst could effect a net oxidative transformation under aerobic conditions.³⁰⁵ In this case, α -silylamines 113.2 were employed as surrogates of iminium species in this asymmetric Mannich-type reaction toward product 113.3. Various aniline derivatives underwent smooth transformation with high yields and excellent enantioselectivities (113.4-113.5). Likewise, the scope with respect to 113.1 was found to be broad (113.6-113.11) (Scheme 113). On the basis of the photophysical studies, the authors proposed coordination complex A as the in situ formed photocatalyst. Thus, upon photoexcitation, A undergoes reductive quenching in the presence of electronrich amine 113.2. The reduced form of A is then reoxidized by oxygen to complete the photoredox cycle. Meanwhile, the formed aminium radical cation desilylates and gets further oxidized to produce iminium cation B, which then reacts with iridium enolate complex C in the asymmetric catalysis cycle to furnish complex D. Exchange of the latter with another substrate molecule affords product 113.3 and regenerates the active photocatalyst.

Chemical Reviews Review pubs.acs.org/CR

Scheme 111. Asymmetric α -Alkylation of Ketones Enabled by a Single Iridium Photocatalyst

Meggers, 2014

7.2.2. Asymmetric Radical-Radical Cross-Coupling. Another example of reductive quenching of photoexcited Ir(III) also came from Meggers' group, in which they reported an

Scheme 112. Asymmetric α -Trichloromethylation and α -Perfluoroalkylation of Ketones

asymmetric radical-radical cross-coupling of trifluoromethyl ketones 114.1 and tertiary amines 114.2 to furnish 1,2aminoalcohols 114.3.³⁰⁶ Various *N*-methyl diarylamines were coupled in moderate to good yields and excellent enantioselectivities (114.4-114.8). A substrate with a pyridyl directing group was also compatible (114.9). Besides, N-aryl THIQ derivatives were also reactive to deliver the cross-coupling products with high level of stereocontrol (114.10). It was proposed that the in situ formed coordination complex A undergoes SET with amine 114.2 upon photoexciation, as described before, thereby producing ketyl radical B and the respective aminium radical cation. A subsequent proton transfer leads to a radical pair C, which upon cross-recombination of radicals affords enantioenriched intermediate D. Finally, incoming substrate releases the coordinated product 114.3 and closes the catalytic cycle (Scheme 114).

7.3. Iridium as Chiral Triplet Sensitizer

In 2017, Yoon and Baik's groups disclosed another class of chiral Ir(III) photocatalyst capable of EnT to alkene-tethered quinolone derivatives 115.1 upon hydrogen-bonding, thereby accomplishing an enantioselective intramolecular [2 + 2] photocycloaddition.²⁹⁷ Structurally related quinolones provided excellent yields and high enantiomeric excess (115.3-115.7). Placing a chlorine atom at the 8-position led to a drastic decrease of enantioselectivity (115.8). In contrast, product 115.9 with a smaller fluorine atom was obtained with high enantiocontrol. Modification of the alkene tether was also feasible, albeit with diminished enantioselectivities (115.10–115.11). Importantly, substrates in which the nitrogen atom was protected or replaced by an oxygen atom delivered the cycloadducts in good yields, however, with loss of enantiocontrol, thus underlining the crucial role of N-H bond in asymmetric induction. The authors ruled out the possibility of SET as both oxidation and reduction potentials of quinolone 115.14 are out of the range of Λ -Ir4 (1.59 V vs 1.27 V and \leftarrow 1.7 V vs -0.78 V, respectively). Besides, a marginal bathochromic shift was observed upon mixing substrate and photocatalyst, indicating that substrate coordina-

Scheme 113. Asymmetric Oxidative α -Aminomethylation of Ketones

tion was not essential for photoexcitation to occur. On the other hand, the values of triplet energy of 115.14 and Λ -Ir4 were found to be 55.0 and 59.6 kcal/mol, respectively, suggesting an exergonic state change upon triplet energy transfer. A computational analysis of complex between 115.14 and Λ -Ir4 indicated several interactions, including strong hydrogen-bonding of the carbonyl moiety with the N-atom of the pyrazole fragment. In addition, a π - π interaction between substrate and the ligand in proximity was identified, which is in agreement with the orbital analysis revealing a coplanar alignment of the substrate π -space with the ligand π -orbitals to attain an appropriate overlap. Moreover, an unusual NH $-\pi$ interaction was also identified, which explained the observed negligible enantioinduction in 115.12 and 115.13. Cumulatively, these three substratecatalyst interactions contributed to the asymmetric induction in this transformation (Scheme 115).

More recently, the same groups reported an enantioselective intermolecular [2+2] photocycloaddition of 3-alkoxyquinolones 116.1 and maleimides 116.2 using a similar catalyst Λ -Ir5. This reaction was not sensitive to substitution at the aromatic ring providing good to excellent yields and enantioselectivities (116.4–116.8). Methyl substituent at the alkene moiety was also tolerated, albeit with diminished stereoselectivity. *N*-Substituted maleimides were effective, suggesting that a catalyst–maleimide coordination was not

Scheme 114. Asymmetric Radical—Radical Cross-Coupling of Trifluoromethyl Tetones and Tertiary Amines

crucial (116.10). Notably, N-protected substrate delivered product 116.11 in 72% e.e., in sharp contrast to the previous report in which the racemates were obtained (Scheme 115), thus indicating a fundamental difference in the interactions involved. Interestingly, Stern-Volmer quenching studies revealed that maleimide was a much more efficient quencher than substrate 116.12. Indeed, reaction of alkene-tethered substrate 115.14 in the presence of maleimide provided the intermolecular [2 + 2] adduct exclusively instead of 115.3. Besides, it was found that the photophysics of Λ -Ir5 was not affected upon substrate coordination. These results support the scenario, in which the exciton of substrate—catalyst complex was localized at iridium center and subsequently transferred to maleimide via intermolecular EnT. To gain further insights into the interactions associated with asymmetric induction, the authors performed computational studies. Thus, DFT calculations of a ternary encounter complex of catalyst, substrate 116.12, and maleimide, suggested that the energy required for EnT to hydrogen-bonded substrate was 3.65 kcal/mol, while that of maleimide was 4.62 kcal/mol. However, the rate of EnT is dependent on the degree of orbital overlap. In this ternary complex, maleimide, instead of substrate, as in the previous case, showed strong π – π interaction with the cyclometalating ligand. Furthermore, two hydrogen-bonding interactions were identified between substrate and maleimide. This binding mode

Scheme 115. Enantioselective Intramolecular [2 + 2] Photocycloaddition

provided a rationale behind the preferential triplet sensitization of maleimide over substrate (Scheme 116).

8. RHODIUM

8.1. General Overview

Similarly to iridium, bis-cyclometalated, chiral-at-metal Rh(III) complexes have been developed for asymmetric Lewis acid catalysis. Phase spaces are activity of this type of catalyst and achieved photoinduced asymmetric α -aminomethylation of ketones. As in analogous iridium photocatalysis, a single rhodium catalyst is responsible for both the chiral induction and the redox events (Figure 8a). In addition to α -functionalization, rhodium photocatalysis also enable access to enantioenriched, β -functionalized carbonyl compounds. In 2017, Meggers' group achieved asymmetric β -C—H functionalization of ketones via radical—radical cross-coupling. In the same year, Kang and co-workers employed enones as substrate for enantioselective β -alkylation. 310

Besides photoredox chemistry, in 2017, Meggers' group disclosed an example of asymmetric photocycloaddition reaction, further highlighting the versatility of photoinduced Rh(III) catalysis.³¹¹ In this case, photoexcitation of the Rh(III)—enone coordination complex occurs at the alkene moiety, directly leading to a triplet biradical, which subsequently adds intermolecularly to another alkene (Figure 8b). As such,

Scheme 116. Enantioselective Intermolecular [2 + 2] Photocycloaddition

the rhodium catalyst facilitates visible light excitation of the substrate rather than serve as a triplet photosensitizer (cf. Schemes 115 and 116).

Later in 2019, Baslé and co-workers described a photoinduced Rh(I)-catalyzed directed C—H borylation, representing the sole example of Rh(I) photocatalysis. In this transformation, visible light irradiation promotes the rate-determining C—H oxidative addition step, thus distinguishing it from the aforementioned examples in which radicals are involved (Figure 8c). The catalysts employed for the transformations described below are depicted in Figure 8d.

8.2. Asymmetric α -Functionalization of Ketones

8.2.1. Radical Addition to Enolates. In 2015, Meggers, Gong, and co-workers employed Λ -Rh1 as chiral photocatalyst to achieve Mannich-type transformation, similarly to that depicted in Scheme 113.³⁰⁸ The reaction proceeds via a photoinduced oxidation of amine 117.2 to the respective iminium cation, which is then trapped by the *in situ* formed rhodium enolate complex to furnish α -aminomethylation product 117.3. Similarly to the iridium-catalyzed method, this protocol was applicable to a wide range of ketones and amines (117.4–117.10). In addition, benzimidazole or pyrazole auxiliary could be used in place of imidazole, albeit with compromised yields and enantioselectivities (117.11–117.12) (Scheme 117).

Meggers, 2016

Figure 8. Outline of visible light-induced rhodium catalysis.

Scheme 117. Asymmetric Oxidative α -Aminomethylation of Ketones

In the following year, Meggers' group utilized N-functionalized carbamates 118.2 (ODN = 2,4-dinitrophenylsulfonyloxy) as a precursor to electrophilic amidyl radical³¹⁴ to access enantioenriched α -amination products 118.3.³¹⁵ In general, excellent yields and enantiomeric excess were obtained (118.4-118.9). The intermediacy of amidyl radical was confirmed based on the radical trapping experiments using N-methylindole and carbamate 118.10. In addition, significant amounts of adduct 118.12 were observed only in the presence of substrate 118.11, which is consistent with the in situ formation of rhodium enolate complex as the actual photocatalyst (Scheme 118). The mechanistic scenario is therefore closely related to that with the iridium counterpart (Scheme 101). However, a quantum yield of 14 indicated that the chain process was the dominant pathway, wherein ketyl radical intermediate A underwent SET with carbamate instead of the oxidized photocatalyst to furnish intermediate B and amidyl radical C. The latter would then react

Scheme 118. Asymmetric α -Amination of Ketones

with enolate complex to propagate the chain. Interestingly, the authors also found that rhodium was superior to iridium for this

transformation, which was rationalized based on a significantly faster ligand exchange of the former. Since amidyl radicals are highly reactive species and prone to reduction, ³¹⁶ a high turnover frequency is required for an efficient chain process.

More recently, the same group disclosed synthesis of Λ -Rh2 bearing bis-cyclometalated indazole ligands and its use in asymmetric α -cyanoalkylation of ketones 119.1. Ketones with different α -(hetero)aryl substituents provided the respective products in good yields and enantioselectivities (119.4–119.8). Aliphatic substituent, however, led to much lower yield and enantioselectivity (119.9). Branched α -cyano bromides were also tested, which delivered the products as a mixture of diastereomers with excellent enantiocontrol for the major isomer (119.10–119.12). However, 2-bromobutyronitrile was unreactive under these reaction conditions (119.13) (Scheme 119). In contrast to the previous case, this reaction did not involve a radical chain mechanism (quantum yield = 0.046).

Scheme 119. Asymmetric α -Cyanoalkylation of Ketones

8.2.2. Radical-Radical Cross-Coupling. In 2019, Meggers and co-workers described another rhodium-catalyzed α aminomethylation reaction.³¹⁸ The use of α -chloroketones 120.1 and glycine derivatives 120.2 rendered this transformation redox-neutral. In general, diverse α -aryl substituents were well tolerated, delivering products in good yields and excellent enantioselectivities (120.4–120.8), with the exception of sterically demanding substrate (120.9). In contrast, glycine derivatives displayed a significant dependence on electronics, with electron-withdrawing groups on the phenyl ring favoring high yields and enantiomeric excess (120.10-120.3). The proposed mechanism begins with the formation of coordination complex A as the photocatalyst, which undergoes a photoinduced SET with glycinate **B** to produce ketyl radical **C** and α aminomethyl radical D. Intermediate C then converts to α carbonyl radical E upon loss of chloride. An enantiodetermining radical—radical cross-coupling then follows to construct the C— C bond in F, which upon product release completes the catalytic cycle (Scheme 120).

8.3. Asymmetric Synthesis of β -Functionalized Ketones

8.3.1. Radical—Radical Cross-Coupling. In 2017, Meggers' group reported an asymmetric β -C—H functionalization of ketones 121.1 with 1,2-dicarbonyl compounds 121.2, leading to products 121.3 with two newly formed contiguous stereo-

Scheme 120. Enantioconvergent Radical—Radical Cross-Coupling of α -Chloroketones and Glycine Derivatives

centers.³⁰⁹ In general, high diastereo- and enantioselectivities were obtained. This reaction showed good tolerance to a range of functionalities (121.4-121.8). However, aryl substituent at the β -position seems to be crucial, as its replacement with a methyl group led to no reaction. Pyridyl group was found to be an appropriate auxiliary (121.9). Employment of various α ketoesters delivered products in excellent yields and stereoselectivities with little electronic effect observed (121.10-**121.12**). 1,2-Diketones were also competent coupling partners, albeit with diminished diastereoselectivity (121.13). Importantly, chiral α -ketoesters provided the respective products in a highly diastereoselective manner (121.14). The suggested mechanism begins with the formation of coordination complex A followed by its deprotonation to produce rhodium enolate B, which also serves as the photocatalyst. Thus, a photoinduced SET to dicarbonyl compound followed by β -proton transfer leads to radical pairs C and D. The following stereocontrolled radical—radical cross-coupling forges the C–C bond in E, thus creating two stereocenters. Enolate E then undergoes protonation and a subsequent product release to furnish product **121.3** and regenerate catalytic complex A (Scheme 121).

8.3.2. β **-Alkylation of Enones.** Several protocols have been developed for enantioselective β -alkylation ofenones **122.1** involving an enantiodetermining radical conjugate addition step. In 2017, Kang group utilized *N*-aryl THIQ derivatives **122.2** as α -amino radical precursor to obtain the corresponding products with two contiguous chiral centers. ³¹⁰ *N*-Aryl THIQ derivatives with various aryl protecting groups, as well as substituents at the aromatic ring, were well tolerated, delivering products in good

Scheme 121. Asymmetric β -Functionalization of Ketones with 1,2-Dicarbonyl Compounds

yields. While the diastereoselectivities were moderate, the major isomer was obtained with excellent enantiomeric excess (122.6–122.7). Likewise, modification of the β -substituent in substrate revealed that other (hetero)aryl- and alkyl groups were compatible (122.8–122.10). Similarly to the works by the groups of Yoon³¹⁹ and Melchiorre,³²⁰ the proposed mechanism involves an enantiodetermining radical conjugate addition step.

H⁺

 $\bar{\mathsf{R}}^1$

F

 \bar{R}^1

121.1

In 2018, Meggers and co-workers photochemically generated alkyl radical from Hantzsch ester derivatives 122.3 to achieve similar transformation with excellent enanatiocontrol. Substrates with either aryl- or alkyl groups at the β -carbon were compatible (122.11–122.13). Hantzsch ester derivatives with different C4 substituents, including a simple isopropyl group, were also successfully applied to this reaction (122.14–122.17). Of note, the authors proposed that both radical conjugate addition and radical–radical cross-coupling (cf. Scheme 121) were plausible mechanisms.

The same group also reported a reductive transformation using N-(acyloxy)phthalimides 122.4 as radical precursor and Hantzsch ester as reductant to access β -functionalized γ aminobutyric acid derivatives.³²² In contrast to the report from Kang group, wherein the photoexcited catalyst oxidized Naryl THIQ derivatives, this method utilized the photocatalyst as a single electron reductant to produce α -amino radical from 122.4, thus enabling a broader substrate scope. As in the previous examples, variation of the β -substituent was feasible (122.18-122.20). Sterically demanding tertiary radicals also underwent efficient reaction, providing product 122.21 with a quaternary carbon center. Besides, other nitrogen protecting groups were found to be compatible (122.22). Notably, this method enabled access to products possessing a fluorinated quaternary stereocenter in good yields and excellent enantioselectivities (122.23) (Scheme 122).

Scheme 122. Asymmetric β -Alkylation of Enones with Different Radical Precursors

8.4. Asymmetric Photocycloaddition

Meggers, 2017

In 2017, Meggers and co-workers disclosed the use of chiral rhodium photocatalyst for [2 + 2] photocycloaddition reaction between enone derivatives 123.1 and olefins 123.2, leading to cyclobutane scaffolds 123.3 bearing three stereogenic centers.³¹¹ High yields and diastereoselectivities, and excellent enantioselectivities were observed regardless of the electronic properties and steric hindrance of the aryl substituent (123.4–123.7). Different auxiliaries were also able to deliver products with comparable efficiencies (123.8–123.10). Remarkably, this method allows for construction of vicinal all-carbon quaternary stereocenters with excellent stereocontrol (123.10–123.12) (Scheme 123). In addition, vinyl ether was found to be a

Scheme 123. Asymmetric [2+2] Photocycloaddition of Enones and Alkenes

competent alkene substrate (123.13). Of note, the iridium analog could also catalyze this reaction, however, failed to induce any enantioselectivity. The proposed mechanism involves the photoexcitation of the *in situ* formed complex **A** to its singlet

state, which upon intersystem crossing (ISC) transitions to a triplet state depicted as \mathbf{A}^* (T_1). This biradical species then reacts with olefin **123.2** in a stereocontrolled fashion, constructing the first chiral center in intermediate \mathbf{B} . A subsequent ISC followed by radical recombination forges the second C—C bond to afford cyclobutane C. The desired product is then released upon exchange with the substrate molecule. Computational studies performed on \mathbf{A}^* (T_1) revealed that spin density was mainly localized at the alkene moiety instead of the metal center, thus refuting the possibility of the triplet sensitization (Schemes 115 and 116). In addition, a redox process was unlikely, as the estimated excited-state potentials of \mathbf{A} were insufficient to oxidize or reduce styrene.

Shortly after, the same group described the use of vinyl azides **124.2** to accomplish an asymmetric [2 + 3] photocycloaddition leading to valuable 1-pyrrolines 124.3 containing two consecutive stereocenters. 323 Examination of the aryl group in substrate revealed that electronic and steric effects had little impact on the reaction outcome (124.4-124.7). Likewise, heteroaromatics could be introduced (124.8-124.9). In addition, quaternary stereocenter could be constructed with high efficiency (124.10-124.11). Various aryl-, vinyl-, and alkyl-substituted vinyl azides were also amenable to this transformation (124.12-124.15). Remarkably, nearly perfect diastereoselectivity and excellent enantiomeric excess were observed for all products. As in the previous report, the iridium counterpart led to the formation of product in racemic form. The catalytic cycle starts with the photoexcitation of the *in situ* formed complex A to its excited state A*. A subsequent reaction with vinyl azide leads to biradical B along with the establishment of the first stereocenter. Intermediate B then extrudes dinitrogen to produce an iminyl radical in C, which undergoes stereoselective radical recombination to forge the C-N bond. Finally, the product release closes the catalytic cycle. To understand why analogous iridium catalyst did not give any enantioselectivity, the authors carried out similar spin density calculation and found that the iridium center possessed the major spin density, indicative of a different mechanistic scenario involving EnT to free substrate 124.1 followed by cycloaddition, thus resulting in no stereocontrol (Scheme 124).

In 2018, a related work came from Meggers' group, where racemic cyclopropanes 125.1 were employed in asymmetric [3+ 2] photocycloaddition with alkenes 125.2.³²⁴ A wide variety of Michael acceptors, as well as styrenes were competent alkene partners, delivering the cyclopentane adducts in high yields and good to excellent stereoselectivities (125.4-125.8). Employment of enyne allowed for synthesis of the product 125.9 with all-carbon quaternary stereocenter. Besides, derivatives of natural product, such as aspartame, provided the respective products in excellent yields and stereoselectivities (125.10). Employment of spirocyclic substrate led to product 125.11 with impressive stereocontrol. However, low diastereoselectivities were observed with nonsymmetrical substrates (125.12-125.13). Unlike the previous two photocycloadditions, the proposed mechanism of this reaction involves photoredox processes, wherein a photoexcited complex A undergoes SET with DIPEA to form ketyl radical B, which upon ring opening produces tertiary alkyl radical C. Intermediate C then undergoes stereodetermining cycloaddition step to construct the cyclopentane motif in D. A subsequent single electron oxidation and exchange with the substrate leads to product 125.3 (Scheme 125).

Scheme 124. Asymmetric [2+3] Photocycloaddition of Enones and Vinyl Azides

In the same report, the authors also demonstrated analogous cycloaddition with alkynes 126.2. This photocycloaddition reaction also demonstrated a broad scope with respect to alkynes, furnishing cyclopentene scaffolds in high yields with excellent enantiomeric excess (126.4–126.9). Similarly, spirocycle 126.10 was obtained with excellent enantioselectivity, while 126.11 was obtained as a mixture of diastereomers. A more complex alkyne was also a competent substrate (126.12) (Scheme 126).

8.5. C(sp²)-H Borylation

The transformations discussed so far involve a photoactive Rh(III) species that initiate the catalytic cycle. In 2019, Baslé and co-workers described the use of NHC–Rh(I) complex Rh6 for directed C–H borylation. Examination of electronically diverse 2-phenylpyridine derivatives revealed that the electron-

Scheme 125. Asymmetric [3 + 2] Photocycloaddition of Cyclopropanes and Alkenes

donating groups favored the reaction (127.3–127.6). Substitution at other positions was also tolerated (127.7–127.8). However, employment of more electron-deficient pyridyl directing group was less efficient (127.9). Interestingly, a modest level of desymmetrization was observed in 127.10. This protocol was also applicable to $C(sp^3)$ —H borylation, as exemplified by 127.11. Stoichiometric experiments between Rh6 and substrate 127.12 indicated the essential role of light in the C–H activation step, as key intermediate aryl Rh(III) hydride 127.13 was formed upon irradiation only. Transmetalation of intermediate 127.13 with B_2Pin_2 , followed by reductive elimination of the resultant aryl Rh(III)—BPin complex, furnishes the borylation product 127.2 (Scheme 127).

9. GOLD

9.1. General Overview

The advent of gold/photoredox dual catalysis has enabled a range of transformations involving redox processes at the gold center, ^{32,5-327} which is uncommon in traditional gold catalysis due to its high oxidation potential. ^{32,8} In 2016, Hashmi and co-

Scheme 126. Asymmetric [3 + 2] Photocycloaddition of Cyclopropanes and Alkynes

Scheme 127. Directed C-H Borylation

workers showed that photoexcited gold complexes can also engage in redox processes without an additional photosensitizer, thus representing the first example of visible light-induced gold catalysis. ³²⁹ In this report, they described an oxyarylation of alkynes with aryldiazonium salts, which features the *in situ* formed Au(I)—aryldiazonium charge-transfer complex capable of transferring a single electron to another diazonium upon photoexcitation, thereby producing the key aryl Au(III) intermediate (Figure 9a). Since then, several reactions involving the photocatalytic generation of this intermediate have been achieved.

More recently in 2019, Hashmi's group disclosed a desulfurizing alkylation of alkenes, which comprises another light-

Figure 9. Outline of visible light-induced gold catalysis.

induced reactivity of gold complexes.³³⁰ In this case, dimeric Au(I) complex forms a coordination complex with thiol. Photoexcitation of this complex and LMCT generates a reduced gold intermediate and a thiol radical cation that subsequently desulfurizes to afford the respective alkyl radical (Figure 9b).

It is worth mentioning that an important branch of gold photocatalysis revolves around the use of gold catalyst as a photosensitizer, which is not directly involved in bond forming/breaking events. These works, which are beyond the scope of this review, have been recently summarized by Hashmi and coworkers. ³³¹

9.2. Carbofunctionalization of Alkynes and Alkenes

In 2016, Hashmi's group reported an oxyarylation of internal alkynes 128.1 with aryldiazonium salts 128.2, representing the first example of visible light-induced gold catalysis. 329 Different 1-aryl-1-hexynes were smoothly converted to the respective ketones in good yields (128.4-128.6). Similarly, the alkyl substituent on alkyne could be altered to incorporate various functionalities (128.7-128.10). Both diaryl- (128.11) and dialkyl-substituted (128.12) alkynes were also found to be effective substrates. In addition, diverse aryldiazonium salts delivered the desired products in moderate to good yields (128.13-128.15). However, a trifluoromethyl group was not tolerated, presumably due to decomposition of the corresponding diazonium salt (128.16). The authors also showed that the same reaction conditions could be applied to the oxyarylation of alkene 128.17, thus demonstrating that this process does not require employment of exogeneous photosensitizers, as reported earlier. 325 The role of visible light irradiation was originally attributed to the extrusion of N₂ from Au(III) complex A to produce aryl Au(III) intermediate B. Later, Zhang, Zhu and coworkers performed detailed DFT studies and proposed a different mechanistic scenario involving the formation of photoactive charge-transfer complex C. 332 Upon visible light excitation, C engages another diazonium salt in SET, affording Au(II) complex **D** and a diazo radical, which gives aryl radical upon extrusion of N₂. The formed aryl radical then recombines with D to form intermediate B (path a), which subsequently forms the key coordination complex E with alkyne substrate. Alternatively, aryl radical can add to Au(I) catalyst to give aryl Au(II) species G (path b). A sequence of SET to 128.2 and coordination to alkyne (i), or vice versa (ii), leads to the same intermediate E, which upon nucleophilic addition of methanol delivers vinyl Au(III) complex F. Finally, reductive elimination followed by hydrolysis furnishes product 128.3 and regenerates the gold catalyst (Scheme 128).

In 2019, Hashmi, Klein, and co-workers described a cyclization reaction featuring light-induced chemodivergent transformations.³³³ Thus, reaction between 2-alkynylphenols **129.1** and aryldiazonium salts **129.2** under photoinduced conditions produced 3-aryl benzofurans **129.3** orazobenzofur-

Scheme 128. Oxyarylation of Alkynes

ans 129.4 under dark. Several examples were demonstrated for each transformation resulting in moderate to good yield of benzofurans (129.5-129.11). Stoichiometric reactions showed that both products 129.13 and 129.14 could be derived from vinyl Au(I) complex 129.12. Thus, both catalytic transformations share a common 5-endo-dig cyclization pathway upon π -coordination of Au(I) catalyst to the alkyne moiety in **129.1** to form vinyl Au(I) intermediate. It then diverges into two paths depending on the reaction conditions. In the upper case, vinyl Au(I) species and diazonium salt form a donor-acceptor complex, which upon photoexcitation leads to C-C bond formation in 129.3. DFT calculations revealed that the triplet excited state of this complex featured an elongated C-N bond of diazonium fragment, thus explaining the extrusion of N₂. On the other hand, vinyl Au(I) can act as a typical organometallic nucleophile and attacks electrophilic diazonium salt, thereby constructing the C-N bond in **129.4** (Scheme 129).

In the same year, Hashmi's group also reported a PPh₃-mediated desulfurizing protocol to access C–C bond formation product 130.3 from vinyl (hetero)arenes 130.1 and mercaptan derivatives 130.2.³³⁰ Various functionalized styrene derivatives were found to be compatible (130.4–130.9). Di- and trisubstituted alkenes (130.9–130.11), as well as vinyl

Scheme 129. Visible Light-Induced Mechanistic Divergence

heteroarenes (130.12), also worked well in this transformation. In addition to ester, mercaptans bearing other electronwithdrawing groups delivered the respective products in good yields (130.13-130.15). Examples of secondary and tertiary alkylation were also demonstrated (130.16-130.17). The proposed catalytic cycle commences with the in situ formation of photoactive coordination complex B from dimeric Au(I) catalyst A and mercaptan 130.2. Photoexcitation of B generates gold complex C and thiol radical cation D via LMCT. The latter is then captured by PPh3 to produce phosphoranyl radical E, which upon β -scission releases alkyl radical F. A subsequent radical addition to alkene affords benzyl radical G, which then abstracts hydrogen atom from another mercaptan to directly furnish product 130.3 (path a). The concomitantly formed thiyl radical H can react with PPh3 to propagate the radical chain. In an alternative scenario, G can undergo SET with intermediate C to afford the product via carbanion I, meanwhile closing the gold catalytic cycle (path b). The authors also proposed that trace amount of molecular oxygen may regenerate gold complex A from C. An experimental quantum yield of 19.5% suggested a gold-catalyzed pathway. However, classical radical conditions using AIBN as an initiator provided the product in comparable yield, indicating that both paths a and b could be operative. The intermediacy of alkyl radical was confirmed by radical clock experiment, while the involvement of S-centered radical D or H was supported by the formation of thiol addition product 130.19 in the absence of PPh₃ (Scheme 130). Of note, deuteriumlabeling experiments indicated that in addition to mercaptan, solvent may also serve as a hydrogen source.

9.3. Cross-Coupling Reactions

In 2017, Hashmi, Xie, and co-workers disclosed the first visible light-induced gold-catalyzed cross-coupling reaction of boronic acids **131.1** and diazonium salts **131.2**, ³³⁴ complementing the reported methods which require an additional photosensi-

Scheme 130. Desulfurizing Alkylation of Vinyl (Hetero)arenes

tizer. 321,331 Using this method, electron-neutral and -deficient arylboronic acids delivered the coupling products in moderate to good yields (131.4-131.6). However, the electron-rich counterparts were much less efficient (131.7). Heteroaryl boronic acids were also effective substrates for this transformation (131.8). Likewise, diazonium salts bearing an electron-withdrawing group reacted more efficiently (131.9-131.12). It is worth mentioning that aryl pinacolboronates were also viable cross-coupling partners (131.13). As established earlier, this transformation also involves the photoinduced generation of aryl Au(III) species A from Au(I) catalyst and aryldiazonium 131.2. In this case, the counterion BF₄ also serves as an activator of boronic acid (B), thereby facilitating the subsequent transmetalation step to produce intermediate C. which upon reductive elimination furnishes product 131.3 and regenerates the gold catalyst (Scheme 131).

In 2018, the same group achieved a chemoselective Hiyama coupling using bifunctionalized arenes 132.1 to access highly valuable biarylboronates 132.3.³³⁵ As in the previous case,

Scheme 131. Cross-Coupling between Boronic Acids and Diazonium Salts Enabled by Visible Light-Induced Gold Catalysis

diazonium salts with electron-withdrawing groups were effective coupling partners, delivering products with BMIDA-, BPin-, or BNep functionality in moderate to good yields (132.4–132.9). Remarkably, an iodo substituent was also tolerated, highlighting the chemoselectivity of this protocol (132.10-132.11). This transformation was also applicable to substrates with different substitution pattern (132.12–132.13), as well as those bearing additional functional groups (132.14–132.16). Besides, other arylsilanes were also viable substrates (132.17–132.18). Notably, iodo- (132.19) and triflyl (132.20) groups on arylsilane also remained intact under the reaction conditions, thus constituting another class of bifunctionalized substrates for this reaction (Scheme 132). The authors also demonstrated a series of iterative modular functionalization of the obtained products, thus further highlighting the synthetic utility of this method.

Shortly after, Hashmi's group demonstrated the viability of several other *B*- and *Si*-based reagents **133.1** for cross-coupling reactions. Thus, MIDA boronates, potassium trifluoroboronates, trimethoxysilanes, and bis(catecolato)silicates, were coupled with aryldiazonium salts in moderate to high yields (**133.4–133.5**). In addition, the authors showed that alkynylation was also feasible using alkynyltrimethylsilanes **133.6**, as exemplified by successful synthesis of products **133.9** and **133.10**. Interestingly, bistrimethylsilylacetylene afforded the double arylation product **133.11** in good yield (Scheme **133**).

10. TUNGSTEN

10.1. General Overview

In recent years, tetrabutylammonium decatungstate (TBADT), a tungsten-based polyoxometalate complex, has gained immense popularity in organic synthesis (Figure 10). 337,338 Photoexcited TBADT is capable of abstracting hydrogen atoms from C–H sites of BDE up to 105 kcal/mol, 339 thus rendering TBADT a superior catalyst for the activation of strong C–H bonds.

Scheme 132. Hiyama Coupling en Route to Biarylboronates

Scheme 133. C-C Cross-Coupling Reactions with Different Transmetalation Reagents

Notably, photoexcited TBADT features highly electrophilic oxygens with partial radical character³⁴⁰ and is therefore primed for HAT at electron-rich C–H sites. As such, polarity-matched hydridic C–H bonds undergo faster HAT than the protic ones. Moreover, due to the larger size of TBADT, HAT occurs preferentially at less hindered sites. Taken together, one can strategically exploit the polar and steric factors for highly site-selective C–H functionalization reactions.

Given the absorption maximum at 324 nm, most of the TBADT-catalyzed reactions are performed under UV-irradiation. ^{341,342,340} Nonetheless, this broad absorption band tails into the violet region, thus indicating that visible light irradiation can also be utilized. ^{343–347} In 2009, Fagnoni's group first demonstrated the viability of sunlight as a light source. ³⁴⁸ Since

then, several transformations using purple LED irradiation have been reported.

10.2. C-H Alkylation

In 2009, Fagnoni's group reported a solar light-driven C–H alkylation of Michael acceptors 134.1 with unactivated- (134.4) and activated (134.5) aliphatics as well as aldehydes (134.6). Several examples of Michael acceptors were also demonstrated (134.7–134.9). 348

Several years later, the groups of Fagnoni and Ryu reported a regioselective β -alkylation of cyclopentanone under very similar conditions. As in the previous case, various Michael acceptors were found to be suitable substrates for this reaction (134.10–134.13). Notably, 3-methylcyclopentanone underwent selective transformation at the methine carbon (134.14) (Scheme 134). Interestingly, a much lower β -selectivity was observed with other cyclic and acyclic ketones. Both transformations share the same mechanism, which involves HAT from the more hydridic and weaker C–H sites of 134.2 to photoexcited decatungstate catalyst to form alkyl radical A. A subsequent radical addition to electron-deficient alkene 134.1 affords electrophilic radical C. Finally, back HAT from reduced decatungstate B affords alkylation product 134.3 and regenerates the catalyst.

In 2020, P.-S. Wang group incorporated chiral phosphoric acid (CPA) catalyst into analogous alkylation reaction to access α -enantioenriched ketones 135.3 from enones 135.1. With cyclohexane as the alkyl source, differently substituted 1tetralones delivered the respective products in moderate to good yields with high enantiocontrol (135.5-135.8). Enones with fused heterocycle (135.9), as well as those of different ring sizes (135.10-135.11), were also viable substrates. Acyclic enone proved to be more challenging, as exemplified by the low yield and enantioselectivity of product 135.12. In addition to cycloalkanes, hydrocarbons containing benzylic- (135.13), allylic- (135.14), as well as aldehydic (135.15) C-H sites, afforded the alkylation products with moderate to high efficiencies (Scheme 135). The authors proposed the proton transfer from CPA to enol intermediate A as enantiodetermining step. Of note, this method requires a substantial excess (5-20)equiv) of hydrocarbons to achieve efficient hydroalkylation.

Very recently, Q. Wang and co-workers reported synthesis of unnatural α-amino acids via C-H alkylation of aldehydes with dehydroalanine methyl ester derivatives. Sterically and electronically diverse benzaldehydes reacted efficiently to provide the corresponding products in good yields (136.4–136.8). Notably, the allylic ether moiety of 136.8 remained intact in this transformation. Likewise, heteroaryl aldehydes were found to be effective substrate (136.9). This protocol could also be applied to nonaromatic aldehydes (136.10–136.11), as well as unactivated hydrocarbons bearing a tertiary C-H site (136.12), albeit with lower efficiency. Moreover, switching the substrate to chiral Karady-Beckwith alkene provided product 136.13 with excellent diastereoselectivity.

Shortly after, P.-S. Wang's group independently reported a closely related asymmetric version of this transformation. ³⁵² Simple cyclic hydrocarbons furnished the products with excellent enantioselectivity (136.15–136.16). Likewise, a broad range of toluene derivatives was found to be suitable substrates for this reaction (136.17–136.21). Other substrates possessing weak C–H bonds also underwent smooth transformation with good enantioselectivity (136.22–136.24) (Scheme 136). Importantly, the N–H bond in substrate is crucial to enantioinduction, as protecting the nitrogen with a

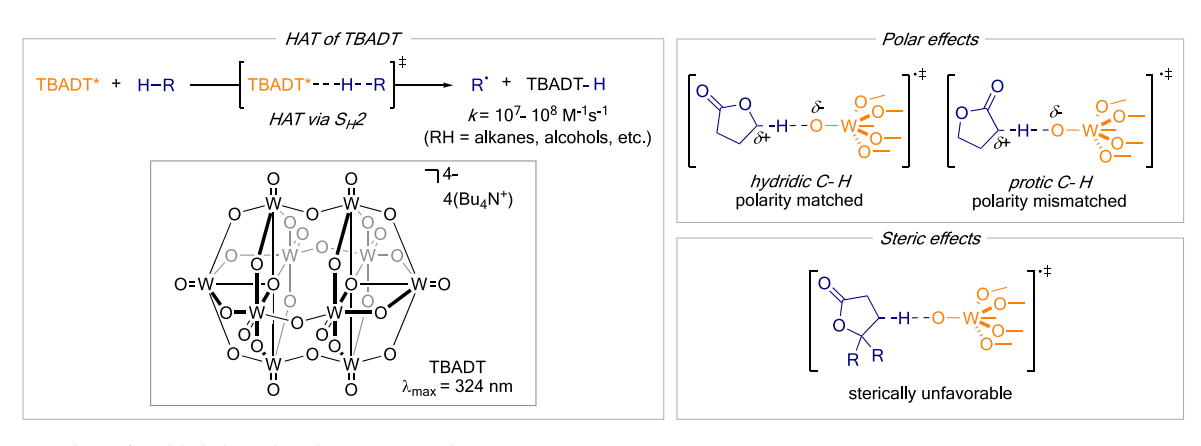
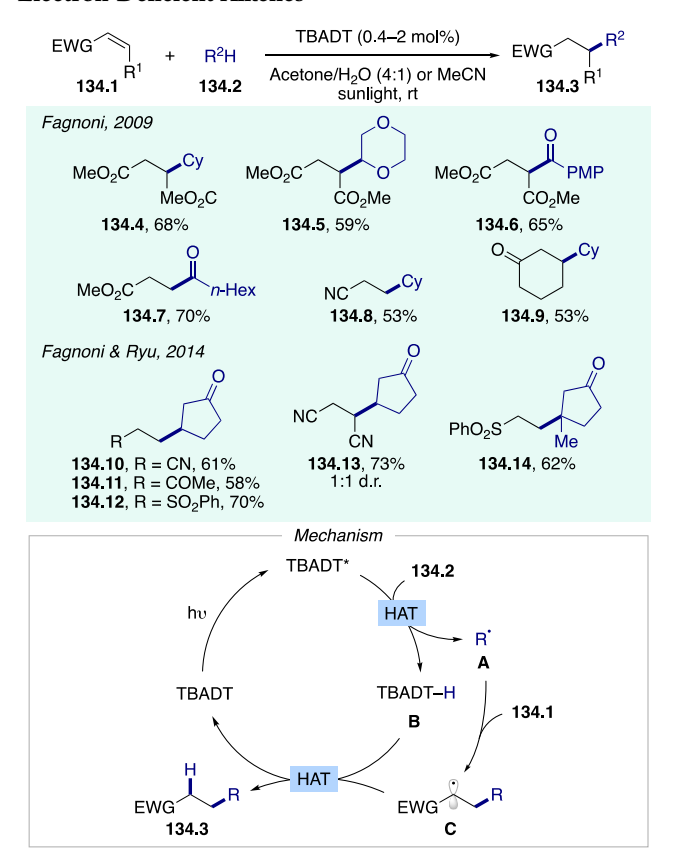


Figure 10. Outline of visible light-induced tungsten catalysis.

Scheme 134. Solar Light-Induced C—H Alkylation with Electron-Deficient Alkenes



methyl group led to the formation of racemic products. Of note, the authors also applied this protocol toward α -aryl carboxylates from the corresponding α -aryl acrylates.

In addition to Michael acceptors, vinyl (hetero)arenes have also been employed for C–H alkylation. In 2019, C. Wang and co-workers reported a hydroacylation reaction of α -trifluoromethylated vinyl (hetero)arenes. Styrene derivatives containing a range of functionalities were compatible (137.4–137.8). Vinyl heteroarenes also provided the respective products uneventfully (137.9). Besides aliphatic aldehydes, the aryl counterparts were also found to be suitable C–H sources (137.10–137.12). N-Phenylformamide also delivered the respective product, albeit with diminished efficiency (137.13). It is noteworthy that β -F elimination, a common

Scheme 135. Tandem Alkylation/Chiral Proton Transfer en Route to Enantioenriched Ketones

side reaction in previous methods, ^{354–356} was not observed in this protocol.

More recently, Prieto and Taillefer employed disulfide as a cocatalyst for C-H alkylation of styrenes. The Various styrene derivatives (137.14–137.17), as well as 2-vinylpyridine (137.18), reacted smoothly with formamide to deliver the corresponding amides in moderate to good yields. N-Alkyl (137.19) and -aryl (137.20) formamides were also found to be suitable reaction partners. However, tertiary amide did not yield the desired product (137.21). Other C-H sources, including aldehydes (137.22–137.23) and 1,3-benzodioxole (137.24), also worked well in this transformation. The authors also demonstrated an example of alkylation with PhSiH₃ (137.25). This protocol features the use of disulfide as a polarity reversal catalyst to circumvent the redox potential mismatch between benzylic radical A and reduced decatungstate B. Thus,

Scheme 136. Synthesis of Unnatural α -Amino Acids

photocatalytically generated thiol radical, which has much lower reduction potential than **A**, undergoes efficient single electron reduction by **B** followed by protonation to form thiol, which in turn, transfers a hydrogen atom to **A** to furnish product **137.20** (Scheme 137).

In 2019, Dilman's group employed *N*-tosyl imines 138.1 as radical acceptor to access alkylation products 138.3. As established in the previous reports, simple aliphatics (138.4), ethers (138.5–138.6), amides (138.7), and aldehydes (138.8) were all found to be viable C–H sources. Aldimines bearing other aryl- (138.9) and alkyl (138.10) substituents also underwent smooth transformation. On the contrary, ketimines afforded much lower yield, presumably due to the steric hindrance (138.11). In addition to a mechanism that resembles the one described before (cf. Scheme 134), the authors proposed an alternative pathway, where electrophilic *N*-centered radical, formed upon radical addition, undergoes HAT with the C–H source to furnish product 138.3 and propagate the radical chain (Scheme 138).

10.3. C-H Alkynylation and Deuteration

Very recently, Capaldo and co-worker reported a C-H alkynylation protocol using methanesulfonyl alkynes 139.1 proceeding via radical addition/elimination pathway. The scope with respect to the C-H sources was similar to the examples presented so far (139.4–139.7). Various functional groups could be introduced at the phenyl ring of substrate (139.8–139.11). Besides, an example of aliphatic substrate was also demonstrated (139.12). The employment of sulfonyl substituent as a radical leaving group was crucial, as the chloro

Scheme 137. C-H Alkylation with Styrene Derivatives

Scheme 138. C-H Alkylation with Imines

analogue 139.13 led to vinylation product 139.14 (Scheme 139).

As detailed in Scheme 95, thiol can be incorporated in decatungstate catalysis to facilitate back HAT to the organic radical intermediate. In 2020, Q. Wang's group reported the deuteration of aldehydes 140.1 via a direct hydrogen isotope exchange (HIE) with D₂O, using thiol 140.3 as a DAT catalyst. A broad range of functionalized (hetero)aryl aldehydes were efficiently deuterated (140.4–140.13). Notably, products 140.10 and 140.11, possessing allylic and benzylic C–H bonds, respectively, were obtained chemoselectively. Aliphatic aldehydes also underwent deuteration with high level of deuterium incorporation (140.14–140.16). In some cases,

Scheme 139. C—H Alkynylation with Methanesulfonyl Alkynes

additional deuteration occurred at the α -C-H site to the carbonyl group. Furthermore, more complex substrates, such as ibuprofen derivative (140.16), can also be selectively deuteriated.

In the same year, Wu and co-workers reported the same transformation under similar conditions.³⁶¹ Likewise, (hetero)-aryl- (140.4, 140.17–140.21) and aliphatic (140.22–140.23) aldehydes underwent efficient isotope exchange to provide the deuterated products. The authors also extended this chemistry toward deuteration of aliphatic C(sp³)–H bonds. Thus, both unactivated and activated C–H sites were successfully deuterated (140.26–140.28). As in the previous cases, further deuteration at other positions may occur (140.29–140.31) (Scheme 140). In addition, a range of pharmaceutical compounds, such as edaravone (140.32), mexiletine (140.33) and sesamol derivative (140.34), were amenable to this transformation, further highlighting the generality of this protocol.

11. OTHER TRANSITION METALS

11.1. Manganese

Although there are reports on manganese-catalyzed organic reactions under visible light irradiation, 362 a majority of them feature an off-cycle, photoassisted generation of active manganese species, which then catalyzes the reaction in its ground state. A notable example is the photolysis of $\rm Mn_2(CO)_{10}$ to its reactive monomeric form. $^{363-368}$ As such, there are only a handful of photocatalytic reactions, where a photoexcited manganese complex undergoes redox events with a substrate molecule via an inner sphere mechanism.

In 2018, Ackermann's group disclosed the first example of visible light-induced manganese catalysis, in which a Mn(I) catalyst for C–H arylation of (hetero)arenes 141.2 with aryldiazonium salts 141.1 was employed. ³⁶⁹ Electron-deficient diazonium salts reacted efficiently with various arenes to form the biaryl products in moderate to good yields (141.4–141.18). Likewise, heteroarenes, including furans (141.9–141.13), pyrroles (141.14), as well as thiophenes (141.15–141.17), were found to be viable substrates for this transformation. Of note, products 141.16 and 141.17 were obtained with excellent regioselectivity. The proposed mechanism begins with an off-cycle ligand exchange between CpMn(CO)₃ and arene 141.2 to form complex A, which undergoes a second exchange with diazonium salt 141.1 to produce visible-light absorbing species B. Then photoexcitation of B triggers an SET from Mn(I) to

Scheme 140. C-H Deuteration at (a) Formyl C-H and (b) Hydridic C(sp³)-H Sites

diazonium salt, leading to the formation of aryl radical C and Mn(II) complex D. A subsequent radical addition of the former to another arene molecule affords intermediate E, which is then oxidized by Mn(II) intermediate D to carbocation F, meanwhile regenerating the Mn(I) catalyst (path a). Alternatively, radical E can be oxidized by diazonium salt (path b). Finally, deprotonation of intermediate F furnishes the reaction product 141.3. In accord with the proposed mechanism, the competition experiment showed that electron-deficient diazonium salt 141.18 reacted preferentially over its electron-rich counterpart 141.19. Besides, a parallel KIE value of 1.0 indicated that the C—H bond cleavage is not the rate-determining step. In addition, the formation of aryl radical was supported by radical trapping experiment with 1,1-diphenylethylene (141.21) (Scheme 141).

In 2020, Wan and co-workers showed that photoexcited Mn(III) complex can be reduced by Langlois' reagent (NaSO₂CF₃), representing an example of reductive quenching cycle in manganese photocatalysis.³⁷⁰ In this work, unactivated

Scheme 141. C—H Arylation of Arenes under Photoflow Conditions

alkenes 142.1 underwent hydroxytrifluoromethylation with $NaSO_2CF_3$ under aerobic conditions. Monosubstituted alkenes with pendant ester functionality were found to be suitable substrates for this transformation (142.3–142.7). Likewise, imides (142.8) and thioesters (142.9) delivered the respective products in good yields. 1,1-Disubstituted alkenes also underwent smooth reaction, furnishing tertiary alcohol with high efficiency (142.10). The catalytic cycle commences with an SET event from $NaSO_2CF_3$ to photoexcited Mn(III) catalyst, producing trifluoromethyl radical and a Mn(II) complex. The former then adds to unactivated alkene 142.1 to afford alkyl radical A, which is subsequently trapped by molecular oxygen to

generate peroxy radical **B**. Finally, intermediate **B** reacts with the Mn(II) complex to deliver product **142.2**, presumably via the respective Mn(III) peroxo intermediate, and complete the cycle (Scheme 142). Radical trapping experiment revealed the formation of TEMPO–CF₃ adduct, thus supporting the radical nature of this reaction.

Scheme 142. Hydroxytrifluoromethylation of Unactivated Alkenes

11.2. Ruthenium

In contrast to its rich chemistry as a conventional photosensitizer, 1,6 ruthenium had not been utilized as a transition metal catalyst in the realm of photocatalysis until recently. In these scarce reports, however, visible light-photoexcited ruthenium catalysis has exhibited interesting reactivity, which is distinct from that in its ground state.

In 2019, the groups of Ackermann and Greaney simultaneously reported a photoinduced Ru(II)-catalyzed *meta*-selective alkylation of arenes 143.1. $^{371-373}$ In the protocol developed by Ackermann and co-workers, a range of tertiary alkyl bromides underwent efficient reaction with 2-phenyl-pyridine to provide the respective alkylation products in good to excellent yields (143.4–143.7). Substrates with substituted phenyl ring were also found to be effective (143.8–143.9). Remarkably, this protocol enables a selective *meta*-alkylation regardless of the steric environment (143.10). Secondary alkyl bromides were generally less efficient, leading to the corresponding products in moderate yields (143.11–143.13). α -Bromo esters also proved to be viable reaction partners (143.14). The authors also showed that in addition to pyridine, other directing groups, such as pyrazole (143.15) and oxazoline (143.16), also delivered the desired products, albeit with lower efficiency.

Greaney's method relies on use of alkyl iodides in this transformation. Thus, alkylation with tertiary (143.17–143.18) and secondary alkyl iodides (143.19–143.22) was achieved with moderate to good efficiencies. This protocol exhibits high functional group tolerance, as exemplified by the efficient

synthesis of products 143.23–143.26. As in the previous case, the authors also demonstrated the viability of other directing groups for this transformation (143.27). It is noteworthy that primary alkyl iodides were also reactive under the same conditions, but delivered *ortho*-alkylation products instead.

The proposed mechanism involves the *in situ* formation of photoactive cyclometalated Ru(II) complex **A** from ruthenium catalyst and substrate **143.1**. Upon photoexcitation, complex **A** undergoes SET with alkyl halide **143.2** to produce alkyl radical **B** and Ru(III) species **C**. A subsequent addition of nucleophilic radical **B** at the position *para*-to-Ru(III) leads to complex **D**, which is then oxidized upon intramolecular SET. Finally, deprotonation followed by protiodemetalation releases alkylation product **143.3** and regenerates Ru(II) catalyst. Mechanistic studies performed by the two groups confirmed the radical nature of this reaction. In addition, fluorescence quenching studies established the role of alkyl halides as the quencher of the photoexcited complex **A** (Scheme **143**).

11.3. Platinum

While an array of platinum photosensitizers has been developed for various applications, such as photodynamic therapies ^{374–377} and synthetic chemistry, ^{378,379} organic transformations wherein the platinum catalyst is directly involved in bond breaking/forming events remain scarce.

In 2004, Tung, Wu, and co-workers disclosed a visible lightinduced Pt(II)-catalyzed hydrogen production from Hantzsch ester derivatives 144.1. Remarkably, platinum catalyst 144.3 efficiently catalyzed the dehydrogenation with quantitative formation of H₂ at catalyst loading as low as 0.1 mol %. On the other hand, Hantzsch esters with secondary alkyl or benzyl substituent at the 4-position underwent dealkylation, delivering pyridines 144.4 and alkanes 144.5. The proposed mechanism begins with the photoinduced excitation of platinum catalyst 144.3 to its MLCT state, which undergoes intermolecular HAT at the 1-position of substrate 144.1 to produce Pt(III) hydride and N-centered radical A in a solvent cage. A subsequent atom transfer affords pyridine derivative 144.2 or 144.5, and Pt(II)— H_2 or Pt(II)-RH complex **B**. The latter then regenerates Pt(II)catalyst upon hydrogen or alkane elimination. Deuteriumlabeling studies revealed a lower photoluminescence quenching constant for Hantzsch ester deuterated at the 1-position compared to the one at 4-position, thus indicating the first HAT occurs at the nitrogen site (Scheme 144).

12. CONCLUSIONS

Visible light-induced transition metal catalysis has emerged as a new area in photocatalysis. Although it has only been studied for a few years, a range of transition metals exhibiting various excited-state reactivities has been already successfully demonstrated, as displayed by the diverse transformations discussed in this Review. It is believed that this exogenous photosensitizer-free and mechanistically distinct subfield of photocatalysis will continue to grow.

Despite the recent advances achieved in visible light-induced transition metal catalysis, this field is still largely underexplored. An inspiration for the development of new protocols under visible light may come from the rich conventional ground state transition metal reactivity. Besides, certain limitations are yet to be overcome. Within the context of photoinduced SET, a majority of transformations presented herein proceed via oxidative quenching of the transition metal complex. Thus, a wide range of organic electrophiles (oxidative quench) can be

Scheme 143. meta-Selective C-H Alkylation of Arenes

converted to the respective radical species using the current methods as in conventional photoredox chemistry. In contrast, the analogous transformations utilizing nucleophiles (reductive quench) are much less explored. Accomplishing the alternative reductive process will not only allow for a substantial expansion of substrate scope but also lead to a transition metal intermediate at a different oxidation state, which, in turn, may display new

С

 R^3

В

Scheme 144. Photocatalytic Dehydrogenation and Dealkylation of Hantzsch Esters

reactivities. Furthermore, a direct generation of C-centered radicals from strong C-H bonds remains underdeveloped in transition metal photocatalysis. Another formidable challenge is achieving high site-selectivity with substrates possessing similar C-H bonds. It should be also mentioned that except for copper, iridium, and rhodium catalysis, for which some enantioselective transformations have been demonstrated, analogous methods for other metals are yet to be developed. While it is expected to be a more challenging task given an added criterion, namely the chiral transition metal complex needs to be a chromophore capable of initiating photochemistry, a rational ligand design will undoubtedly bring valuable insights into the development of this type of asymmetric catalysis. Naturally, it is also expected that development toward the utilization of less explored first-row transition metals will constitute an important future direction of this field.

In addition to these limitations, in-depth mechanistic investigations are required to provide a more comprehensive understanding of the reaction mechanisms. While many of the mechanistic studies are reasonably focused on the excited state reactivity of the catalyst or the catalyst—substrate complex, there are considerably less information regarding the subsequently formed transition metal intermediates. These, in turn, may also be photoactive and therefore noninnocent, thus potentially altering the reaction mechanism. Furthermore, systematic studies on how ligands affect the photophysical properties of the transition metal complexes are highly warranted, as they can provide guiding principles on the design of catalytic systems with enhanced photochemical and catalytic properties.

We anticipate that this mode of photocatalysis will become a versatile strategy and find broad applications in synthetic chemistry, pharmaceutical chemistry, and material science.

AUTHOR INFORMATION

Corresponding Author

Vladimir Gevorgyan — Department of Chemistry and Biochemistry, The University of Texas at Dallas, Richardson, Texas 75080, United States; ⊚ orcid.org/0000-0002-7836-7596; Email: vlad@utdallas.edu

Authors

Kelvin Pak Shing Cheung — Department of Chemistry and Biochemistry, The University of Texas at Dallas, Richardson, Texas 75080, United States

Sumon Sarkar — Department of Chemistry and Biochemistry, The University of Texas at Dallas, Richardson, Texas 75080, United States

Complete contact information is available at: https://pubs.acs.org/10.1021/acs.chemrev.1c00403

Notes

The authors declare no competing financial interest.

Biographies

Kelvin Pak Shing Cheung received his BSc and MPhil in chemistry from the Chinese University of Hong Kong. In 2018, he joined Gevorgyan group at the University of Illinois at Chicago as a PhD student, and later at the University of Texas at Dallas. His research work has focused on the development of visible light-induced transition metal-catalyzed transformations.

Sumon Sarkar received his BSc from Jadavpur University, Kolkata and MSc from Indian Institute of Technology Kanpur. In 2017, he joined the Gevorgyan group at the University of Illinois at Chicago as a PhD student and later moved to the University of Texas at Dallas. His research interest is focused on development of novel photoinduced methodologies.

Vladimir Gevorgyan received his PhD from the Latvian Institute of Organic Synthesis. After two years of postdoctoral research (1992–1994, JSPS- and CibaGeigy International Postdoctoral Fellowships) at Tohoku University, Japan, and a visiting professorship (1995) at CNR, Bologna, Italy, he joined the faculty at Tohoku University (Assistant Professor, 1996; Associate Professor, 1997–1999). In 1999, Vladimir Gevorgyan moved to USA to join UIC (Associate Professor, 1999; Professor, 2003; LAS Distinguished Professor, 2012). In 2019, he joined the University of Texas at Dallas to become a Robert. A. Welch Distinguished Chair in Chemistry. Vladimir also holds a Professor position at the University of Texas Southwestern Medical Center. His group is interested in the development of novel synthetic methodology, particularly toward biologically relevant molecules.

ACKNOWLEDGMENTS

We thank the National Institute of Health (GM120281), National Science Foundation (CHE-1955663), and Welch Foundation (Chair, AT-0041) for financial support. S.S. thanks the Eugene McDermott Graduate Fellowship, UT Dallas.

REFERENCES

- (1) Narayanam, J. M.; Stephenson, C. R. Visible Light Photoredox Catalysis: Applications in Organic Synthesis. *Chem. Soc. Rev.* **2011**, *40*, 102–113
- (2) Tucker, J. W.; Stephenson, C. R. Shining Light on Photoredox Catalysis: Theory and Synthetic Applications. *J. Org. Chem.* **2012**, *77*, 1617–1622.

- (3) Prier, C. K.; Rankic, D. A.; MacMillan, D. W. Visible Light Photoredox Catalysis with Transition Metal Complexes: Applications in Organic Synthesis. *Chem. Rev.* **2013**, *113*, 5322–5363.
- (4) Schultz, D. M.; Yoon, T. P. Solar Synthesis: Prospects in Visible Light Photocatalysis. *Science* **2014**, *343*, 1239176.
- (5) Romero, N. A.; Nicewicz, D. A. Organic Photoredox Catalysis. *Chem. Rev.* **2016**, *116*, 10075–10166.
- (6) Shaw, M. H.; Twilton, J.; MacMillan, D. W. Photoredox Catalysis in Organic Chemistry. *J. Org. Chem.* **2016**, *81*, 6898–6926.
- (7) Skubi, K. L.; Blum, T. R.; Yoon, T. P. Dual Catalysis Strategies in Photochemical Synthesis. *Chem. Rev.* **2016**, *116*, 10035–10074.
- (8) Tellis, J. C.; Kelly, C. B.; Primer, D. N.; Jouffroy, M.; Patel, N. R.; Molander, G. A. Single-Electron Transmetalation via Photoredox/Nickel Dual Catalysis: Unlocking a New Paradigm for sp³-sp² Cross-Coupling. *Acc. Chem. Res.* **2016**, *49*, 1429–1439.
- (9) Twilton, J.; Le, C.; Zhang, P.; Shaw, M. H.; Evans, R. W.; MacMillan, D. W. C. The Merger of Transition Metal and Photocatalysis. *Nat. Rev. Chem.* **2017**, *1*, 0052.
- (10) Marzo, L.; Pagire, S. K.; Reiser, O.; Konig, B. Visible-Light Photocatalysis: Does It Make a Difference in Organic Synthesis? *Angew. Chem., Int. Ed.* **2018**, *57*, 10034–10072.
- (11) Strieth-Kalthoff, F.; James, M. J.; Teders, M.; Pitzer, L.; Glorius, F. Energy Transfer Catalysis Mediated by Visible Light: Principles, Applications, Directions. *Chem. Soc. Rev.* **2018**, *47*, 7190–7202.
- (12) Sandoval, B. A.; Hyster, T. K. Emerging Strategies for Expanding the Toolbox of Enzymes in Biocatalysis. *Curr. Opin. Chem. Biol.* **2020**, *55*, 45–51.
- (13) Parasram, M.; Gevorgyan, V. Visible Light-Induced Transition Metal-Catalyzed Transformations: Beyond Conventional Photosensitizers. *Chem. Soc. Rev.* **2017**, *46*, 6227–6240.
- (14) Kancherla, R.; Muralirajan, K.; Sagadevan, A.; Rueping, M. Visible Light-Induced Excited-State Transition-Metal Catalysis. *Trends Chem.* **2019**, *1*, 510–523.
- (15) Cheng, W. M.; Shang, R. Transition Metal-Catalyzed Organic Reactions under Visible Light: Recent Developments and Future Perspectives. ACS Catal. 2020, 10, 9170–9196.
- (16) For an example of dual photocatalysis in which transition metal complex is also light-absorbing, see: Zhang, Z.; Rogers, C. R.; Weiss, E. A. Energy Transfer from CdS QDs to a Photogenerated Pd Complex Enhances the Rate and Selectivity of a Pd-Photocatalyzed Heck Reaction. *J. Am. Chem. Soc.* **2020**, 142, 495–501.
- (17) Pattenden, G. Simonsen Lecture. Cobalt-Mediated Radical Reactions in Organic Synthesis. *Chem. Soc. Rev.* **1988**, *17*, 361–382.
- (18) Demarteau, J.; Debuigne, A.; Detrembleur, C. Organocobalt Complexes as Sources of Carbon-Centered Radicals for Organic and Polymer Chemistries. *Chem. Rev.* **2019**, *119*, 6906–6955.
- (19) Scheffold, R.; Rytz, G.; Walder, L.; Orlinski, R.; Chilmonczyk, Z. Formation of (C-C) Bonds Catalyzed by Vitamin-B12. *Pure Appl. Chem.* 1983, 55, 1791–1797.
- (20) Branchaud, B. P.; Detlefsen, W. D. Cobaloxime-Catalyzed Radical Alkyl-Styryl Cross Couplings. *Tetrahedron Lett.* **1991**, *32*, 6273–6276.
- (21) Weiss, M. E.; Kreis, L. M.; Lauber, A.; Carreira, E. M. Cobalt-Catalyzed Coupling of Alkyl Iodides with Alkenes: Deprotonation of Hydridocobalt Enables Turnover. *Angew. Chem., Int. Ed.* **2011**, *50*, 11125–11128.
- (22) Giedyk, M.; Goliszewska, K.; Proinsias, K.; Gryko, D. Cobalt(I)-Catalysed CH-Alkylation of Terminal Olefins, and Beyond. *Chem. Commun.* **2016**, *52*, 1389–1392.
- (23) Prina Cerai, G.; Morandi, B. Atom-Economical Cobalt-Catalysed Regioselective Coupling of Epoxides and Aziridines with Alkenes. *Chem. Commun.* **2016**, *52*, 9769–9772.
- (24) Ociepa, M.; Baka, O.; Narodowiec, J.; Gryko, D. Light-Driven Vitamin B₁₂-Catalysed Generation of Acyl Radicals from 2-S-Pyridyl Thioesters. *Adv. Synth. Catal.* **2017**, 359, 3560–3565.
- (25) Ociepa, M.; Wierzba, A. J.; Turkowska, J.; Gryko, D. Polarity-Reversal Strategy for the Functionalization of Electrophilic Strained Molecules via Light-Driven Cobalt Catalysis. *J. Am. Chem. Soc.* **2020**, 142, 5355–5361.

- (26) Komeyama, K.; Michiyuki, T.; Teshima, Y.; Osaka, I. Visible Light-Driven Giese Reaction with Alkyl Tosylates Catalysed by Nucleophilic Cobalt. RSC Adv. 2021, 11, 3539—3546.
- (27) Ravetz, B. D.; Wang, J. Y.; Ruhl, K. E.; Rovis, T. Photoinduced Ligand-to-Metal Charge Transfer Enables Photocatalyst-Independent Light-Gated Activation of Co(II). *ACS Catal.* **2019**, *9*, 200–204.
- (28) Liu, W. Q.; Lei, T.; Zhou, S.; Yang, X. L.; Li, J.; Chen, B.; Sivaguru, J.; Tung, C. H.; Wu, L. Z. Cobaloxime Catalysis: Selective Synthesis of Alkenylphosphine Oxides under Visible Light. *J. Am. Chem. Soc.* 2019, 141, 13941–13947.
- (29) Scheffold, R.; Orlinski, R. Synthesis and Reactions of Porphine-Type Metal Complexes. 15. Carbon-Carbon Bond Formation by Light Assisted B12-Catalysis. Nucleophilic Acylation of Michael Olefins. *J. Am. Chem. Soc.* 1983, 105, 7200–7202.
- (30) Busato, S.; Tinembart, O.; Zhang, Z.-d.; Scheffold, R. Vitamin B_{12} , a Catalyst in the Synthesis of Prostaglandins. *Tetrahedron* **1990**, *46*, 3155–3166.
- (31) Giedyk, M.; Goliszewska, K.; Gryko, D. Vitamin B₁₂ Catalysed Reactions. *Chem. Soc. Rev.* **2015**, *44*, 3391–3404.
- (32) Gryko, D.; Wincenciuk, A.; Smoleń, S.; Drapała, O. Vitamin B₁₂-Catalyzed Dicarbofunctionalization of Bromoalkenes Under Visible Light Irradiation. *Synthesis* **2021**, *53*, 1645–1653.
- (33) Potrzasaj, A.; Ociepa, M.; Baka, O.; Spólnik, G.; Gryko, D. Vitamin B_{12} Enables Consecutive Generation of Acyl and Alkyl Radicals from One Reagent. *Eur. J. Org. Chem.* **2020**, 2020, 1567–1571.
- (34) Giese, B.; Erdmann, P.; Gobel, T.; Springer, R. Cobalt-Catalyzed Carbon-Carbon Bond Formation via Radicals. *Tetrahedron Lett.* **1992**, 33, 4545–4548.
- (35) Tada, M.; Kaneko, K. (Triphenyltin) cobaloxime as a Reagent for Radical Generation from Bromides. *J. Org. Chem.* **1995**, *60*, *66*35–6636
- (36) Weiss, M. E.; Carreira, E. M. Total Synthesis of (+)-Daphmanidin E. *Angew. Chem., Int. Ed.* **2011**, *50*, 11501–11505.
- (37) Kreis, L. M.; Krautwald, S.; Pfeiffer, N.; Martin, R. E.; Carreira, E. M. Photocatalytic Synthesis of Allylic Trifluoromethyl Substituted Styrene Derivatives in Batch and Flow. *Org. Lett.* **2013**, *15*, 1634–1637.
- (38) Karczewski, M.; Ociepa, M.l; Pluta, K.; o Proinsias, K.; Gryko, D. Vitamin B₁₂ Catalysis: Probing the Structure/Efficacy Relationship. *Chem. Eur. J.* **2017**, 23, 7024–7030.
- (39) Lebel, H.; Marcoux, J. F.; Molinaro, C.; Charette, A. B. Stereoselective Cyclopropanation Reactions. *Chem. Rev.* **2003**, *103*, 977–1050.
- (40) Xu, X.; Zhu, S.; Cui, X.; Wojtas, L.; Zhang, X. P. Cobalt(II)-Catalyzed Asymmetric Olefin Cyclopropanation with α -Ketodiazoacetates. *Angew. Chem., Int. Ed.* **2013**, *52*, 11857–11861.
- (41) Otte, M.; Kuijpers, P. F.; Troeppner, O.; Ivanovic-Burmazovic, I.; Reek, J. N.; de Bruin, B. Encapsulated Cobalt-Porphyrin as a Catalyst for Size-Selective Radical-Type Cyclopropanation Reactions. *Chem. Eur. J.* **2014**, *20*, 4880–4884.
- (42) Choi, M.-Y.; Chan, M. C.-W.; Zhang, S.; Cheung, K.-K.; Che, C.-M.; Wong, K.-Y. MLCT and LMCT Transitions in Acetylide Complexes. Structural, Spectroscopic, and Redox Properties of Ruthenium(II) and -(III) $\operatorname{Bis}(\sigma$ -arylacetylide) Complexes Supported by a Tetradentate Macrocyclic Tertiary Amine Ligand. *Organometallics* 1999, 18, 2074–2080.
- (43) Gesing, E. R. F.; Tane, J. P.; Vollhardt, K. P. C. Cobalt Mediated [2 + 2+2]-Cycloadditions A Simple Route to Substituted Cyclopentadienones. *Angew. Chem., Int. Ed. Engl.* **1980**, *19*, 1023–1024.
- (44) Brien, D. J.; Naiman, A.; Vollhardt, K. P. C. Catalytic Cocyclisation of α , ω -Cyanoalkynes with Alkynes: a Versatile Chemo- and Regio-Selective Synthesis of 2,3-Substituted 5,6,7,8-Tetrahydroquinolines and Other Cycloalka[1,2-b]pyridines. *J. Chem. Soc., Chem. Commun.* 1982, 133–134.
- (45) Schulz, W.; Pracejus, H.; Oehme, G. Photoassisted Cocyclization of Acetylene and Nitriles Catalyzed by Cobalt Complexes at Ambient-Temperature and Normal Pressure. *Tetrahedron Lett.* **1989**, *30*, 1229–1232.

- (46) Heller, B.; Oehme, G. First Cobalt(I)-Catalyzed Heterocyclotrimerization of Ethyne with Nitriles to Pyridines in Water under Mild Conditions. *J. Chem. Soc., Chem. Commun.* **1995**, 179–180.
- (47) Lei, T.; Liang, G.; Cheng, Y. Y.; Chen, B.; Tung, C. H.; Wu, L. Z. Cobaloxime Catalysis for Enamine Phosphorylation with Hydrogen Evolution. *Org. Lett.* **2020**, *22*, 5385–5389.
- (48) Reiser, O. Shining Light on Copper: Unique Opportunities for Visible-Light-Catalyzed Atom Transfer Radical Addition Reactions and Related Processes. *Acc. Chem. Res.* **2016**, *49*, 1990–1996.
- (49) Hossain, A.; Bhattacharyya, A.; Reiser, O. Copper's Rapid Ascent in Visible-Light Photoredox Catalysis. *Science* **2019**, *364*, No. eaav9713. (50) Creutz, S. E.; Lotito, K. J.; Fu, G. C.; Peters, J. C. Photoinduced
- Ullmann C-N Coupling: Demonstrating the Viability of a Radical Pathway. *Science* **2012**, 338, 647–651.
- (51) Chinchilla, R.; Najera, C. Recent Advances in Sonogashira Reactions. *Chem. Soc. Rev.* **2011**, *40*, 5084–5121.
- (52) Kanwal, I.; Mujahid, A.; Rasool, N.; Rizwan, K.; Malik, A.; Ahmad, G.; Shah, S. A. A.; Rashid, U.; Nasir, N. M. Palladium and Copper Catalyzed Sonogashira Cross Coupling an Excellent Methodology for C-C Bond Formation over 17 Years: A Review. *Catalysts* **2020**, *10*, 443.
- (53) Sagadevan, A.; Hwang, K. C. Photo-Induced Sonogashira C-C Coupling Reaction Catalyzed by Simple Copper(I) Chloride Salt at Room Temperature. *Adv. Synth. Catal.* **2012**, *354*, 3421–3427.
- (54) Tang, X. J.; Dolbier, W. R., Jr. Efficient Cu-Catalyzed Atom Transfer Radical Addition Reactions of Fluoroalkylsulfonyl Chlorides with Electron-Deficient Alkenes Induced by Visible Light. *Angew. Chem., Int. Ed.* **2015**, *54*, 4246–4249.
- (55) Bagal, D. B.; Kachkovskyi, G.; Knorn, M.; Rawner, T.; Bhanage, B. M.; Reiser, O. Trifluoromethylchlorosulfonylation of Alkenes: Evidence for an Inner-Sphere Mechanism by a Copper Phenanthroline Photoredox Catalyst. *Angew. Chem., Int. Ed.* **2015**, *54*, 6999–7002.
- (56) Kochi, J. K. Photolyses of Metal Compounds Cupric Chloride in Organic Media. J. Am. Chem. Soc. 1962, 84, 2121–2127.
- (57) Abderrazak, Y.; Bhattacharyya, A.; Reiser, O. Visible-Light-Induced Homolysis of Earth-Abundant Metal-Substrate Complexes: A Complementary Activation Strategy in Photoredox Catalysis. *Angew. Chem., Int. Ed.* **2021**, *60*, 21100.
- (58) Hossain, A.; Vidyasagar, A.; Eichinger, C.; Lankes, C.; Phan, J.; Rehbein, J.; Reiser, O. Visible-Light-Accelerated Copper(II)-Catalyzed Regio- and Chemoselective Oxo-Azidation of Vinyl Arenes. *Angew. Chem., Int. Ed.* **2018**, *57*, 8288–8292.
- (59) Li, Y.; Zhou, K.; Wen, Z.; Cao, S.; Shen, X.; Lei, M.; Gong, L. Copper(II)-Catalyzed Asymmetric Photoredox Reactions: Enantioselective Alkylation of Imines Driven by Visible Light. *J. Am. Chem. Soc.* **2018**, *140*, 15850–15858.
- (60) Lian, P.; Long, W.; Li, J.; Zheng, Y.; Wan, X. Visible-Light-Induced Vicinal Dichlorination of Alkenes through LMCT Excitation of CuCl₂. Angew. Chem., Int. Ed. 2020, 59, 23603–23608.
- (61) Treacy, S. M.; Rovis, T. Copper Catalyzed C(sp³)-H Bond Alkylation via Photoinduced Ligand-to-Metal Charge Transfer. *J. Am. Chem. Soc.* **2021**, *143*, 2729–2735.
- (62) Fayad, R.; Engl, S.; Danilov, E. O.; Hauke, C. E.; Reiser, O.; Castellano, F. N. Direct Evidence of Visible Light-Induced Homolysis in Chlorobis(2,9-dimethyl-1,10-phenanthroline)copper(II). *J. Phys. Chem. Lett.* **2020**, *11*, 5345–5349.
- (63) Lei, W. L.; Wang, T.; Feng, K. W.; Wu, L. Z.; Liu, Q. Visible-Light-Driven Synthesis of 4-Alkyl/Aryl-2-Aminothiazoles Promoted by In Situ Generated Copper Photocatalyst. *ACS Catal.* **2017**, *7*, 7941–7945
- (64) Bissember, A. C.; Lundgren, R. J.; Creutz, S. E.; Peters, J. C.; Fu, G. C. Transition-Metal-Catalyzed Alkylations of Amines with Alkyl Halides: Photoinduced, Copper-Catalyzed Couplings of Carbazoles. *Angew. Chem., Int. Ed.* **2013**, *52*, 5129–5133.
- (65) Uyeda, C.; Tan, Y.; Fu, G. C.; Peters, J. C. A New Family of Nucleophiles for Photoinduced, Copper-Catalyzed Cross-Couplings via Single-Electron Transfer: Reactions of Thiols with Aryl Halides under Mild Conditions (0 °C). *J. Am. Chem. Soc.* **2013**, *135*, 9548–9552.

- (66) Ziegler, D. T.; Choi, J.; Munoz-Molina, J. M.; Bissember, A. C.; Peters, J. C.; Fu, G. C. A Versatile Approach to Ullmann C-N Couplings at Room Temperature: New Families of Nucleophiles and Electrophiles for Photoinduced, Copper-Catalyzed Processes. *J. Am. Chem. Soc.* 2013, 135, 13107–13112.
- (67) Do, H. Q.; Bachman, S.; Bissember, A. C.; Peters, J. C.; Fu, G. C. Photoinduced, Copper-Catalyzed Alkylation of Amides with Unactivated Secondary Alkyl Halides at Room Temperature. *J. Am. Chem. Soc.* **2014**, *136*, 2162–2167.
- (68) Tan, Y. C.; Munoz-Molina, J. M.; Fu, G. C.; Peters, J. C. Oxygen Nucleophiles as Reaction Partners in Photoinduced, Copper-Catalyzed Cross-Couplings: *O*-Arylations of Phenols at Room Temperature. *Chem. Sci.* **2014**, *5*, 2831–2835.
- (69) Ratani, T. S.; Bachman, S.; Fu, G. C.; Peters, J. C. Photoinduced, Copper-Catalyzed Carbon-Carbon Bond Formation with Alkyl Electrophiles: Cyanation of Unactivated Secondary Alkyl Chlorides at Room Temperature. *J. Am. Chem. Soc.* **2015**, *137*, 13902–13907.
- (70) Yang, F.; Koeller, J.; Ackermann, L. Photoinduced Copper-Catalyzed C-H Arylation at Room Temperature. *Angew. Chem., Int. Ed.* **2016**, *55*, 4759–4762.
- (71) Ahn, J. M.; Ratani, T. S.; Hannoun, K. I.; Fu, G. C.; Peters, J. C. Photoinduced, Copper-Catalyzed Alkylation of Amines: A Mechanistic Study of the Cross-Coupling of Carbazole with Alkyl Bromides. *J. Am. Chem. Soc.* **2017**, *139*, 12716–12723.
- (72) Gandeepan, P.; Mo, J.; Ackermann, L. Photo-Induced Copper-Catalyzed C-H Chalcogenation of Azoles at Room Temperature. *Chem. Commun.* **2017**, *53*, 5906–5909.
- (73) Hernandez-Perez, A. C.; Vlassova, A.; Collins, S. K. Toward a Visible Light Mediated Photocyclization: Cu-Based Sensitizers for the Synthesis of [5]Helicene. *Org. Lett.* **2012**, *14*, 2988–2991.
- (74) Pirtsch, M.; Paria, S.; Matsuno, T.; Isobe, H.; Reiser, O. [Cu(dap)₂Cl] as an Efficient Visible-Light-Driven Photoredox Catalyst in Carbon-Carbon Bond-Forming Reactions. *Chem. Eur. J.* **2012**, *18*, 7336–7340.
- (75) Hernandez-Perez, A. C.; Collins, S. K. A Visible-Light-Mediated Synthesis of Carbazoles. *Angew. Chem., Int. Ed.* **2013**, *52*, 12696–12700.
- (76) Paria, S.; Pirtsch, M.; Kais, V.; Reiser, O. Visible-Light-Induced Intermolecular Atom-Transfer Radical Addition of Benzyl Halides to Olefins: Facile Synthesis of Tetrahydroquinolines. *Synthesis* **2013**, *45*, 2689–2698.
- (77) Fumagalli, G.; Rabet, P. T.; Boyd, S.; Greaney, M. F. Three-Component Azidation of Styrene-Type Double Bonds: Light-Switchable Behavior of a Copper Photoredox Catalyst. *Angew. Chem., Int. Ed.* **2015**, *54*, 11481–11484.
- (78) Hernandez-Perez, A. C.; Caron, A.; Collins, S. K. Photochemical Synthesis of Complex Carbazoles: Evaluation of Electronic Effects in Both UV- and Visible-Light Methods in Continuous Flow. *Chem. Eur. J.* **2015**, *21*, 16673–16678.
- (79) Knorn, M.; Rawner, T.; Czerwieniec, R.; Reiser, O. [Copper(phenanthroline)(bisisonitrile)(+)-Complexes for the Visible-Light-Mediated Atom Transfer Radical Addition and Allylation Reactions. *ACS Catal.* **2015**, *5*, 5186–5193.
- (80) Hernandez-Perez, A. C.; Collins, S. K. Heteroleptic Cu-Based Sensitizers in Photoredox Catalysis. *Acc. Chem. Res.* **2016**, *49*, 1557–1565.
- (81) Ahn, J. M.; Peters, J. C.; Fu, G. C. Design of a Photoredox Catalyst that Enables the Direct Synthesis of Carbamate-Protected Primary Amines via Photoinduced, Copper-Catalyzed N-Alkylation Reactions of Unactivated Secondary Halides. J. Am. Chem. Soc. 2017, 139, 18101–18106.
- (82) Minozzi, C.; Caron, A.; Grenier-Petel, J. C.; Santandrea, J.; Collins, S. K. Heteroleptic Copper(I)-Based Complexes for Photocatalysis: Combinatorial Assembly, Discovery, and Optimization. *Angew. Chem., Int. Ed.* **2018**, *57*, 5477–5481.
- (83) Lyu, X. L.; Huang, S. S.; Song, H. J.; Liu, Y. X.; Wang, Q. M. Visible-Light-Induced Copper-Catalyzed Decarboxylative Coupling of Redox-Active Esters with N-Heteroarenes. *Org. Lett.* **2019**, *21*, 5728–5732.

- (84) Zheng, L.; Jiang, Q.; Bao, H.; Zhou, B.; Luo, S. P.; Jin, H.; Wu, H.; Liu, Y. Tertiary Amines Acting as Alkyl Radical Equivalents Enabled by a P/N Heteroleptic Cu(I) Photosensitizer. *Org. Lett.* **2020**, 22, 8888–8893.
- (85) Xu, P.; Lopez-Rojas, P.; Ritter, T. Radical Decarboxylative Carbometalation of Benzoic Acids: A Solution to Aromatic Decarboxylative Fluorination. *J. Am. Chem. Soc.* **2021**, *143*, 5349–5354.
- (86) Kainz, Q. M.; Matier, C. D.; Bartoszewicz, A.; Zultanski, S. L.; Peters, J. C.; Fu, G. C. Asymmetric Copper-Catalyzed C-N Cross-Couplings Induced by Visible Light. *Science* **2016**, *351*, *681*–*684*.
- (87) Matier, C. D.; Schwaben, J.; Peters, J. C.; Fu, G. C. Copper-Catalyzed Alkylation of Aliphatic Amines Induced by Visible Light. *J. Am. Chem. Soc.* **2017**, 139, 17707–17710.
- (88) He, J.; Chen, C.; Fu, G. C.; Peters, J. C. Visible-Light-Induced, Copper-Catalyzed Three-Component Coupling of Alkyl Halides, Olefins, and Trifluoromethylthiolate to Generate Trifluoromethyl Thioethers. ACS Catal. 2018, 8, 11741–11748.
- (89) Xiong, Y.; Ma, X.; Zhang, G. Copper-Catalyzed Intermolecular Carboamination of Alkenes Induced by Visible Light. *Org. Lett.* **2019**, 21, 1699–1703.
- (90) Xiong, Y.; Zhang, G. Visible-Light-Induced Copper-Catalyzed Intermolecular Markovnikov Hydroamination of Alkenes. *Org. Lett.* **2019**, *21*, 7873–7877.
- (91) Ganley, J. M.; Murray, P. R. D.; Knowles, R. R. Photocatalytic Generation of Aminium Radical Cations for C-N Bond Formation. *ACS Catal.* **2020**, *10*, 11712–11738.
- (92) Lu, B.; Cheng, Y.; Chen, L. Y.; Chen, J. R.; Xiao, W. J. Photoinduced Copper-Catalyzed Radical Aminocarbonylation of Cycloketone Oxime Esters. *ACS Catal.* **2019**, *9*, 8159–8164.
- (93) Thathagar, M. B.; Beckers, J.; Rothenberg, G. Palladium-Free and Ligand-Free Sonogashira Cross-Coupling. *Green Chem.* **2004**, *6*, 215–218
- (94) Zuidema, E.; Bolm, C. Sub-Mol % Catalyst Loading and Ligand-Acceleration in the Copper-Catalyzed Coupling of Aryl Iodides and Terminal Alkyenes. *Chem. Eur. J.* **2010**, *16*, 4181–4185.
- (95) Le, C.; Chen, T. Q.; Liang, T.; Zhang, P.; MacMillan, D. W. C. A Radical Approach to the Copper Oxidative Addition Problem: Trifluoromethylation of Bromoarenes. *Science* **2018**, *360*, 1010–1014.
- (96) Majek, M.; Jacobi von Wangelin, A. Ambient-Light-Mediated Copper-Catalyzed C-C and C-N Bond Formation. *Angew. Chem., Int. Ed.* **2013**, 52, 5919–5921.
- (97) Yam, V. W.-W.; Kam-Wing Lo, K.; Man-Chung Wong, K. Luminescent Polynuclear Metal Acetylides. *J. Organomet. Chem.* **1999**, 578, 3–30.
- (98) Hazra, A.; Lee, M. T.; Chiu, J. F.; Lalic, G. Photoinduced Copper-Catalyzed Coupling of Terminal Alkynes and Alkyl Iodides. *Angew. Chem., Int. Ed.* **2018**, *57*, 5492–5496.
- (99) Isse, A. A.; Lin, C. Y.; Coote, M. L.; Gennaro, A. Estimation of Standard Reduction Potentials of Halogen Atoms and Alkyl Halides. *J. Phys. Chem. B* **2011**, *115*, 678–684.
- (100) Dong, X. Y.; Zhang, Y. F.; Ma, C. L.; Gu, Q. S.; Wang, F. L.; Li, Z. L.; Jiang, S. P.; Liu, X. Y. A General Asymmetric Copper-Catalysed Sonogashira C(sp³)-C(sp) Coupling. *Nat. Chem.* **2019**, *11*, 1158–1166.
- (101) Xia, H. D.; Li, Z. L.; Gu, Q. S.; Dong, X. Y.; Fang, J. H.; Du, X. Y.; Wang, L. L.; Liu, X. Y. Photoinduced Copper-Catalyzed Asymmetric Decarboxylative Alkynylation with Terminal Alkynes. *Angew. Chem., Int. Ed.* **2020**, *59*, 16926–16932.
- (102) Chen, J.; He, B. Q.; Wang, P. Z.; Yu, X. Y.; Zhao, Q. Q.; Chen, J. R.; Xiao, W. J. Photoinduced, Copper-Catalyzed Radical Cross-Coupling of Cycloketone Oxime Esters, Alkenes, and Terminal Alkynes. *Org. Lett.* **2019**, *21*, 4359–4364.
- (103) Zhang, Y.; Sun, Y.; Chen, B.; Xu, M.; Li, C.; Zhang, D.; Zhang, G. Copper-Catalyzed Photoinduced Enantioselective Dual Carbofunctionalization of Alkenes. *Org. Lett.* **2020**, *22*, 1490–1494.
- (104) Parasram, M.; Chuentragool, P.; Wang, Y.; Shi, Y.; Gevorgyan, V. General, Auxiliary-Enabled Photoinduced Pd-Catalyzed Remote Desaturation of Aliphatic Alcohols. *J. Am. Chem. Soc.* **2017**, *139*, 14857–14860.

- (105) Chuentragool, P.; Yadagiri, D.; Morita, T.; Sarkar, S.; Parasram, M.; Wang, Y.; Gevorgyan, V. Aliphatic Radical Relay Heck Reaction at Unactivated C(sp³)-H Sites of Alcohols. *Angew. Chem., Int. Ed.* **2019**, 58, 1794–1798.
- (106) Kurandina, D.; Yadagiri, D.; Rivas, M.; Kavun, A.; Chuentragool, P.; Hayama, K.; Gevorgyan, V. Transition-Metal- and Light-Free Directed Amination of Remote Unactivated C(sp³)-H Bonds of Alcohols. *J. Am. Chem. Soc.* **2019**, *141*, 8104–8109.
- (107) Cao, Z.; Li, J.; Sun, Y.; Zhang, H.; Mo, X.; Cao, X.; Zhang, G. Photo-Induced Copper-Catalyzed Alkynylation and Amination of Remote Unactivated C(sp³)-H Bonds. *Chem. Sci.* **2021**, *12*, 4836–4840.
- (108) Sagadevan, A.; Ragupathi, A.; Hwang, K. C. Visible-Light-Induced, Copper(I)-Catalysed C-N Coupling between o-Phenylenediamine and Terminal Alkynes: One-Pot Synthesis of 3-Phenyl-2-Hydroxy-Quinoxalines. *Photochem. Photobiol. Sci.* **2013**, *12*, 2110–2118.
- (109) Sagadevan, A.; Ragupathi, A.; Hwang, K. C. Photoinduced Copper-Catalyzed Regioselective Synthesis of Indoles: Three-Component Coupling of Arylamines, Terminal Alkynes, and Quinones. *Angew. Chem., Int. Ed.* **2015**, *54*, 13896–13901.
- (110) Ragupathi, A.; Sagadevan, A.; Charpe, V. P.; Lin, C. C.; Hwu, J. R.; Hwang, K. C. Visible-Light-Driven Copper-Catalyzed Aerobic Oxidative Cascade Cyclization of *N*-Tosylhydrazones and Terminal Alkynes: Regioselective Synthesis of 3-Arylcoumarins. *Chem. Commun.* **2019**, *55*, 5151–5154.
- (111) Sagadevan, A.; Ragupathi, A.; Lin, C.-C.; Hwu, J. R.; Hwang, K. C. Visible-Light Initiated Copper(I)-Catalysed Oxidative C-N Coupling Of Anilines with Terminal Alkynes: One-Step Synthesis of α -Ketoamides. *Green Chem.* **2015**, *17*, 1113–1119.
- (112) Ragupathi, A.; Sagadevan, A.; Lin, C. C.; Hwu, J. R.; Hwang, K. C. Copper(I)-Catalysed Oxidative C-N Coupling of 2-Aminopyridine with Terminal Alkynes Featuring a C≡C Bond Cleavage Promoted by Visible Light. *Chem. Commun.* **2016**, *52*, 11756−11759.
- (113) Das, D. K.; Kumar Pampana, V. K.; Hwang, K. C. Copper Catalyzed Photoredox Synthesis of α -Keto Esters, Quinoxaline, and Naphthoquinone: Controlled Oxidation of Terminal Alkynes to Glyoxals. *Chem. Sci.* **2018**, *9*, 7318–7326.
- (114) Ragupathi, A.; Charpe, V. P.; Sagadevan, A.; Hwang, K. C. Visible Light-Mediated Copper(I)-Catalysed Aerobic Oxidation of Ynamides/Ynamines at Room Temperature: A Sustainable Approach to the Synthesis of α -Ketoimides/ α -Ketoamides. *Adv. Synth. Catal.* **2017**, 359, 1138–1143.
- (115) Charpe, V. P.; Sagadevan, A.; Hwang, K. C. Visible Light-Induced Aerobic Oxidation of Diarylalkynes to α -Diketones Catalyzed by Copper-Superoxo at Room Temperature. *Green Chem.* **2020**, 22, 4426-4432
- (116) Sagadevan, A.; Charpe, V. P.; Ragupathi, A.; Hwang, K. C. Visible Light Copper Photoredox-Catalyzed Aerobic Oxidative Coupling of Phenols and Terminal Alkynes: Regioselective Synthesis of Functionalized Ketones via C≡C Triple Bond Cleavage. *J. Am. Chem. Soc.* 2017, 139, 2896–2899.
- (117) Allen, S. E.; Walvoord, R. R.; Padilla-Salinas, R.; Kozlowski, M. C. Aerobic Copper-Catalyzed Organic Reactions. *Chem. Rev.* **2013**, *113*, 6234–6458.
- (118) Bosch, E.; Hubig, S. M.; Kochi, J. K. Paterno-Buchi Coupling of (Diaryl)Acetylenes and Quinone via Photoinduced Electron Transfer. *J. Am. Chem. Soc.* **1998**, *120*, 386–395.
- (119) Pampana, V. K. K.; Sagadevan, A.; Ragupathi, A.; Hwang, K. C. Visible Light-Promoted Copper Catalyzed Regioselective Acetamidation of Terminal Alkynes by Arylamines. *Green Chem.* **2020**, 22, 1164–1170.
- (120) Sagadevan, A.; Lyu, P.-C.; Hwang, K. C. Visible-Light-Activated Copper(I) Catalyzed Oxidative C_{sp}-C_{sp} Cross-Coupling Reaction: Efficient Synthesis of Unsymmetrical Conjugated Diynes without Ligands and Base. *Green Chem.* **2016**, *18*, 4526–4530.
- (121) Siemsen, P.; Livingston, R. C.; Diederich, F. Acetylenic Coupling: A Powerful Tool in Molecular Construction. *Angew. Chem., Int. Ed.* **2000**, *39*, 2632–2657.

- (122) Shi, W.; Luo, Y.; Luo, X.; Chao, L.; Zhang, H.; Wang, J.; Lei, A. Investigation of an Efficient Palladium-Catalyzed C(sp)-C(sp) Cross-Coupling Reaction Using Phosphine-Olefin Ligand: Application and Mechanistic Aspects. *J. Am. Chem. Soc.* **2008**, *130*, 14713–14720.
- (123) Yin, W.; He, C.; Chen, M.; Zhang, H.; Lei, A. Nickel-Catalyzed Oxidative Coupling Reactions of Two Different Terminal Alkynes Using O₂ as the Oxidant at Room Temperature: Facile Syntheses of Unsymmetric 1,3-Diynes. *Org. Lett.* **2009**, *11*, 709–712.
- (124) Jia, X. S.; Yin, K.; Li, C. J.; Li, J.; Bian, H. S. Copper-Catalyzed Oxidative Alkyne Homocoupling without Palladium, Ligands and Bases. *Green Chem.* **2011**, *13*, 2175–2178.
- (125) Wang, S. H.; Yu, L.; Li, P. H.; Meng, L. G.; Wang, L. Copper(I) Iodide Catalyzed Cross-Coupling Reaction of Terminal Alkynes with 1-Bromoalkynes: A Simple Synthesis of Unsymmetrical Buta-1,3-diynes. *Synthesis* **2011**, 2011, 1541–1546.
- (126) Yin, K.; Li, C. J.; Li, J. A.; Jia, X. S. CuCl-Catalyzed Green Oxidative Alkyne Homocoupling without Palladium, Ligands and Bases. *Green Chem.* **2011**, *13*, 591–593.
- (127) Zhang, S. L.; Liu, X. Y.; Wang, T. Q. An Efficient Copper-Catalyzed Homocoupling of Terminal Alkynes to Give Symmetrical 1,4-Disubstituted 1,3-Diynes. *Adv. Synth. Catal.* **2011**, 353, 1463–1466.
- (128) Niu, X. J.; Li, C. J.; Li, J.; Jia, X. S. Importance of Bases on the Copper-Catalyzed Oxidative Homocoupling of Terminal Alkynes to 1,4-Disubstituted 1,3-Diynes. *Tetrahedron Lett.* **2012**, *53*, 5559–5561.
- (129) Peng, H.; Xi, Y.; Ronaghi, N.; Dong, B.; Akhmedov, N. G.; Shi, X. Gold-Catalyzed Oxidative Cross-Coupling of Terminal Alkynes: Selective Synthesis of Unsymmetrical 1,3-Diynes. *J. Am. Chem. Soc.* **2014**, *136*, 13174–13177.
- (130) Sagadevan, A.; Charpe, V. P.; Hwang, K. C. Copper(I) Chloride Catalysed Room Temperature Csp-Csp Homocoupling of Terminal Alkynes Mediated by Visible Light. *Catal. Sci. Technol.* **2016**, *6*, 7688–7692.
- (131) Charpe, V. P.; Hande, A. A.; Sagadevan, A.; Hwang, K. C. Visible-Light Induced Copper(I)-Catalysed Denitrogenative Oxidative Coupling of Hydrazinylpyridines with Terminal Alkynes. *Green Chem.* **2018**, *20*, 4859–4864.
- (132) Sagadevan, A.; Pampana, V. K. K.; Hwang, K. C. Copper Photoredox Catalyzed A3' Coupling of Arylamines, Terminal Alkynes, and Alcohols through a Hydrogen Atom Transfer Process. *Angew. Chem., Int. Ed.* **2019**, *58*, 3838–3842.
- (133) Guo, Q. P.; Wang, M. R.; Peng, Q.; Huo, Y. M.; Liu, Q.; Wang, R.; Xu, Z. Q. Dual-Functional Chiral Cu-Catalyst-Induced Photoredox Asymmetric Cyanofluoroalkylation of Alkenes. *ACS Catal.* **2019**, *9*, 4470–4476.
- (134) Ma, X.; Zhang, G. Visible Light-Induced Copper-Catalyzed C—H Arylation of Benzoxazoles. *Chin. J. Chem.* **2020**, *38*, 1299–1303. (135) Li, C.; Chen, B.; Ma, X.; Mo, X.; Zhang, G. Light-Promoted Copper-Catalyzed Enantioselective Alkylation of Azoles. *Angew. Chem., Int. Ed.* **2021**, *60*, 2130–2134.
- (136) Rawner, T.; Knorn, M.; Lutsker, E.; Hossain, A.; Reiser, O. Synthesis of Trifluoromethylated Sultones from Alkenols Using a Copper Photoredox Catalyst. *J. Org. Chem.* **2016**, *81*, 7139–7147.
- (137) Hossain, A.; Engl, S.; Lutsker, E.; Reiser, O. Visible-Light-Mediated Regioselective Chlorosulfonylation of Alkenes and Alkynes: Introducing the Cu(II) Complex [Cu(dap)Cl₂] to Photochemical ATRA Reactions. *ACS Catal.* **2019**, *9*, 1103–1109.
- (138) Engl, S.; Reiser, O. Making Copper Photocatalysis Even More Robust and Economic: Photoredox Catalysis with [Cu^{II}(dmp)₂Cl]Cl. *Eur. J. Org. Chem.* **2020**, 2020, 1523–1533.
- (139) Rawner, T.; Lutsker, E.; Kaiser, C. A.; Reiser, O. The Different Faces of Photoredox Catalysts: Visible-Light-Mediated Atom Transfer Radical Addition (ATRA) Reactions of Perfluoroalkyl Iodides with Styrenes and Phenylacetylenes. *ACS Catal.* **2018**, *8*, 3950–3956.
- (140) Engl, S.; Reiser, O. Copper Makes the Difference: Visible Light-Mediated Atom Transfer Radical Addition Reactions of Iodoform with Olefins. ACS Catal. **2020**, *10*, 9899–9906.

- (141) Liu, Z.; Chen, H.; Lv, Y.; Tan, X.; Shen, H.; Yu, H. Z.; Li, C. Radical Carbofluorination of Unactivated Alkenes with Fluoride Ions. *J. Am. Chem. Soc.* **2018**, *140*, 6169–6175.
- (142) Yu, X. Y.; Zhao, Q. Q.; Chen, J.; Chen, J. R.; Xiao, W. J. Copper-Catalyzed Radical Cross-Coupling of Redox-Active Oxime Esters, Styrenes, and Boronic Acids. *Angew. Chem., Int. Ed.* **2018**, *57*, 15505–15509
- (143) Zhao, W.; Wurz, R. P.; Peters, J. C.; Fu, G. C. Photoinduced, Copper-Catalyzed Decarboxylative C-N Coupling to Generate Protected Amines: An Alternative to the Curtius Rearrangement. *J. Am. Chem. Soc.* **2017**, *139*, 12153–12156.
- (144) Liu, D. Y.; Liu, X.; Gao, Y.; Wang, C. Q.; Tian, J. S.; Loh, T. P. Decarboxylative C-H Alkylation of Heteroarene N-Oxides by Visible Light/Copper Catalysis. *Org. Lett.* **2020**, *22*, 8978–8983.
- (145) Han, B.; Li, Y.; Yu, \dot{Y} .; Gong, L. Photocatalytic Enantioselective α -Aminoalkylation of Acyclic Imine Derivatives by a Chiral Copper Catalyst. *Nat. Commun.* **2019**, *10*, 3804.
- (146) Kochi, J. K. Photolyses of Metal Compounds: Cupric Chloride in Organic Media. J. Am. Chem. Soc. 1962, 84, 2121–2127.
- (147) Takaki, K.; Yamamoto, J.; Matsushita, Y.; Morii, H.; Shishido, T.; Takehira, L. Oxidation of Alkanes with Dioxygen Induced by Visible Light and Cu(II) and Fe(III) Chlorides. *Bull. Chem. Soc. Jpn.* **2003**, *76*, 393–398.
- (148) Takaki, K.; Yamamoto, J.; Komeyama, K.; Kawabata, T.; Takehira, K. Photocatalytic Oxidation of Alkanes with Dioxygen by Visible Light and Copper(II) and Iron(III) Chlorides: Preference Oxidation of Alkanes over Alcohols and Ketones. *Bull. Chem. Soc. Jpn.* **2004**, *77*, 2251–2255.
- (149) Mereshchenko, A. S.; Olshin, P. K.; Karimov, A. M.; Skripkin, M. Y.; Burkov, K. A.; Tveryanovich, Y. S.; Tarnovsky, A. N. Photochemistry of Copper(II) Chlorocomplexes in Acetonitrile: Trapping the Ligand-to-Metal Charge Transfer Excited State Relaxations Pathways. *Chem. Phys. Lett.* **2014**, *615*, 105–110.
- (150) For an example of EnT from photoexcited Cu(I) complex to molecular oxygen, see: Meng, Q. Y.; Gao, X. W.; Lei, T.; Liu, Z.; Zhan, F.; Li, Z. J.; Zhong, J. J.; Xiao, H.; Feng, K.; Chen, B.; Tao, Y.; Tung, C. H.; Wu, L. Z. Identifying Key Intermediates Generated In Situ from Cu(II) Salt-Catalyzed C-H Functionalization of Aromatic Amines under Illumination. *Sci. Adv.* **2017**, *3*, No. e1700666.
- (151) Rajam, S.; Jadhav, A. V.; Li, Q.; Sarkar, S. K.; Singh, P. N.; Rohr, A.; Pace, T. C.; Li, R.; Krause, J. A.; Bohne, C.; Ault, B. S.; Gudmundsdottir, A. D. Triplet Sensitized Photolysis of a Vinyl Azide: Direct Detection of a Triplet Vinyl Azide and Nitrene. *J. Org. Chem.* **2014**, *79*, 9325–9334.
- (152) Wang, Q.; Huang, J.; Zhou, L. Synthesis of Quinolines by Visible-Light Induced Radical Reaction of Vinyl Azides and α -Carbonyl Benzyl Bromides. *Adv. Synth. Catal.* **2015**, *357*, 2479–2484.
- (153) Monat, J. E.; McCusker, J. K. Femtosecond Excited-State Dynamics of an Iron(II) Polypyridyl Solar Cell Sensitizer Model. *J. Am. Chem. Soc.* **2000**, *122*, 4092–4097.
- (154) Creutz, C.; Chou, M.; Netzel, T. L.; Okumura, M.; Sutin, N. Lifetimes, Spectra, and Quenching of the Excited States of Polypyridine Complexes of Iron(II), Ruthenium(II), And Osmium(II). *J. Am. Chem. Soc.* **1980**, *102*, 1309–1319.
- (155) Chábera, P.; Liu, Y.; Prakash, O.; Thyrhaug, E.; Nahhas, A. E.; Honarfar, A.; Essén, S.; Fredin, L. A.; Harlang, T. C.; Kjær, K. S.; Handrup, K.; Ericson, F.; Tatsuno, H.; Morgan, K.; Schnadt, J.; Häggström, L.; Ericsson, T.; Sobkowiak, A.; Lidin, S.; Huang, P.; Styring, S.; Uhlig, J.; Bendix, J.; Lomoth, R.; Sundström, V.; Persson, P.; Wärnmark, K. A Low-Spin Fe(III) Complex with 100-ps Ligand-to-Metal Charge Transfer Photoluminescence. *Nature* **2017**, *543*, 695–690
- (156) Kjær, K. S.; Kaul, N.; Prakash, O.; Chábera, P.; Rosemann, N. W.; Honarfar, A.; Gordivska, O.; Fredin, L. A.; Bergquist, K.-E.; Häggström, L.; Ericsson, T.; Lindh, L.; Yartsev, A.; Styring, S.; Huang, P.; Uhlig, J.; Bendix, J.; Strand, D.; Sundström, V.; Persson, P.; Lomoth, R.; Wärnmark, K. Luminescence and Reactivity of a Charge-Transfer Excited Iron Complex with Nanosecond Lifetime. *Science* **2019**, *363*, 249–253.

- (157) Zhou, W. J.; Wu, X. D.; Miao, M.; Wang, Z. H.; Chen, L.; Shan, S. Y.; Cao, G. M.; Yu, D. G. Light Runs Across Iron Catalysts in Organic Transformations. *Chem. Eur. J.* **2020**, *26*, 15052–15064.
- (158) Li, Z.; Wang, X.; Xia, S.; Jin, J. Ligand-Accelerated Iron Photocatalysis Enabling Decarboxylative Alkylation of Heteroarenes. *Org. Lett.* **2019**, *21*, 4259–4265.
- (159) Huang, B. B.; Li, Y. N.; Yang, C.; Xia, W. J. Three-Component Aminoselenation of Alkenes via Visible-Light Enabled Fe-Catalysis. *Green Chem.* **2020**, 22, 2804–2809.
- (160) Wei, X. J.; Abdiaj, I.; Sambiagio, C.; Li, C.; Zysman-Colman, E.; Alcazar, J.; Noel, T. Visible-Light-Promoted Iron-Catalyzed C(sp²)-C(sp³) Kumada Cross-Coupling in Flow. *Angew. Chem., Int. Ed.* **2019**, 58, 13030–13034.
- (161) Feng, G. S.; Wang, X. F.; Jin, J. Decarboxylative C-C and C-N Bond Formation by Ligand-Accelerated Iron Photocatalysis. *Eur. J. Org. Chem.* **2019**, 2019, 6728–6732.
- (162) Xia, S.; Hu, K.; Lei, C.; Jin, J. Intramolecular Aromatic C-H Acyloxylation Enabled by Iron Photocatalysis. *Org. Lett.* **2020**, 22, 1385–1389.
- (163) Rushworth, P. J.; Hulcoop, D. G.; Fox, D. J. Iron/Tetramethylethylenediamine-Catalyzed Ambient-Temperature Coupling of Alkyl Grignard Reagents and Aryl Chlorides. *J. Org. Chem.* **2013**, *78*, 9517–9521.
- (164) Cahiez, G.; Lefevre, G.; Moyeux, A.; Guerret, O.; Gayon, E.; Guillonneau, L.; Lefevre, N.; Gu, Q.; Zhou, E. Gram-Scale, Cheap, and Eco-Friendly Iron-Catalyzed Cross-Coupling between Alkyl Grignard Reagents and Alkenyl or Aryl Halides. *Org. Lett.* **2019**, *21*, 2679–2683.
- (165) Hatakeyama, T.; Hashimoto, S.; Ishizuka, K.; Nakamura, M. Highly Selective Biaryl Cross-Coupling Reactions between Aryl Halides and Aryl Grignard Reagents: A New Catalyst Combination of N-Heterocyclic Carbenes and Iron, Cobalt, and Nickel Fluorides. *J. Am. Chem. Soc.* **2009**, *131*, 11949–11963.
- (166) Perry, M. C.; Gillett, A. N.; Law, T. C. An Unprecedented Iron-Catalyzed Cross-Coupling of Primary and Secondary Alkyl Grignard Reagents with Non-Activated Aryl Chlorides. *Tetrahedron Lett.* **2012**, 53, 4436–4439.
- (167) Kunkely, H.; Vogler, A. Photo-Oxidation of Bis[1,2-Bis-(Diphenylphosphino)Ferrocene]-Palladium(0) In CCl₄ Induced by Ferrocene to Solvent Charge Transfer Excitation. *J. Organomet. Chem.* **1998**, 559, 215–217.
- (168) Caspar, J. V. Long-Lived Reactive Excited States of Zero-Valent Phosphine, Phosphite, and Arsine Complexes of Nickel, Palladium and Platinum. *J. Am. Chem. Soc.* **1985**, *107*, 6718–6719.
- (169) Harvey, P. D.; Gray, H. B. Low-Lying Singlet and Triplet Electronic Excited States of Binuclear (d¹⁰-d¹⁰) Palladium(0) And Platinum(0) Complexes. *J. Am. Chem. Soc.* **1988**, *110*, 2145–2147.
- (170) Harvey, P. D.; Schaefer, W. P.; Gray, H. B. Emission Properties of Tetrahedral Bis[bis(diphenylphosphino)propane] palladium and -platinum, Complexes. Crystal and Molecular Structure of Pt(dppp)₂. *Inorg. Chem.* **1988**, *27*, 1101–1104.
- (171) Ohkubo, T.; Takao, K.; Tsubomura, T. Blue to Orange Emitters; Palladium(0) Monodentate Phosphine Complexes. *Inorg. Chem. Commun.* **2012**, *20*, 27–29.
- (172) Riese, S.; Holzapfel, M.; Schmiedel, A.; Gert, I.; Schmidt, D.; Wurthner, F.; Lambert, C. Photoinduced Dynamics of Bis-dipyrrinato-palladium(II) and Porphodimethenato-palladium(II) Complexes: Governing Near Infrared Phosphorescence by Structural Restriction. *Inorg. Chem.* **2018**, *57*, 12480–12488.
- (173) Sumino, S.; Fusano, A.; Fukuyama, T.; Ryu, I. Carbonylation Reactions of Alkyl Iodides through the Interplay of Carbon Radicals and Pd Catalysts. *Acc. Chem. Res.* **2014**, *47*, 1563–1574.
- (174) Parasram, M.; Chuentragool, P.; Sarkar, D.; Gevorgyan, V. Photoinduced Formation of Hybrid Aryl Pd-Radical Species Capable of 1,5-HAT: Selective Catalytic Oxidation of Silyl Ethers into Silyl Enol Ethers. J. Am. Chem. Soc. 2016, 138, 6340–6343.
- (175) Chuentragool, P.; Kurandina, D.; Gevorgyan, V. Catalysis with Palladium Complexes Photoexcited by Visible Light. *Angew. Chem., Int. Ed.* **2019**, *58*, 11586–11598.

- (176) Zhou, W. J.; Cao, G. M.; Zhang, Z. P.; Yu, D. G. Visible Light-induced Palladium-Catalysis in Organic Synthesis. *Chem. Lett.* **2019**, 48, 181–191.
- (177) Firmansjah, L.; Fu, G. C. Intramolecular Heck Reactions of Unactivated Alkyl Halides. *J. Am. Chem. Soc.* **2007**, *129*, 11340–11341. (178) Bloome, K. S.; Alexanian, E. J. Palladium-Catalyzed Carbonylative Heck-Type Reactions of Alkyl Iodides. *J. Am. Chem. Soc.* **2010**, *132*, 12823–12825.
- (179) McMahon, C. M.; Alexanian, E. J. Palladium-Catalyzed Heck-Type Cross-Couplings of Unactivated Alkyl Iodides. *Angew. Chem., Int. Ed.* **2014**, *53*, 5974–5977.
- (180) Zou, Y.; Zhou, J. S. Palladium-Catalyzed Intermolecular Heck Reaction of Alkyl Halides. *Chem. Commun.* **2014**, *50*, 3725–3728.
- (181) Torres, G. M.; Liu, Y.; Arndtsen, B. A. A Dual Light-Driven Palladium Catalyst: Breaking the Barriers in Carbonylation Reactions. *Science* **2020**, *368*, 318–323.
- (182) Abdiaj, I.; Huck, L.; Mateo, J. M.; de la Hoz, A.; Gomez, M. V.; Diaz-Ortiz, A.; Alcazar, J. Photoinduced Palladium-Catalyzed Negishi Cross-Couplings Enabled by the Visible-Light Absorption of Palladium-Zinc Complexes. *Angew. Chem., Int. Ed.* **2018**, 57, 13231–13236.
- (183) Rakshit, A.; Kumar, P.; Alam, T.; Dhara, H.; Patel, B. K. Visible-Light-Accelerated Pd-Catalyzed Cascade Addition/Cyclization of Arylboronic Acids to γ and β -Ketodinitriles for the Construction of 3-Cyanopyridines and 3-Cyanopyrrole Analogues. *J. Org. Chem.* **2020**, 85, 12482–12504.
- (184) Kurandina, D.; Parasram, M.; Gevorgyan, V. Visible Light-Induced Room-Temperature Heck Reaction of Functionalized Alkyl Halides with Vinyl Arenes/Heteroarenes. *Angew. Chem., Int. Ed.* **2017**, *56*, 14212–14216.
- (185) Zhou, W. J.; Cao, G. M.; Shen, G.; Zhu, X. Y.; Gui, Y. Y.; Ye, J. H.; Sun, L.; Liao, L. L.; Li, J.; Yu, D. G. Visible-Light-Driven Palladium-Catalyzed Radical Alkylation of C-H Bonds with Unactivated Alkyl Bromides. *Angew. Chem., Int. Ed.* **2017**, *56*, 15683–15687.
- (186) Wang, G. Z.; Shang, R.; Cheng, W. M.; Fu, Y. Irradiation-Induced Heck Reaction of Unactivated Alkyl Halides at Room Temperature. *J. Am. Chem. Soc.* **2017**, *139*, 18307–18312.
- (187) Kurandina, D.; Rivas, M.; Radzhabov, M.; Gevorgyan, V. Heck Reaction of Electronically Diverse Tertiary Alkyl Halides. *Org. Lett.* **2018**, *20*, 357–360.
- (188) Ratushnyy, M.; Parasram, M.; Wang, Y.; Gevorgyan, V. Palladium-Catalyzed Atom-Transfer Radical Cyclization at Remote Unactivated $C(sp^3)$ -H Sites: Hydrogen-Atom Transfer of Hybrid Vinyl Palladium Radical Intermediates. *Angew. Chem., Int. Ed.* **2018**, *57*, 2712–2715.
- (189) Ratushnyy, M.; Kvasovs, N.; Sarkar, S.; Gevorgyan, V. Visible-Light-Induced Palladium-Catalyzed Generation of Aryl Radicals from Aryl Triflates. *Angew. Chem., Int. Ed.* **2020**, *59*, 10316–10320.
- (190) Lee, G. S.; Kim, D.; Hong, S. H. Pd-Catalyzed Formal Mizoroki-Heck Coupling of Unactivated Alkyl Chlorides. *Nat. Commun.* **2021**, *12*, 991.
- (191) Koy, M.; Sandfort, F.; Tlahuext-Aca, A.; Quach, L.; Daniliuc, C. G.; Glorius, F. Palladium-Catalyzed Decarboxylative Heck-Type Coupling of Activated Aliphatic Carboxylic Acids Enabled by Visible Light. *Chem. Eur. J.* **2018**, *24*, 4552–4555.
- (192) Wang, G. Z.; Shang, R.; Fu, Y. Irradiation-Induced Palladium-Catalyzed Decarboxylative Heck Reaction of Aliphatic N-(Acyloxy)-phthalimides at Room Temperature. *Org. Lett.* **2018**, *20*, 888–891.
- (193) Xing, W. L.; Shang, R.; Wang, G. Z.; Fu, Y. Visible Light-Induced Palladium-Catalyzed Ring Opening β -H Elimination and Addition of Cyclobutanone Oxime Esters. *Chem. Commun.* **2019**, *55*, 14291–14294.
- (194) For an example of aryl radical generation from Pd(I) complex, see: Manolikakes, G.; Knochel, P. Radical Catalysis of Kumada Cross-Coupling Reactions Using Functionalized Grignard Reagents. *Angew. Chem., Int. Ed.* **2009**, 48, 205–209.
- (195) Stateman, L. M.; Nakafuku, K. M.; Nagib, D. A. Remote C-H Functionalization via Selective Hydrogen Atom Transfer. *Synthesis* **2018**, *50*, 1569–1586.

- (196) Sarkar, S.; Cheung, K. P. S.; Gevorgyan, V. C-H Functionalization Reactions Enabled by Hydrogen Atom Transfer to Carbon-Centered Radicals. *Chem. Sci.* **2020**, *11*, 12974–12993.
- (197) Kvasovs, N.; Gevorgyan, V. Contemporary Methods for Generation of Aryl Radicals. Chem. Soc. Rev. 2021, 50, 2244–2259.
- (198) Chuentragool, P.; Parasram, M.; Shi, Y.; Gevorgyan, V. General, Mild, and Selective Method for Desaturation of Aliphatic Amines. *J. Am. Chem. Soc.* **2018**, *140*, 2465–2468.
- (199) Voica, A. F.; Mendoza, A.; Gutekunst, W. R.; Fraga, J. O.; Baran, P. S. Guided Desaturation of Unactivated Aliphatics. *Nat. Chem.* **2012**, *4*, 629–635.
- (200) Blanksby, S. J.; Ellison, G. B. Bond Dissociation Energies of Organic Molecules. *Acc. Chem. Res.* **2003**, *36*, 255–263.
- (201) Hsu, Y. C.; Wang, V. C.; Au-Yeung, K. C.; Tsai, C. Y.; Chang, C. C.; Lin, B. C.; Chan, Y. T.; Hsu, C. P.; Yap, G. P. A.; Jurca, T.; Ong, T. G. One-Pot Tandem Photoredox and Cross-Coupling Catalysis with a Single Palladium Carbodicarbene Complex. *Angew. Chem., Int. Ed.* **2018**, *57*, 4622–4626.
- (202) Kalyani, D.; McMurtrey, K. B.; Neufeldt, S. R.; Sanford, M. S. Room-Temperature C-H Arylation: Merger of Pd-Catalyzed C-H Functionalization and Visible-Light Photocatalysis. *J. Am. Chem. Soc.* **2011**, *133*, 18566–18569.
- (203) Chen, X.; Engle, K. M.; Wang, D. H.; Yu, J. Q. Palladium(II)-Catalyzed C-H Activation/C-C Cross-Coupling Reactions: Versatility and Practicality. *Angew. Chem., Int. Ed.* **2009**, 48, 5094–5115.
- (204) Lyons, T. W.; Sanford, M. S. Palladium-Catalyzed Ligand-Directed C-H Functionalization Reactions. *Chem. Rev.* **2010**, *110*, 1147–1169.
- (205) Liu, X. Y.; Jensen, K. F. Direct Oxidative Amidation of Aromatic Aldehydes Using Aqueous Hydrogen Peroxide in Continuous Flow Microreactor Systems. *Green Chem.* **2012**, *14*, 1471–1474.
- (206) Leow, D. Phenazinium Salt-Catalyzed Aerobic Oxidative Amidation of Aromatic Aldehydes. *Org. Lett.* **2014**, *16*, 5812–5815.
- (207) Zhou, Z. Z.; Zhao, J. H.; Gou, X. Y.; Chen, X. M.; Liang, Y. M. Visible-Light-Mediated Hydrodehalogenation and Br/D Exchange of Inactivated Aryl and Alkyl Halides with a Palladium Complex. *Org. Chem. Front.* **2019**, *6*, 1649–1654.
- (208) Shaughnessy, K. H.; Hamann, B. C.; Hartwig, J. F. Palladium-Catalyzed Inter- and Intramolecular α -Arylation of Amides. Application of Intramolecular Amide Arylation to the Synthesis of Oxindoles. *J. Org. Chem.* **1998**, *63*, *6546*–*6553*.
- (209) Lee, S.; Hartwig, J. F. Improved Catalysts for the Palladium-Catalyzed Synthesis of Oxindoles by Amide α -Arylation. Rate Acceleration, Use of Aryl Chloride Substrates, and a New Carbene Ligand for Asymmetric Transformations. *J. Org. Chem.* **2001**, *66*, 3402–3415.
- (210) Chen, Y. Q.; Wang, Z.; Wu, Y.; Wisniewski, S. R.; Qiao, J. X.; Ewing, W. R.; Eastgate, M. D.; Yu, J. Q. Overcoming the Limitations of γ and δ -C-H Arylation of Amines through Ligand Development. *J. Am. Chem. Soc.* **2018**, *140*, 17884–17894.
- (211) Koreeda, M.; Hamann, L. G. Chirality Transmission Involving a Free-Radical-Mediated 6-Exo Cyclization Process. Stereocontrolled Synthesis of Branched-Chain 1,4-Diols. *J. Am. Chem. Soc.* **1990**, *112*, 8175–8177.
- (212) Parasram, M.; Iaroshenko, V. O.; Gevorgyan, V. Endo-Selective Pd-Catalyzed Silyl Methyl Heck Reaction. *J. Am. Chem. Soc.* **2014**, *136*, 17926–17929.
- (213) Murarka, S. N-(Acyloxy)phthalimides as Redox-Active Esters in Cross-Coupling Reactions. *Adv. Synth. Catal.* **2018**, *360*, 1735–1753.
- (214) Parida, S. K.; Hota, S. K.; Kumar, R.; Murarka, S. Late-Stage Alkylation of Heterocycles Using *N*-(Acyloxy)phthalimides. *Chem. Asian J.* **2021**, *16*, 879–889.
- (215) Cheng, W. M.; Shang, R.; Fu, Y. Irradiation-Induced Palladium-Catalyzed Decarboxylative Desaturation Enabled by a Dual Ligand System. *Nat. Commun.* **2018**, *9*, 5215.
- (216) Frisch, A. C.; Beller, M. Catalysts for Cross-Coupling Reactions with Non-Activated Alkyl Halides. *Angew. Chem., Int. Ed.* **2005**, *44*, 674–688.

- (217) Fu, G. C. Transition-Metal Catalysis of Nucleophilic Substitution Reactions: A Radical Alternative to S_N1 and S_N2 Processes. ACS Cent. Sci. 2017, 3, 692–700.
- (218) Shiner, V. J. Substitution and Elimination Rate Studies on Some Deutero-Isopropyl Bromides. *J. Am. Chem. Soc.* **1952**, *74*, 5285–5288. (219) Shmidt, A. F.; Smirnov, V. V. Kinetic Study of the Heck Reaction by the Method of Competing Reactions. *Kinet. Catal.* **2001**, *42*, 800–804.
- (220) Adamik, R.; Foldesi, T.; Novak, Z. Photocatalytic Palladium-Catalyzed Fluoroalkylation of Styrene Derivatives. *Org. Lett.* **2020**, 22, 8091–8095.
- (221) Zhao, B.; Shang, R.; Wang, G.-Z.; Wang, S.; Chen, H.; Fu, Y. Palladium-Catalyzed Dual Ligand-Enabled Alkylation of Silyl Enol Ether and Enamide under Irradiation: Scope, Mechanism, and Theoretical Elucidation of Hybrid Alkyl Pd(I)-Radical Species. *ACS Catal.* 2020, 10, 1334–1343.
- (222) Li, M.; Qiu, Y. F.; Wang, C. T.; Li, X. S.; Wei, W. X.; Wang, Y. Z.; Bao, Q. F.; Ding, Y. N.; Shi, W. Y.; Liang, Y. M. Visible-Light-Induced Pd-Catalyzed Radical Strategy for Constructing C-Vinyl Glycosides. *Org. Lett.* **2020**, *22*, 6288–6293.
- (223) Adlington, R. M.; Baldwin, J. E.; Basak, A.; Kozyrod, R. P. Applications of Radical-Addition Reactions to the Synthesis of a C-Glucoside and a Functionalized Amino-Acid. *J. Chem. Soc., Chem. Commun.* **1983**, 944–945.
- (224) Giese, B.; Dupuis, J. Diastereoselective Syntheses of C-Glycopyranosides. *Angew. Chem., Int. Ed. Engl.* **1983**, 22, 622–623.
- (225) Andrews, R. S.; Becker, J. J.; Gagne, M. R. Intermolecular Addition of Glycosyl Halides to Alkenes Mediated by Visible Light. *Angew. Chem., Int. Ed.* **2010**, *49*, 7274–7276.
- (226) Andrews, R. S.; Becker, J. J.; Gagne, M. R. Investigating the Rate of Photoreductive Glucosyl Radical Generation. *Org. Lett.* **2011**, *13*, 2406–2409.
- (227) Kancherla, R.; Muralirajan, K.; Maity, B.; Zhu, C.; Krach, P. E.; Cavallo, L.; Rueping, M. Oxidative Addition to Palladium(0) Made Easy through Photoexcited-State Metal Catalysis: Experiment and Computation. *Angew. Chem., Int. Ed.* **2019**, *58*, 3412–3416.
- (228) Friestad, G. K. Addition of Carbon-Centered Radicals to Imines and Related Compounds. *Tetrahedron* **2001**, *57*, 5461–5496.
- (229) Naito, T.; Miyabe, H.; Ueda, M. Carbon-Carbon Bond Construction Based on Radical Addition to C = N Bond. *Synlett* **2004**, 1140–1157.
- (230) Kvasovs, N.; Iziumchenko, V.; Palchykov, V.; Gevorgyan, V. Visible Light-Induced Pd-Catalyzed Alkyl-Heck Reaction of Oximes. *ACS Catal.* **2021**, *11*, 3749–3754.
- (231) Koy, M.; Bellotti, P.; Katzenburg, F.; Daniliuc, C. G.; Glorius, F. Synthesis of All-Carbon Quaternary Centers by Palladium-Catalyzed Olefin Dicarbofunctionalization. *Angew. Chem., Int. Ed.* **2020**, *59*, 2375–2379.
- (232) Fournet, G.; Balme, G.; Gore, J. Attaque Nucleophile Intramoleculaire D'organopalladiques Issus de la Carbopalladation D'alkylidenecyclopropanes. *Tetrahedron Lett.* **1987**, *28*, 4533–4536.
- (233) Xu, T.; Dong, G. Rhodium-Catalyzed Regioselective Carboacylation of Olefins: A C-C Bond Activation Approach for Accessing Fused-Ring Systems. *Angew. Chem., Int. Ed.* **2012**, *51*, 7567–7571
- (234) Souillart, L.; Parker, E.; Cramer, N. Highly Enantioselective Rhodium(I)-Catalyzed Activation of Enantiotopic Cyclobutanone C-C Bonds. *Angew. Chem., Int. Ed.* **2014**, *53*, 3001–3005.
- (235) Donald, J. R.; Unsworth, W. P. Ring-Expansion Reactions in the Synthesis of Macrocycles and Medium-Sized Rings. *Chem. Eur. J.* **2017**, 23, 8780–8799.
- (236) Huber, T.; Wildermuth, R. E.; Magauer, T. 9-Membered Carbocycles: Strategies and Tactics for their Synthesis. *Chem. Eur. J.* **2018**, 24, 12107–12120.
- (237) Chen, L.; Guo, L. N.; Liu, S.; Liu, L.; Duan, X. H. Visible-Light-Driven Palladium-Catalyzed Dowd-Beckwith Ring Expansion/C-C Bond Formation Cascade. *Chem. Sci.* **2021**, *12*, 1791–1795.
- (238) Bartling, H.; Eisenhofer, A.; Konig, B.; Gschwind, R. M. The Photocatalyzed Aza-Henry Reaction of *N*-Aryltetrahydroisoquinolines:

- Comprehensive Mechanism, H*-versus H*-Abstraction, and Background Reactions. J. Am. Chem. Soc. 2016, 138, 11860–11871.
- (239) Yang, Q.; Zhang, L.; Ye, C.; Luo, S.; Wu, L. Z.; Tung, C. H. Visible-Light-Promoted Asymmetric Cross-Dehydrogenative Coupling of Tertiary Amines to Ketones by Synergistic Multiple Catalysis. *Angew. Chem., Int. Ed.* **2017**, *56*, 3694–3698.
- (240) Wang, G. Z.; Shang, R.; Fu, Y. Irradiation-Induced Palladium-Catalyzed Direct C-H Alkylation of Heteroarenes with Tertiary and Secondary Alkyl Bromides. *Synthesis* **2018**, *50*, 2908–2914.
- (241) Jiao, Z.; Lim, L. H.; Hirao, H.; Zhou, J. S. Palladium-Catalyzed para-Selective Alkylation of Electron-Deficient Arenes. *Angew. Chem., Int. Ed.* **2018**, *57*, 6294–6298.
- (242) Kim, D.; Lee, G. S.; Kim, D.; Hong, S. H. Direct C(sp²)-H Alkylation of Unactivated Arenes Enabled by Photoinduced Pd Catalysis. *Nat. Commun.* **2020**, *11*, 5266.
- (243) Shelton, J. R.; Uzelmeier, C. W. Homolytic Aromatic Cyclohexylation. J. Am. Chem. Soc. 1966, 88, 5222-5228.
- (244) Sharma, K. K.; Patel, D. I.; Jain, R. Metal-Free Synthesis of N-Fused Heterocyclic Iodides via C-H Functionalization Mediated by Tert-Butylhydroperoxide. *Chem. Commun.* **2015**, *51*, 15129–15132.
- (245) Sun, L.; Ye, J. H.; Zhou, W. J.; Zeng, X.; Yu, D. G. Oxy-Alkylation of Allylamines with Unactivated Alkyl Bromides and CO_2 via Visible-Light-Driven Palladium Catalysis. *Org. Lett.* **2018**, *20*, 3049–3052.
- (246) Dell'Amico, D. B.; Calderazzo, F.; Labella, L.; Marchetti, F.; Pampaloni, G. Converting Carbon Dioxide into Carbamato Derivatives. *Chem. Rev.* **2003**, *103*, 3857–3897.
- (247) Sun, S.; Zhou, C.; Yu, J. T.; Cheng, J. Visible-Light-Driven Palladium-Catalyzed Oxy-Alkylation of 2-(1-Arylvinyl)anilines by Unactivated Alkyl Bromides and CO₂: Multicomponent Reactions toward 1,4-Dihydro-2*H*-3,1-benzoxazin-2-ones. *Org. Lett.* **2019**, *21*, 6579–6583.
- (248) Huang, H.-M.; Koy, M.; Serrano, E.; Pflüger, P. M.; Schwarz, J. L.; Glorius, F. Catalytic Radical Generation of π -Allylpalladium Complexes. *Nat. Catal.* **2020**, *3*, 393–400.
- (249) Trost, B. M.; Van Vranken, D. L. Asymmetric Transition Metal-Catalyzed Allylic Alkylations. *Chem. Rev.* **1996**, *96*, 395–422.
- (250) Lu, Z.; Ma, S. Metal-Catalyzed Enantioselective Allylation in Asymmetric Synthesis. *Angew. Chem., Int. Ed.* **2008**, 47, 258–297.
- (251) Huang, H. M.; Bellotti, P.; Pfluger, P. M.; Schwarz, J. L.; Heidrich, B.; Glorius, F. Three-Component, Interrupted Radical Heck/Allylic Substitution Cascade Involving Unactivated Alkyl Bromides. *J. Am. Chem. Soc.* **2020**, *142*, 10173–10183.
- (252) Bellotti, P.; Koy, M.; Gutheil, C.; Heuvel, S.; Glorius, F. Three-Component Three-Bond Forming Cascade via Palladium Photoredox Catalysis. *Chem. Sci.* **2021**, *12*, 1810–1817.
- (253) Cheung, K. P. S.; Kurandina, D.; Yata, T.; Gevorgyan, V. Photoinduced Palladium-Catalyzed Carbofunctionalization of Conjugated Dienes Proceeding via Radical-Polar Crossover Scenario: 1,2-Aminoalkylation and Beyond. *J. Am. Chem. Soc.* **2020**, 142, 9932–9937.
- (254) Wu, X. F.; Fang, X.; Wu, L.; Jackstell, R.; Neumann, H.; Beller, M. Transition-Metal-Catalyzed Carbonylation Reactions of Olefins and Alkynes: A Personal Account. *Acc. Chem. Res.* **2014**, *47*, 1041–1053.
- (255) Peng, J. B.; Geng, H. Q.; Wu, X. F. The Chemistry of CO: Carbonylation. *Chem.* **2019**, *5*, 526–552.
- (256) Peng, J. B.; Wu, F. P.; Wu, X. F. First-Row Transition-Metal-Catalyzed Carbonylative Transformations of Carbon Electrophiles. *Chem. Rev.* **2019**, *119*, 2090–2127.
- (257) Schoenberg, A.; Bartoletti, I.; Heck, R. F. Palladium-Catalyzed Carboalkoxylation of Aryl, Benzyl, and Vinylic Halides. *J. Org. Chem.* **1974**, 39, 3318–3326.
- (258) Schoenberg, A.; Heck, R. F. Palladium-Catalyzed Amidation of Aryl, Heterocyclic, and Vinylic Halides. *J. Org. Chem.* **1974**, *39*, 3327–3331.
- (259) Kobayashi, T.; Tanaka, M. Cleavage of C-N Bonds of Tertiary-Amines and Carbonylation of Organic Halides with Palladium Complexes as Catalysts Leading to Formation of Tertiary Amides. *J. Organomet. Chem.* **1982**, 231, C12—C14.

- (260) Kondo, T.; Tsuji, Y.; Watanabe, Y. Photochemical Carbonylation of Alkyl Iodides in the Presence of Various Metal-Carbonyls. *Tetrahedron Lett.* **1988**, 29, 3833–3836.
- (261) Ishiyama, T.; Miyaura, N.; Suzuki, A. Palladium-Catalyzed Carbonylative Cross-Coupling Reaction of Iodoalkanes with 9-Alkyl-9-BBN Derivatives A Direct and Selective Synthesis of Ketones. *Tetrahedron Lett.* **1991**, 32, 6923–6926.
- (262) Ryu, I.; Kreimerman, S.; Araki, F.; Nishitani, S.; Oderaotoshi, Y.; Minakata, S.; Komatsu, M. Cascade Radical Reactions Catalyzed by a Pd/Light System: Cyclizative Multiple Carbonylation of 4-Alkenyl Iodides. *J. Am. Chem. Soc.* **2002**, *124*, 3812–3813.
- (263) Fukuyama, T.; Nishitani, S.; Inouye, T.; Morimoto, K.; Ryu, I. Effective Acceleration of Atom Transfer Carbonylation of Alkyl Iodides by Metal Complexes. Application to the Synthesis of the Hinokinin Precursor and Dihydrocapsaicin. *Org. Lett.* **2006**, *8*, 1383–1386.
- (264) Fukuyama, T.; Inouye, T.; Ryu, I. Atom Transfer Carbonylation Using Ionic Liquids as Reaction Media. *J. Organomet. Chem.* **2007**, 692, 685–690.
- (265) Fusano, A.; Fukuyama, T.; Nishitani, S.; Inouye, T.; Ryu, I. Synthesis of Alkyl Alkynyl Ketones by Pd/Light-Induced Three-Component Coupling Reactions of Iodoalkanes, Co, and 1-Alkynes. *Org. Lett.* **2010**, *12*, 2410–2413.
- (266) Fusano, A.; Sumino, S.; Fukuyama, T.; Ryu, I. Vicinal C-Functionalization of Alkenes. Pd/Light-Induced Multicomponent Coupling Reactions Leading to Functionalized Esters and Lactones. *Org. Lett.* **2011**, *13*, 2114–2117.
- (267) Fusano, A.; Sumino, S.; Nishitani, S.; Inouye, T.; Morimoto, K.; Fukuyama, T.; Ryu, I. Pd/Light-Accelerated Atom-Transfer Carbonylation of Alkyl Iodides: Applications in Multicomponent Coupling Processes Leading to Functionalized Carboxylic Acid Derivatives. *Chem. Eur. J.* 2012, *18*, 9415–9422.
- (268) Ryu, I.; Sumino, S.; Fusano, A.; Fukuyama, T. Synthesis of Carbamoylacetates from α -Iodoacetate, CO, and Amines under Pd/Light Combined Conditions. *Synlett* **2012**, 23, 1331–1334.
- (269) Sumino, S.; Ui, T.; Ryu, I. Synthesis of Alkyl Aryl Ketones by Pd/Light Induced Carbonylative Cross-Coupling of Alkyl Iodides and Arylboronic Acids. *Org. Lett.* **2013**, *15*, 3142–3145.
- (270) Sargent, B. T.; Alexanian, E. J. Palladium-Catalyzed Alkoxycarbonylation of Unactivated Secondary Alkyl Bromides at Low Pressure. *J. Am. Chem. Soc.* **2016**, *138*, 7520–7523.
- (271) Quesnel, J. S.; Arndtsen, B. A. A Palladium-Catalyzed Carbonylation Approach to Acid Chloride Synthesis. *J. Am. Chem. Soc.* **2013**, *135*, 16841–16844.
- (272) Yang, Z.; Koenigs, R. M. Photoinduced Palladium-Catalyzed Dicarbofunctionalization of Terminal Alkynes. *Chem. Eur. J.* **2021**, *27*, 3694–3699.
- (273) Zhao, G.; Yao, W.; Mauro, J. N.; Ngai, M. Y. Excited-State Palladium-Catalyzed 1,2-Spin-Center Shift Enables Selective C-2 Reduction, Deuteration, and Iodination of Carbohydrates. *J. Am. Chem. Soc.* **2021**, *143*, 1728–1734.
- (274) Czyz, M. L.; Weragoda, G. K.; Horngren, T. H.; Connell, T. U.; Gomez, D.; O'Hair, R. A. J.; Polyzos, A. Photoexcited Pd(II) Auxiliaries Enable Light-Induced Control in C(sp³)-H Bond Functionalisation. *Chem. Sci.* **2020**, *11*, 2455–2463.
- (275) Zhao, J. H.; Zhou, Z. Z.; Zhang, Y.; Su, X.; Chen, X. M.; Liang, Y. M. Visible-Light-Mediated Borylation of Aryl and Alkyl Halides with a Palladium Complex. *Org. Biomol. Chem.* **2020**, *18*, 4390–4394.
- (276) Ma, J. W.; Chen, X.; Zhou, Z. Z.; Liang, Y. M. Visible-Light-Induced Palladium-Catalyzed Carbocyclization of Unactivated Alkyl Bromides with Alkenes Involving C-I or C-B Coupling. *J. Org. Chem.* **2020**, *85*, 9301–9312.
- (277) Feng, L.; Guo, L.; Yang, C.; Zhou, J.; Xia, W. Visible-Light-Induced Palladium-Catalyzed Intermolecular Narasaka-Heck Reaction at Room Temperature. *Org. Lett.* **2020**, *22*, 3964–3968.
- (278) Bao, X.; Wang, Q.; Zhu, J. Palladium-Catalyzed Enantiose-lective Narasaka-Heck Reaction/Direct C-H Alkylation of Arenes: Iminoarylation of Alkenes. *Angew. Chem., Int. Ed.* **2017**, *56*, 9577–9581.
- (279) Fu, W.; Yu, A.; Jiang, H.; Zuo, M.; Wu, H.; Yang, Z.; An, Q.; Sun, Z.; Chu, W. A Visible-Light-Induced Cascade Reaction of

- Etherification/C-C Cyclization: Efficient Synthesis of Dibenzo[b,d]-Oxepin-7(6H)-Ones. Org. Biomol. Chem. **2019**, 17, 3324–3327.
- (280) Shields, B. J.; Kudisch, B.; Scholes, G. D.; Doyle, A. G. Long-Lived Charge-Transfer States of Nickel(II) Aryl Halide Complexes Facilitate Bimolecular Photoinduced Electron Transfer. *J. Am. Chem. Soc.* 2018, 140, 3035–3039.
- (281) Shen, X.; Li, Y. J.; Wen, Z. R.; Cao, S.; Hou, X. Y.; Gong, L. A Chiral Nickel DBFOX Complex as a Bifunctional Catalyst for Visible-Light-Promoted Asymmetric Photoredox Reactions. *Chem. Sci.* **2018**, *9*, 4562–4568.
- (282) Lim, C. H.; Kudisch, M.; Liu, B.; Miyake, G. M. C-N Cross-Coupling via Photoexcitation of Nickel-Amine Complexes. *J. Am. Chem. Soc.* **2018**, *140*, 7667–7673.
- (283) Abdiaj, I.; Fontana, A.; Gomez, M. V.; de la Hoz, A.; Alcazar, J. Visible-Light-Induced Nickel-Catalyzed Negishi Cross-Couplings by Exogenous-Photosensitizer-Free Photocatalysis. *Angew. Chem., Int. Ed.* **2018**, *57*, 8473–8477.
- (284) Ting, S. I.; Garakyaraghi, S.; Taliaferro, C. M.; Shields, B. J.; Scholes, G. D.; Castellano, F. N.; Doyle, A. G. ³d-d Excited States of Ni(II) Complexes Relevant to Photoredox Catalysis: Spectroscopic Identification and Mechanistic Implications. *J. Am. Chem. Soc.* **2020**, 142, 5800–5810.
- (285) Kariofillis, S. K.; Doyle, A. G. Synthetic and Mechanistic Implications of Chlorine Photoelimination in Nickel/Photoredox C(sp³)-H Cross-Coupling. *Acc. Chem. Res.* **2021**, *54*, 988–1000.
- (286) Yang, L.; Lu, H. H.; Lai, C. H.; Li, G.; Zhang, W.; Cao, R.; Liu, F.; Wang, C.; Xiao, J.; Xue, D. Light-Promoted Nickel Catalysis: Etherification of Aryl Electrophiles with Alcohols Catalyzed by a Ni(II)-Aryl Complex. *Angew. Chem., Int. Ed.* **2020**, *59*, 12714–12719. (287) Li, G.; Yang, L.; Liu, J. J.; Zhang, W.; Cao, R.; Wang, C.; Zhang, Z.; Xiao, J.; Xue, D. Light-Promoted C-N Coupling of Aryl Halides with Nitroarenes. *Angew. Chem., Int. Ed.* **2021**, *60*, 5230–5234.
- (288) Abdiaj, I.; Horn, C. R.; Alcazar, J. Scalability of Visible-Light-Induced Nickel Negishi Reactions: A Combination of Flow Photochemistry, Use of Solid Reagents, and In-Line NMR Monitoring. *J. Org. Chem.* **2019**, *84*, 4748–4753.
- (289) Nicewicz, D. A.; MacMillan, D. W. Merging Photoredox Catalysis with Organocatalysis: The Direct Asymmetric Alkylation of Aldehydes. *Science* **2008**, 322, 77–80.
- (290) Nagib, D. A.; Scott, M. E.; MacMillan, D. W. Enantioselective α -Trifluoromethylation of Aldehydes via Photoredox Organocatalysis. *J. Am. Chem. Soc.* **2009**, *131*, 10875–10877.
- (291) Shih, H. W.; Vander Wal, M. N.; Grange, R. L.; MacMillan, D. W. Enantioselective α-Benzylation of Aldehydes via Photoredox Organocatalysis. *J. Am. Chem. Soc.* **2010**, *132*, 13600–13603.
- (292) DiRocco, D. A.; Rovis, T. Catalytic Asymmetric Alpha-Acylation of Tertiary Amines Mediated by a Dual Catalysis Mode: N-Heterocyclic Carbene and Photoredox Catalysis. *J. Am. Chem. Soc.* **2012**, *134*, 8094–8097.
- (293) Rono, L. J.; Yayla, H. G.; Wang, D. Y.; Armstrong, M. F.; Knowles, R. R. Enantioselective Photoredox Catalysis Enabled by Proton-Coupled Electron Transfer: Development of an Asymmetric Aza-Pinacol Cyclication. *J. Am. Chem. Soc.* **2013**, 135, 17735–17738.
- (294) Du, J. N.; Skubi, K. L.; Schultz, D. M.; Yoon, T. P. A Dual-Catalysis Approach to Enantioselective [2 + 2] Photocycloadditions Using Visible Light. *Science* **2014**, *344*, 392–396.
- (295) Bergonzini, G.; Schindler, C. S.; Wallentin, C. J.; Jacobsen, E. N.; Stephenson, C. R. J. Photoredox Activation and Anion Binding Catalysis in the Dual Catalytic Enantioselective Synthesis of Bamino Esters. *Chem. Sci.* **2014**, *5*, 112–116.
- (296) Huo, H.; Shen, X.; Wang, C.; Zhang, L.; Rose, P.; Chen, L. A.; Harms, K.; Marsch, M.; Hilt, G.; Meggers, E. Asymmetric Photoredox Transition-Metal Catalysis Activated by Visible Light. *Nature* **2014**, *515*, 100–103.
- (297) Skubi, K. L.; Kidd, J. B.; Jung, H.; Guzei, I. A.; Baik, M. H.; Yoon, T. P. Enantioselective Excited-State Photoreactions Controlled by a Chiral Hydrogen-Bonding Iridium Sensitizer. *J. Am. Chem. Soc.* **2017**, 139, 17186–17192.

- (298) Zheng, J.; Swords, W. B.; Jung, H.; Skubi, K. L.; Kidd, J. B.; Meyer, G. J.; Baik, M. H.; Yoon, T. P. Enantioselective Intermolecular Excited-State Photoreactions Using a Chiral Ir Triplet Sensitizer: Separating Association from Energy Transfer in Asymmetric Photocatalysis. J. Am. Chem. Soc. 2019, 141, 13625–13634.
- (299) Meggers, E. Exploiting Octahedral Stereocenters: From Enzyme Inhibition to Asymmetric Photoredox Catalysis. *Angew. Chem., Int. Ed.* **2017**, *56*, 5668–5675.
- (300) Zhang, L.; Meggers, E. Stereogenic-Only-at-Metal Asymmetric Catalysts. *Chem. Asian J.* **2017**, *12*, 2335–2342.
- (301) Zhang, L.; Meggers, E. Steering Asymmetric Lewis Acid Catalysis Exclusively with Octahedral Metal-Centered Chirality. *Acc. Chem. Res.* **2017**, *50*, 320–330.
- (302) Ma, J.; Zhang, X.; Huang, X.; Luo, S.; Meggers, E. Preparation of Chiral-at-Metal Catalysts and Their Use in Asymmetric Photoredox Chemistry. *Nat. Protoc.* **2018**, *13*, 605–632.
- (303) Huo, H.; Wang, C.; Harms, K.; Meggers, E. Enantioselective, Catalytic Trichloromethylation through Visible-Light-Activated Photoredox Catalysis with a Chiral Iridium Complex. *J. Am. Chem. Soc.* **2015**, 137, 9551–9554.
- (304) Meggers, E.; Huo, H.; Huang, X.; Shen, X.; Harms, K. Visible-Light-Activated Enantioselective Perfluoroalkylation with a Chiral Iridium Photoredox Catalyst. *Synlett* **2016**, *27*, 749–753.
- (305) Wang, C.; Zheng, Y.; Huo, H.; Rose, P.; Zhang, L.; Harms, K.; Hilt, G.; Meggers, E. Merger of Visible Light Induced Oxidation and Enantioselective Alkylation with a Chiral Iridium Catalyst. *Chem. Eur. J.* **2015**, *21*, 7355–7359.
- (306) Wang, C.; Qin, J.; Shen, X.; Riedel, R.; Harms, K.; Meggers, E. Asymmetric Radical-Radical Cross-Coupling through Visible-Light-Activated Iridium Catalysis. *Angew. Chem., Int. Ed.* **2016**, *55*, 685–688.
- (307) Huang, X.; Meggers, E. Asymmetric Photocatalysis with Biscyclometalated Rhodium Complexes. *Acc. Chem. Res.* **2019**, *52*, 833–847.
- (308) Tan, Y. Q.; Yuan, W.; Gong, L.; Meggers, E. Aerobic Asymmetric Dehydrogenative Cross-Coupling between Two C_{sp3} -H Groups Catalyzed by a Chiral-at-Metal Rhodium Complex. *Angew. Chem., Int. Ed.* **2015**, *54*, 13045–13048.
- (309) Ma, J.; Rosales, A. R.; Huang, X.; Harms, K.; Riedel, R.; Wiest, O.; Meggers, E. Visible-Light-Activated Asymmetric β -C-H Functionalization of Acceptor-Substituted Ketones with 1,2-Dicarbonyl Compounds. *J. Am. Chem. Soc.* **2017**, *139*, 17245–17248.
- (310) Lin, S. X.; Sun, G. J.; Kang, Q. A Visible-Light-Activated Rhodium Complex in Enantioselective Conjugate Addition of α -Amino Radicals with Michael Acceptors. *Chem. Commun.* **2017**, *53*, 7665–7668.
- (311) Huang, X.; Quinn, T. R.; Harms, K.; Webster, R. D.; Zhang, L.; Wiest, O.; Meggers, E. Direct Visible-Light-Excited Asymmetric Lewis Acid Catalysis of Intermolecular [2 + 2] Photocycloadditions. *J. Am. Chem. Soc.* **2017**, *139*, 9120–9123.
- (312) Thongpaen, J.; Manguin, R.; Dorcet, V.; Vives, T.; Duhayon, C.; Mauduit, M.; Basle, O. Visible Light Induced Rhodium(I)-Catalyzed C-H Borylation. *Angew. Chem., Int. Ed.* **2019**, *58*, 15244–15248.
- (313) Min, X. T.; Ji, D. W.; Guan, Y. Q.; Guo, S. Y.; Hu, Y. C.; Wan, B.; Chen, Q. A. Visible Light Induced Bifunctional Rhodium Catalysis for Decarbonylative Coupling of Imides with Alkynes. *Angew. Chem., Int. Ed.* **2021**, *60*, 1583–1587.
- (314) Cecere, G.; Konig, C. M.; Alleva, J. L.; MacMillan, D. W. C. Enantioselective Direct α -Annination of Aldehydes via a Photoredox Mechanism: A Strategy for Asymmetric Amine Fragment Coupling. *J. Am. Chem. Soc.* **2013**, *135*, 11521–11524.
- (315) Shen, X.; Harms, K.; Marsch, M.; Meggers, E. A Rhodium Catalyst Superior to Iridium Congeners for Enantioselective Radical Amination Activated by Visible Light. *Chem. Eur. J.* **2016**, 22, 9102–9105.
- (316) Zard, S. Z. Recent Progress in the Generation and Use of Nitrogen-Centred Radicals. Chem. Soc. Rev. 2008, 37, 1603-1618.
- (317) Steinlandt, P. S.; Zuo, W.; Harms, K.; Meggers, E. Bis-Cyclometalated Indazole Chiral-at-Rhodium Catalyst for Asymmetric Photoredox Cyanoalkylations. *Chem. Eur. J.* **2019**, *25*, 15333–15340.

- (318) Zhou, Z. J.; Nie, X.; Harms, K.; Riedel, R.; Zhang, L. L.; Meggers, E. Enantioconvergent Photoredox Radical-Radical Coupling Catalyzed by a Chiral-at-Rhodium Complex. *Sci. China: Chem.* **2019**, 62, 1512–1518.
- (319) Ruiz Espelt, L.; McPherson, I. S.; Wiensch, E. M.; Yoon, T. P. Enantioselective Conjugate Additions of α -Amino Radicals via Cooperative Photoredox and Lewis Acid Catalysis. *J. Am. Chem. Soc.* **2015**, *137*, 2452–2455.
- (320) Murphy, J. J.; Bastida, D.; Paria, S.; Fagnoni, M.; Melchiorre, P. Asymmetric Catalytic Formation of Quaternary Carbons by Iminium Ion Trapping of Radicals. *Nature* **2016**, *532*, 218–222.
- (321) de Assis, F. F.; Huang, X. Q.; Akiyama, M.; Pilli, R. A.; Meggers, E. Visible-Light-Activated Catalytic Enantioselective β -Alkylation of α , β -Unsaturated 2-Acyl Imidazoles Using Hantzsch Esters as Radical Reservoirs. *J. Org. Chem.* **2018**, 83, 10922–10932.
- (322) Ma, J. J.; Lin, J. H.; Zhao, L. F.; Harms, K.; Marsch, M.; Xie, X. L.; Meggers, E. Synthesis of β -Substituted γ -Aminobutyric Acid Derivatives through Enantioselective Photoredox Catalysis. *Angew. Chem., Int. Ed.* **2018**, *57*, 11193–11197.
- (323) Huang, X.; Li, X.; Xie, X.; Harms, K.; Riedel, R.; Meggers, E. Catalytic Asymmetric Synthesis of a Nitrogen Heterocycle through Stereocontrolled Direct Photoreaction from Electronically Excited State. *Nat. Commun.* **2017**, *8*, 2245.
- (324) Huang, X. Q.; Lin, J. H.; Shen, T. Q.; Harms, K.; Marchini, M.; Ceroni, P.; Meggers, E. Asymmetric [3 + 2] Photocycloadditions of Cyclopropanes with Alkenes or Alkynes through Visible-Light Excitation of Catalyst-Bound Substrates. *Angew. Chem., Int. Ed.* **2018**, 57, 5454–5458.
- (325) Sahoo, B.; Hopkinson, M. N.; Glorius, F. Combining Gold and Photoredox Catalysis: Visible Light-Mediated Oxy- and Aminoarylation of Alkenes. *J. Am. Chem. Soc.* **2013**, *135*, 5505–5508.
- (326) Hopkinson, M. N.; Sahoo, B.; Glorius, F. Dual Photoredox and Gold Catalysis: Intermolecular Multicomponent Oxyarylation of Alkenes. *Adv. Synth. Catal.* **2014**, *356*, 2794–2800.
- (327) Shu, X. Z.; Zhang, M.; He, Y.; Frei, H.; Toste, F. D. Dual Visible Light Photoredox and Gold-Catalyzed Arylative Ring Expansion. *J. Am. Chem. Soc.* **2014**, *136*, 5844–5847.
- (328) Bratsch, S. G. Standard Electrode-Potentials and Temperature Coefficients in Water at 298.15-K. *J. Phys. Chem. Ref. Data* **1989**, *18*, 1–21
- (329) Huang, L.; Rudolph, M.; Rominger, F.; Hashmi, A. S. Photosensitizer-Free Visible-Light-Mediated Gold-Catalyzed 1,2-Difunctionalization of Alkynes. *Angew. Chem., Int. Ed.* **2016**, *55*, 4808–4813.
- (330) Zhang, L. M.; Si, X. J.; Yang, Y. Y.; Witzel, S.; Sekine, K.; Rudolph, M.; Rominger, F.; Hashmi, A. S. K. Reductive C-C Coupling by Desulfurizing Gold-Catalyzed Photoreactions. *ACS Catal.* **2019**, *9*, 6118–6123.
- (331) Witzel, S.; Hashmi, A. S. K.; Xie, J. Light in Gold Catalysis. *Chem. Rev.* **2021**, *121*, 8868–8925.
- (332) Liu, Y.; Yang, Y.; Zhu, R.; Liu, C.; Zhang, D. The Dual Role of Gold(I) Complexes in Photosensitizer-Free Visible-Light-Mediated Gold-Catalyzed 1,2-Difunctionalization of Alkynes: A DFT Study. Chem. Eur. J. 2018, 24, 14119–14126.
- (333) Taschinski, S.; Dopp, R.; Ackermann, M.; Rominger, F.; de Vries, F.; Menger, M.; Rudolph, M.; Hashmi, A. S. K.; Klein, J. Light-Induced Mechanistic Divergence in Gold(I) Catalysis: Revisiting the Reactivity of Diazonium Salts. *Angew. Chem., Int. Ed.* **2019**, *58*, 16988–16993.
- (334) Witzel, S.; Xie, J.; Rudolph, M.; Hashmi, A. S. K. Photosensitizer-Free, Gold-Catalyzed C-C Cross-Coupling of Boronic Acids and Diazonium Salts Enabled by Visible Light. *Adv. Synth. Catal.* **2017**, 359, 1522–1528.
- (335) Xie, J.; Sekine, K.; Witzel, S.; Kramer, P.; Rudolph, M.; Rominger, F.; Hashmi, A. S. K. Light-Induced Gold-Catalyzed Hiyama Arylation: A Coupling Access to Biarylboronates. *Angew. Chem., Int. Ed.* **2018**, *57*, 16648–16653.
- (336) Witzel, S.; Sekine, K.; Rudolph, M.; Hashmi, A. S. K. New Transmetalation Reagents for the Gold-Catalyzed Visible Light-

- Enabled C(sp or sp²)-C(sp²) Cross-Coupling with Aryldiazonium Salts in the Absence of a Photosensitizer. *Chem. Commun.* **2018**, *54*, 13802–13804.
- (337) Tzirakis, M. D.; Lykakis, I. N.; Orfanopoulos, M. Decatungstate as an Efficient Photocatalyst in Organic Chemistry. *Chem. Soc. Rev.* **2009**, 38, 2609–2621.
- (338) Ravelli, D.; Fagnoni, M.; Fukuyama, T.; Nishikawa, T.; Ryu, I. Site-Selective C-H Functionalization by Decatungstate Anion Photocatalysis: Synergistic Control by Polar and Steric Effects Expands the Reaction Scope. *ACS Catal.* **2018**, *8*, 701–713.
- (339) Laudadio, G.; Deng, Y.; van der Wal, K.; Ravelli, D.; Nuño, M.; Fagnoni, M.; Guthrie, D.; Sun, Y.; Noël, T. C(sp³)-H Functionalizations of Light Hydrocarbons Using Decatungstate Photocatalysis in Flow. *Science* **2020**, *369*, 92–96.
- (340) Waele, V. D.; Poizat, O.; Fagnoni, M.; Bagno, A.; Ravelli, D. Unraveling the Key Features of the Reactive State of Decatungstate Anion in Hydrogen Atom Transfer (HAT) Photocatalysis. *ACS Catal.* **2016**, *6*, 7174–7182.
- (341) Renneke, R. F.; Hill, C. L. Homogeneous Catalytic Photochemical Functionalization of Alkanes by Polyoxometalates. *J. Am. Chem. Soc.* **1986**, *108*, 3528–3529.
- (342) Duncan, D. C.; Netzel, T. L.; Hill, C. L. Early-Time Dynamics and Reactivity of Polyoxometalate Excited States. Identification of a Short-Lived LMCT Excited State and a Reactive Long-Lived Charge-Transfer Intermediate following Picosecond Flash Excitation of $\left[W_{10}O_{32}\right]^4$ in Acetonitrile. *Inorg. Chem.* 1995, 34, 4640–4646.
- (343) Ravelli, D.; Montanaro, S.; Zema, M.; Fagnoni, M.; Albini, A. A Tin-Free, Radical Photocatalyzed Addition to Vinyl Sulfones. *Adv. Synth. Catal.* **2011**, *353*, 3295–3300.
- (344) Qrareya, H.; Ravelli, D.; Fagnoni, M.; Albini, A. Decatungstate Photocatalyzed Benzylation of Alkenes with Alkylaromatics. *Adv. Synth. Catal.* **2013**, 355, 2891–2899.
- (345) Ryu, I.; Tani, A.; Fukuyama, T.; Ravelli, D.; Montanaro, S.; Fagnoni, M. Efficient C-H/C-N and C-H/C-CO-N Conversion via Decatungstate-Photoinduced Alkylation of Diisopropyl Azodicarboxylate. *Org. Lett.* **2013**, *15*, 2554–2557.
- (346) Ravelli, D.; Zoccolillo, M.; Mella, M.; Fagnoni, M. Photocatalytic Synthesis of Oxetane Derivatives by Selective C-H Activation. *Adv. Synth. Catal.* **2014**, 356, 2781–2786.
- (347) Qrareya, H.; Dondi, D.; Ravelli, D.; Fagnoni, M. Decatungstate-Photocatalyzed Si-H/C-H Activation in Silyl Hydrides: Hydrosilylation of Electron-Poor Alkenes. *ChemCatChem* **2015**, *7*, 3350–3357.
- (348) Protti, S.; Ravelli, D.; Fagnoni, M.; Albini, A. Solar Light-Driven Photocatalyzed Alkylations. Chemistry on the Window Ledge. *Chem. Commun.* **2009**, 7351–7353.
- (349) Okada, M.; Fukuyama, T.; Yamada, K.; Ryu, I.; Ravelli, D.; Fagnoni, M. Sunlight Photocatalyzed Regioselective β -Alkylation and Acylation of Cyclopentanones. *Chem. Sci.* **2014**, *5*, 2893–2898.
- (350) Dai, Z. Y.; Nong, Z. S.; Wang, P. S. Light-Mediated Asymmetric Aliphatic C-H Alkylation with Hydrogen Atom Transfer Catalyst and Chiral Phosphoric Acid. *ACS Catal.* **2020**, *10*, 4786–4790.
- (351) Wang, X.; Chen, Y.; Song, H.; Liu, Y.; Wang, Q. Synthesis of Unnatural α-Amino Acids via Photoinduced Decatungstate-Catalyzed Giese Reactions of Aldehydes. *Org. Lett.* **2021**, 23, 2199–2204.
- (352) Dai, Z. Y.; Nong, Z. S.; Song, S.; Wang, P. S. Asymmetric Photocatalytic $C(sp^3)$ -H Bond Addition to α -Substituted Acrylates. *Org. Lett.* **2021**, 23, 3157–3161.
- (353) Fan, P.; Zhang, C.; Lan, Y.; Lin, Z.; Zhang, L.; Wang, C. Photocatalytic Hydroacylation of Trifluoromethyl Alkenes. *Chem. Commun.* **2019**, *55*, 12691–12694.
- (354) Xiao, T.; Li, L.; Zhou, L. Synthesis of Functionalized gem-Difluoroalkenes via a Photocatalytic Decarboxylative/Defluorinative Reaction. J. Org. Chem. 2016, 81, 7908—7916.
- (355) Lang, S. B.; Wiles, R. J.; Kelly, C. B.; Molander, G. A. Photoredox Generation of Carbon-Centered Radicals Enables the Construction of 1,1-Difluoroalkene Carbonyl Mimics. *Angew. Chem., Int. Ed.* **2017**, *56*, 15073–15077.
- (356) Phelan, J. P.; Lang, S. B.; Sim, J.; Berritt, S.; Peat, A. J.; Billings, K.; Fan, L.; Molander, G. A. Open-Air Alkylation Reactions in

- Photoredox-Catalyzed DNA-Encoded Library Synthesis. J. Am. Chem. Soc. 2019, 141, 3723–3732.
- (357) Prieto, A.; Taillefer, M. Visible-Light Decatungstate/Disulfide Dual Catalysis for the Hydro-Functionalization of Styrenes. *Org. Lett.* **2021**, 23, 1484–1488.
- (358) Supranovich, V. I.; Levin, V. V.; Dilman, A. D. Radical Addition to N-Tosylimines via C-H Activation Induced by Decatungstate Photocatalyst. *Org. Lett.* **2019**, *21*, 4271–4274.
- (359) Capaldo, L.; Ravelli, D. Decatungstate as Direct Hydrogen Atom Transfer Photocatalyst for SOMOphilic Alkynylation. *Org. Lett.* **2021**, 23, 2243–2247.
- (360) Dong, J.; Wang, X.; Wang, Z.; Song, H.; Liu, Y.; Wang, Q. Formyl-Selective Deuteration of Aldehydes with D_2O via Synergistic Organic and Photoredox Catalysis. *Chem. Sci.* **2020**, *11*, 1026–1031.
- (361) Kuang, Y.; Cao, H.; Tang, H.; Chew, J.; Chen, W.; Shi, X.; Wu, J. Visible Light Driven Deuteration of Formyl C-H and Hydridic C(sp³)-H Bonds in Feedstock Chemicals and Pharmaceutical Molecules. *Chem. Sci.* **2020**, *11*, 8912–8918.
- (362) Jamatia, R.; Mondal, A.; Srimani, D. Visible-Light-Induced Manganese-Catalyzed Reactions: Present Approach and Future Prospects. *Adv. Synth. Catal.* **2021**, 363, 2969–2995.
- (363) Nuhant, P.; Oderinde, M. S.; Genovino, J.; Juneau, A.; Gagné, Y.; Allais, C.; Chinigo, G. M.; Choi, C.; Sach, N. W.; Bernier, L.; Fobian, Y. M.; Bundesmann, M. W.; Khunte, B.; Frenette, M.; Fadeyi, O. O. Visible-Light-Initiated Manganese Catalysis for C-H Alkylation of Heteroarenes: Applications and Mechanistic Studies. *Angew. Chem., Int. Ed.* **2017**, *56*, 15309—15313.
- (364) Wang, L.; Lear, J. M.; Rafferty, S. M.; Fosu, S. C.; Nagib, D. A. Ketyl Radical Reactivity via Atom Transfer Catalysis. *Science* **2018**, 362, 225–229.
- (365) Liang, H.; Ji, Y. X.; Wang, R. H.; Zhang, Z. H.; Zhang, B. Visible-Light-Initiated Manganese-Catalyzed *E*-Selective Hydrosilylation and Hydrogermylation of Alkynes. *Org. Lett.* **2019**, *21*, 2750–2754.
- (366) Weng, W. Z.; Liang, H.; Liu, R. Z.; Ji, Y. X.; Zhang, B. Visible-Light-Promoted Manganese-Catalyzed Atom Transfer Radical Cyclization of Unactivated Alkyl Iodides. *Org. Lett.* **2019**, *21*, 5586–5590.
- (367) Liu, R. Z.; Li, J.; Sun, J.; Liu, X. G.; Qu, S.; Li, P.; Zhang, B. Generation and Reactivity of Amidyl Radicals: Manganese-Mediated Atom-Transfer Reaction. *Angew. Chem., Int. Ed.* **2020**, *59*, 4428–4433. (368) Ji, Y. X.; Li, J.; Li, C. M.; Qu, S.; Zhang, B. Manganese-Catalyzed N-F Bond Activation for Hydroamination and Carboamination of Alkenes. *Org. Lett.* **2021**, *23*, 207–212.
- (369) Liang, Y. F.; Steinbock, R.; Yang, L.; Ackermann, L. Continuous Visible-Light Photoflow Approach for a Manganese-Catalyzed (Het)-Arene C-H Arylation. *Angew. Chem., Int. Ed.* **2018**, *57*, 10625–10629. (370) Long, W.; Lian, P.; Li, J.; Wan, X. Mn-Catalysed Photoredox Hydroxytrifluoromethylation of Aliphatic Alkenes Using CF₃SO₂Na. *Org. Biomol. Chem.* **2020**, *18*, 6483–6486.
- (371) Gandeepan, P.; Koeller, J.; Korvorapun, K.; Mohr, J.; Ackermann, L. Visible-Light-Enabled Ruthenium-Catalyzed meta-C-H Alkylation at Room Temperature. *Angew. Chem., Int. Ed.* **2019**, 58, 9820–9825.
- (372) Sagadevan, A.; Greaney, M. F. meta-Selective C-H Activation of Arenes at Room Temperature Using Visible Light: Dual-Function Ruthenium Catalysis. *Angew. Chem., Int. Ed.* **2019**, *58*, 9826–9830.
- (373) For a related work in which visible light is not involved in the catalytic cycle, see: Sagadevan, A.; Charitou, A.; Wang, F.; Ivanova, M.; Vuagnat, M.; Greaney, M. F. Ortho C-H arylation of Arenes at Room Temperature Using Visible Light Ruthenium C-H Activation. *Chem. Sci.* **2020**, *11*, 4439–4443.
- (374) Sakai, K.; Ozawa, H. Homogeneous Catalysis of Platinum(II) Complexes in Photochemical Hydrogen Production from Water. *Coord. Chem. Rev.* **2007**, *251*, 2753–2766.
- (375) Naik, A.; Rubbiani, R.; Gasser, G.; Spingler, B. Visible-Light-Induced Annihilation of Tumor Cells with Platinum-Porphyrin Conjugates. *Angew. Chem., Int. Ed.* **2014**, *53*, 6938–6941.
- (376) Doherty, R. E.; Sazanovich, I. V.; McKenzie, L. K.; Stasheuski, A. S.; Coyle, R.; Baggaley, E.; Bottomley, S.; Weinstein, J. A.; Bryant, H.

- E. Photodynamic Killing of Cancer Cells by a Platinum(II) Complex with Cyclometallating Ligand. Sci. Rep. 2016, 6, 22668.
- (377) Ranieri, A. M.; Burt, L. K.; Stagni, S.; Zacchini, S.; Skelton, B. W.; Ogden, M. I.; Bissember, A. C.; Massi, M. Anionic Cyclometalated Platinum(II) Tetrazolato Complexes as Viable Photoredox Catalysts. *Organometallics* **2019**, *38*, 1108–1117.
- (378) Li, K.; Ming Tong, G. S.; Wan, Q.; Cheng, G.; Tong, W. Y.; Ang, W. H.; Kwong, W. L.; Che, C. M. Highly Phosphorescent Platinum(II) Emitters: Photophysics, Materials and Biological Applications. *Chem. Sci.* **2016**, *7*, 1653–1673.
- (379) Gee, J. C.; Fuller, B. A.; Lockett, H. M.; Sedghi, G.; Robertson, C. M.; Luzyanin, K. V. Visible Light Accelerated Hydrosilylation of Alkynes Using Platinum-[Acyclic Diaminocarbene] Photocatalysts. *Chem. Commun.* **2018**, *54*, 9450–9453.
- (380) Zhang, D.; Wu, L. Z.; Zhou, L.; Han, X.; Yang, Q. Z.; Zhang, L. P.; Tung, C. H. Photocatalytic Hydrogen Production from Hantzsch 1,4-Dihydropyridines by Platinum(II) Terpyridyl Complexes in Homogeneous Solution. *J. Am. Chem. Soc.* **2004**, *126*, 3440–3441.